Journal of Medicinal Chemistry

pubs.acs.org/jmc

Article

Discovery and Evaluation of C6-Substituted Pyrazolopyrimidine-Based Bisphosphonate Inhibitors of the Human Geranylgeranyl Pyrophosphate Synthase and Evaluation of Their Antitumor Efficacy in Multiple Myeloma, Pancreatic Ductal Adenocarcinoma, and Colorectal Cancer

Rebecca Boutin, Hiu-Fung Lee, Tian Lai Guan, Tan Trieu Nguyen, Xian Fang Huang, Daniel D. Waller, Jordan Lu, Iok In Christine Chio, René P. Michel, Michael Sebag, and Youla S. Tsantrizos*

Cite This: J. Med. Chem. 2023, 66, 15776−15800

Read Online

ACCESS | Metrics & More | Article Recommendations | Supporting Information

ABSTRACT: Novel C6-substituted pyrazolo[3,4-*d*]pyrimidine- and C2-substituted purine-based bisphosphonate (C6-PyraP-BP and C2-Pur-BP, respectively) inhibitors of the human geranylgeranyl pyrophosphate synthase (hGGPPS) were designed and evaluated for their ability to block the proliferation of multiple myeloma (MM), pancreatic ductal adenocarcinoma (PDAC), and colorectal cancer (CRC) cells. Pyrazolo[3,4-*d*]pyrimidine analogs were identified that induce selective intracellular target engagement leading to apoptosis and downregulate the prenylation of Rap-1A in MM, PDAC, and CRC cells. The C6-PyraP-BP inhibitor RB-07-16 was found to exhibit antitumor efficacy in xenograft mouse models of MM and PDAC, significantly reducing tumor growth without substantially increasing liver enzymes or causing significant histopathologic damage, usually associated with hepatotoxicity. RB-07-16 is a metabolically stable compound in cross-species liver microsomes, does not inhibit key CYP 450 enzymes, and exhibits good systemic circulation in rat. Collectively, the current studies provide encouraging support for further optimization of the pyrazolo[3,4-*d*]pyrimidine-based GGPPS inhibitors as potential human therapeutics for various cancers.

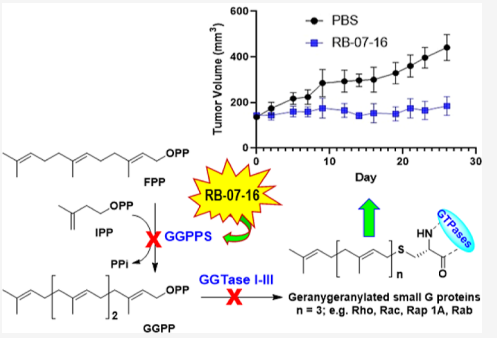

1. INTRODUCTION

Optimization of exploratory compounds to clinical candidates almost invariably involves bioisosteric replacements of key structural motifs in order to simultaneously optimize all of the biopharmaceutical properties in a class of exploratory compounds, including their in vitro and cell-based potency,[1] target selectivity, protein binding, ADME/PK profile,[2] and oral bioavailability.[3] In the course of our own medicinal chemistry efforts toward the discovery of novel therapeutics for the treatment of hematological cancers[4] and other human diseases,[5] we investigated several structurally diverse classes of compounds that can downregulate the prenylation of small GTP-binding proteins (GTPases). Mutated GTPases, such as the farnesylated H/K/N-RAS[6] and the geranylgeranylated Rho family (e.g., RhoA/B/C) and Ras-related proteins (e.g., Rap-1A and Rab),[7] are known to mediate cancer cell proliferation, differentiation, metastasis, and cell survival and have been of interest in oncology for several decades. Downregulation of GTPases' prenylation can be achieved in numerous ways, including by directly blocking the transferase enzymes FTase or GGTase I/II/III, which catalyze the attachment of the C-15 and C-20 lipidic carbon chains of farnesyl pyrophosphate (FPP) and geranylgeranyl pyrophosphate (GGPP), respectively, to the GTPases (Figure 1). Alternatively, inhibition of the upstream enzymes in the mevalonate/isoprenoid metabolic pathway, the human farnesyl pyrophosphate synthase (hFPPS) or the human geranylgeranyl pyrophosphate synthase (hGGPPS), can lead to intracellular depletion of their corresponding catalytic products (FPP and GGPP, respectively), thus also resulting in the intracellular decrease of prenylated GTPases. All of these approaches have been explored for cancer chemotherapy, leading to the identification of several preclinical and clinical candidates for the treatment of various cancers, unfortunately, with modest or minimal success. However, investigations focusing specifically on novel and selective inhibitors of hGGPPS have been relatively limited, and none of the inhibitors reported so far have advanced to clinical development.[8]

Received: July 13, 2023
Published: November 20, 2023

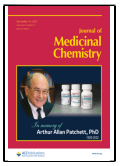

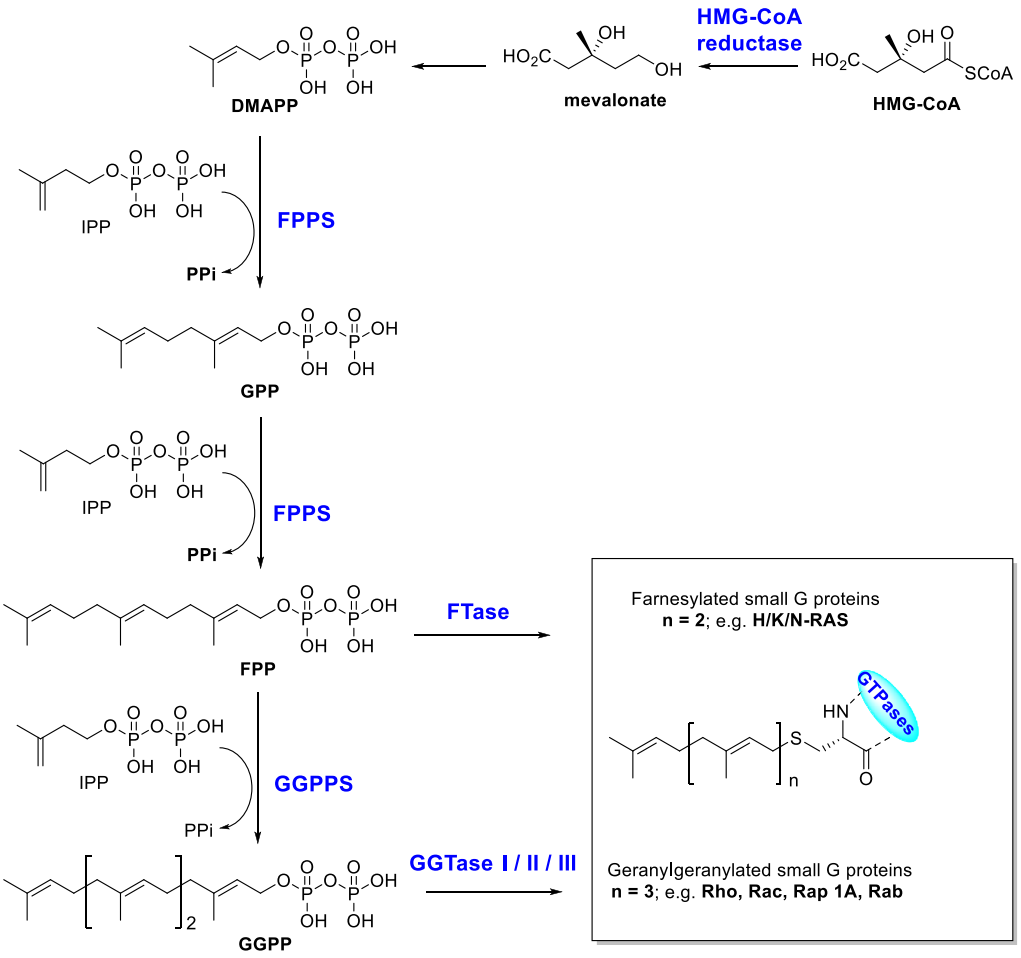

Figure 1. Biosynthetic pathway of isoprenoid metabolites leading to post-translational prenylation of GTPases.

We previously reported the identification of C2-substituted thienopyrimidine-based bisphosphonate (C2-ThP-BP) inhibitors of the hGGPPS with general structures **11** and **12** (Figure 2).[9] We showed that these compounds can block the biosynthesis of GGPP in multiple myeloma (MM) cells, thus downregulating the post-translational geranylgeranylation of common GTPases, such as Rap-1A;[9a] this is the expected outcome of blocking GGPP biosynthesis.[10,11] Analogs for these series of compounds include inhibitor CML-07-119 (**12c**), which exhibits antimyeloma efficacy in vivo.[9a] We also demonstrated that structurally related thienopyrimidine analogs, which are potent inhibitors of hFPPS and have very similar physicochemical properties, were far less potent in blocking the proliferation of MM cells. We proposed that the latter observation is likely due to the significantly higher expression of hFPPS compared to that of hGGPPS in many MM cells and in bone marrow samples of MM patients, resulting in much higher levels of target engagement for hGGPPS than for hFPPS with equipotent inhibitors independently targeting these two enzymes.[9a] Further investigations in our group[9a] revealed that impairment of GGPP biosynthesis disrupts the secretory pathway functions in MM and pancreatic ductal adenocarcinoma (PDAC) cells, an observation also reported by other groups,[12b] leading to endoplasmic reticulum (ER) stress-induced activation of the unfolded protein response and cell apoptosis.[12a] Additionally, we demonstrated the induction of apoptosis in MM cells (RPMI-8226) when treated with inhibitor CML-07-119 (Figure 2; **12c**), which was completely abrogated by simultaneous cotreatment of these cells with inhibitor **12c** and geranylgeraniol (GGOH).[9a] It is known that GGOH gets phosphorylated in cells to GGPP, which is required for cell survival, thus also providing strong evidence of the selective intracellular target engagement of hGGPPS by inhibitor CML-07-119 (**12c**) and direct correlation between MM cellular apoptosis and hGGPPS inhibition. Western blot analysis also demonstrated that XBP1s (the protein product of spliced XBP1 mRNA) increased upon the treatment of MM cells (RPMI-8226) with our hGGPPS inhibitors, and this effect was also mitigated by GGOH cotreatment. Increased and decreased phosphorylation of ERK and AKT, respectively, was also observed.[9a] Similar observations have been reported using statins and various nitrogen-based bisphosphonates (*N*-BP) that target HMG-CoA reductase and hFPPS (Figure 1), respectively, thus indirectly blocking both protein farnesylation and geranylgeranylation.

Previously, we also demonstrated that hGGPPS inhibitors can block the proliferation of PDAC cells, such as MIA PaCa-2.[9a] More recently, the triazole-based GGPPS inhibitor RAM2061 (**7**) was used to demonstrate similar effects in PDAC cells.[12b] It is noteworthy that in earlier studies by scientists from Merck, the prenyl transferase inhibitor L-778,123 (**10**), a dual inhibitor of FTase and GGTase I, was advanced to Phase I clinical trials for the treatment of PDAC.[13] In spite of the fact that the development of L-778,123 was discontinued due to clinical toxicity, the preclinical investigations of this compound (**10**) provided strong support for the hypothesis that blocking protein

https://doi.org/10.1021/acs.jmedchem.3c01271
J. Med. Chem. 2023, 66, 15776−15800

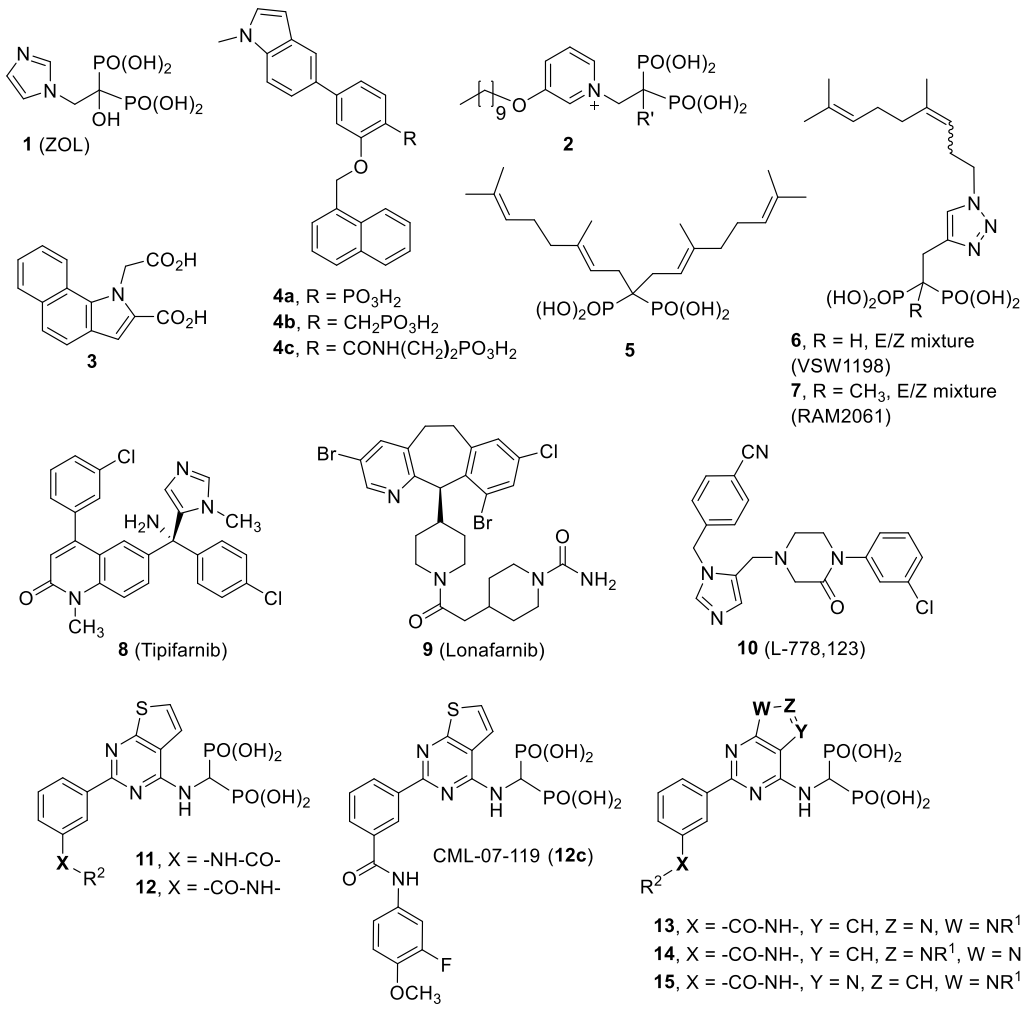

Figure 2. Examples of compounds that block protein prenylation in mammalian cells; bisphosphonate active site inhibitor of FPPS (**1**), dual active site FPPS/GGPPS inhibitor (**2**),[8b,c] allosteric inhibitors of FPPS (**3**, **4**),[21] active site inhibitors of GGPPS (**5**,[8a] **6**[8d] and **7**[8e] and **11**−**15**), inhibitors of FTase (**8**, **9**), and a dual inhibitor of FTase and GGTase I (**10**[13]).

farnesylation and/or geranylgeranylation may be a valuable mechanism for the treatment of pancreatic cancer.

In summary, numerous studies have shown that inhibition of post-translational prenylation of small GTPases can block the ability of these proteins to specifically associate with cellular membranes and act as molecular switches that regulate the proliferation of several cancers.[14,15] More specifically, accumulating evidence supports the hypothesis that direct intracellular inhibition of the human GGPPS may be a more viable mechanism for treating MM, PDAC, and potentially other types of cancers, as opposed to inhibition of the upstream enzymes HMG-CoA reductase, the human FPPS, or the farnesyl transferase enzyme FTase.[16] In our own studies, knockout of the *GGPSI* and *FDPS* genes (encoding hGGPPS and hFPPS, respectively) in MM (RPMI-8226) cells, using CRISPR/Cas9 (Figure S1) and genome-wide RNAi analysis by Penn's group,[17] provided strong evidence that hGGPPS activity is essential for tumor progression in various cancers. Furthermore, it was recently shown that GGPP is a pivotal metabolite for activating K-RAS/MEK/ERK signaling,[18] which are oncogenic drivers for various cancers, including MM, PDAC,[19,20] colorectal cancer (CRC),[18,20] and non-small-cell lung cancer (NSCLC).[20] In this report, we describe the synthesis and biological evaluation of novel hGGPPS inhibitors having pyrazolo[3,4-*d*]pyrimidinyl (**13**) and purinyl (**15**) scaffolds (Figure 2). Select examples of these chemotypes are presented, which were found to be equipotent (or slightly better) inhibitors of hGGPPS to our previously reported analogs **12**.[9b] For example, analogs **13** were found to block the proliferation of MM, PDAC, and CRC cells, without exhibiting significant toxicity to normal human bronchial epithelial (NHBE) cells and normal human fibroblast (IMR-90) cells at the highest concentration tested of 10 μM. Intracellular inhibition of Rap-1A geranylgeranylation and cell apoptosis were also observed with analogs in this series, such as inhibitor RB-07-16 (analog **13e**, Scheme 1), in MM, PDAC, and CRC cells. Consistent with our previous results,[9a] complete cell rescue was observed upon coincubation of the cells with this hGGPPS inhibitor and GGOH. Inhibitor RB-07-16 was used to demonstrate significant antimyeloma activity in vivo, without any overt signs of toxicity. This inhibitor was also tested in a xenograft mouse model of PDAC and primary mouse PDAC organoids, providing promising experimental data for the potential treatment of this high-mortality cancer with more optimized analogs of C6-substituted pyrazolo[3,4-*d*]-pyrimidine-based bisphosphonate (C6-PyraP-BP) hGGPPS inhibitors.

https://doi.org/10.1021/acs.jmedchem.3c01271
J. Med. Chem. 2023, 66, 15776−15800

Scheme 1. Synthesis of Pyrazolopyrimidine-Based Inhibitors 13 and 14[a]

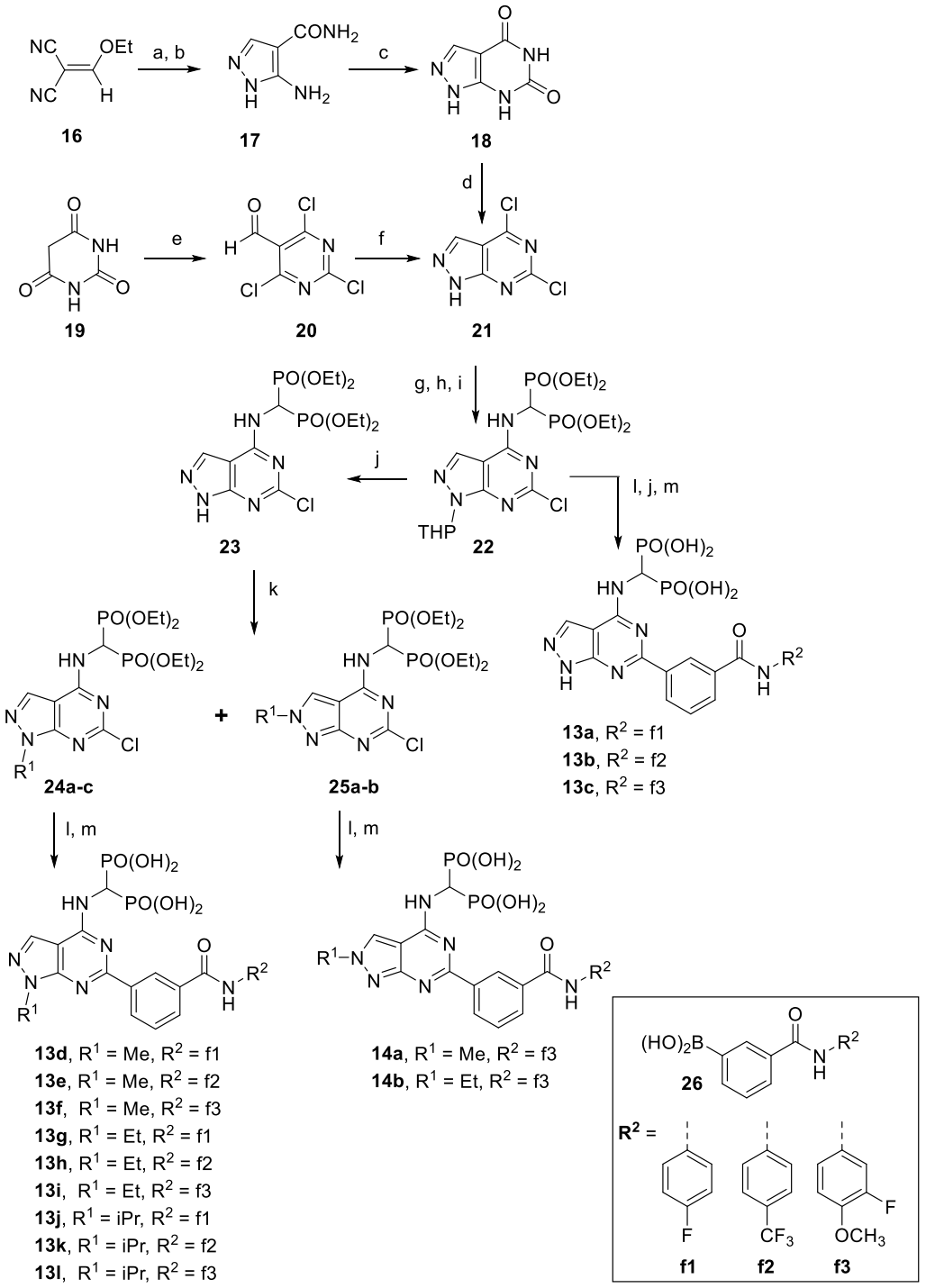

[a]Conditions: (a) $NH_2NH_2{\cdot}H_2O$, 100 °C, 62%; (b) (i) conc. H_2SO_4, rt, (ii) H_2O, 87%; (c) urea, 190 °C, 45%; (d) $POCl_3$, DBU, 105 °C, 32%; (e) $POCl_3$, DMF, 120 °C, 76%; (f) $NH_2NH_2{\cdot}H_2O$, Et_3N, MeOH, 0 °C, 54%; (g) *p*-TsOH, dihydropyran, DCM/THF (1:1), rt, 93%; (h) 28% aqueous NH_4OH, THF, rt, 91%; (i) $HPO(OEt)_2$, $HC(OEt)_3$, toluene, 130 °C, 50%; (j) 4 M HCl in dioxane, MeOH, 40 °C, 44−82%; (k) K_2CO_3, DMF, RI, rt, 62−68% yield for **24**, 16−25% for **25**; (l) **26**, $Pd(PPh_3)_4$, KF or 2 M K_2CO_3, dioxane or dioxane and MeOH, 80−90 °C, 28−76%; (m) (i) TMSI, DCM, 0 °C, (ii) MeOH, 29−93%.

2. CHEMISTRY

Synthesis of 6-Phenyl-1*H*-pyrazolo[3,4-*d*]pyrimidinyl Analogs 13, 6-Phenyl-2*H*-pyrazolo [3,4-*d*]pyrimidinyl Analogs 14 and 2-Phenyl-9*H*-purinyl Analogs 15. During our initial investigations into selective hGGPPS inhibitors, we reported the synthesis and biological evaluation of hGGPPS inhibitors **11** and **12** (Figure 2), having a 2-phenylthieno[2,3-*d*]pyrimidin-4-amine core structure.[9] Several other analogs with various scaffold modifications were also explored and found to inhibit the human GGPPS and block cancer cell proliferation.[22] We have been evaluating the overall biopharmaceutical properties of these compounds and comparing analogs with different core scaffolds in order to identify the most promising

https://doi.org/10.1021/acs.jmedchem.3c01271
J. Med. Chem. 2023, 66, 15776−15800

compounds that could be advanced to preclinical multidose toxicology studies in rat and dog and eventually to clinical development (more studies are ongoing).

The synthesis of hGGPPS inhibitors having a pyrazolo[3,4-*d*]pyrimidin-4-amine scaffold, with or without an N1-alkylation (**13**) or N2-alkylation (**14**), preferably with a small alkyl group, such as a methyl, ethyl, or isopropyl, was undertaken (Scheme 1). As an example, a subset of these analogs, having three of our previously described best R^2 side chains[9b] (e.g., R^2 = f1−f3; Scheme 1), is presented herein. The pyrazolopyrimidine scaffold has been explored in numerous medicinal chemistry projects, and consequently, various methodologies for its preparation have been reported. Initially, we investigated the preparation of these compounds via Knoevenagel/Gewald-type cyclization of 2-(ethoxymethylene)malononitrile (**16**) with hydrazine to give 5-amino-1*H*-pyrazole-4-carbonitrile, as previously reported (Scheme 1).[23] The nitrile substituent was converted to the amide (**17**) under acidic conditions before reacting intermediate **17** with urea to give the 1,7-dihydro-4*H*-pyrazolo[3,4-*d*]-pyrimidine-4,6(5*H*)-dione scaffold (**18**). However, the subsequent chlorination of the pyrimidinedione moiety,[24] in our hands, led to a low yield of the desired product **21** and formation of dimeric and trimeric side products.

As an alternative approach, we began with the synthesis of barbituric acid (**19**), obtained from diethylmalonate and urea (Scheme 1).[25] Chlorination and installation of the aldehyde were achieved using Vilsmeier−Haack conditions to give **20**, which upon treatment with hydrazine gave the key intermediate 4,6-dichloro-1*H*-pyrazolo[3,4-*d*]pyrimidine (**21**) in a good overall yield.[26] For a more modular approach (amenable to parallel library synthesis), we decided to first protect the N1 of the pyrazolopyrimidine with a tetrahydropyranyl (THP) group, following a previously reported protocol.[27] Subsequently, S_NAr displacement of the C-4 chloro with ammonia gave 6-chloro-1-(tetrahydro-2*H*-pyran-2-yl)-1*H*-pyrazolo[3,4-*d*]pyrimidin-4-amine, which upon treatment with diethyl phosphite and triethyl orthoformate gave compound **22**, as we previously reported.[9] Removal of the THP group under acidic conditions gave intermediate **23**, which was used as the precursor to the N1- and N2-alkylated intermediates **24a−c** and **25a,b**, respectively (Scheme 1). Interestingly, although pyridinium *p*-toluenesulfonate (PPTS) in EtOH[28] and TFA in DCM[29] have been previously reported for the removal of the THP group from a heterocyclic nitrogen, these reagents did not give satisfactory results in our hands, whereas 4 M HCl in dioxane gave the desired product in a good yield.[30]

Various conditions for alkylation at either the N1 or the N2 of the pyrazole moiety within the pyrazolopyrimidine scaffold, as well as other related heterocyclic compounds, have been reported. A systematic investigation of the reaction conditions that modulate site-selectivity was recently reported by Bookser and co-workers.[31] In this report, it was shown that the polarity of the solvent was the primary factor controlling the ratio of N1:N2 alkylation, with less polar solvents, such as dioxane and THF, favoring N2 alkylation (achieving ratios of N1:N2 alkylation ranging from 1:5 to 1:10), whereas polar solvents such as DMSO, DMF, and DMPU showed selectivity for N1 alkylation (unfortunately, with a regioselectivity ratio of a maximum of 5:1).[31] Surprisingly, under Mitsunobu-type conditions,[32] we observed preferential dialkylation of N1 and the exocyclic C-4 nitrogen with intermediate **23**, in almost equal amounts, and before the complete consumption of all the starting material. Alkylation with an alkyl iodide in DMF, using K_2CO_3 as the base, provided the highest yield of the desired N1-alkylated products **24**, with a ratio of **24**:**25** that varied from 2.5:1 to 4:1 (depending on the alkyl iodide used) and an overall yield of 84−87%.[33] The subsequent Pd-catalyzed Suzuki-type coupling of intermediates **24** and **25** with the boronic acids **26** using K_2CO_3 or KF as the base gave the tetraester precursors of inhibitors **13** and **14**. In the majority of literature reports, deprotection of the bisphosphonate tetraethyl esters is usually carried out using the classical McKenna reaction with TMSBr followed by MeOH.[34] However, for most compounds in series **11**−**12** and **13**−**14** (Figure 1), this reaction was extremely slow, often taking more than 5−7 days at 40 °C to achieve complete deprotection and requiring large excess of TMSBr (∼25 equiv). Consequently, we replaced TMSBr with TMSI, in a two-step reaction starting with the generation of TMSI, following a slightly modified protocol to that reported by Olah.[35] Deprotection of the bisphosphonate tetraethyl esters using freshly prepared TMSI led to a dramatic improvement in the reaction rates (from 5 to 7 days at 40 °C to an average of 2−4 h at 0 °C) with as little as 6 equiv of TMSI. After transesterification of the tetraethyl bisphosphonate to the silyl esters, methanolysis of the silyl esters resulted in the isolation of the desired bisphosphonic acid inhibitors **13d−l** and **14a,b** in a good overall yield and high purity.

Finally, preparation of analogs **13a−c** required a slight modification to the above synthetic route. The Suzuki coupling reaction of the biaryl side chain **26** with intermediate **23** (having the free amine in the pyrazolopyrimidine scaffold) led to low yields, and consequently, the THP-protected intermediate **22** was used to obtain analogs **13a−c**, with otherwise the same overall reaction protocols (Scheme 1).

Synthesis of purine-based derivatives **15** was initiated with the alkylation of commercially available 2,6-dichloropurine (**27**) at either the N9 or N7 nitrogen, leading to intermediates **28** and **29**, respectively (Scheme 2). As previously reported,[31] solvent effects played a significant role in controlling regioselectivity, with DMF leading to the best yield and a 2:1 ratio of **28**:**29**. Based on previous SAR studies, we presumed that inhibitors derived from intermediate **29** would be less active and decided to proceed with only analogs with core structure **28**. Solvent selection also played a critical role in the subsequent S_NAr amination reaction to give intermediate **30**. Several polar solvents were explored, and dioxane was found to give the highest yield (90%). Installation of the bisphosphonate moiety on intermediate **30**, using the same reaction conditions as we previously reported for the thienopyrimidine-based intermediates[9] and pyrazolopyrimidine-based intermediates in this study (e.g., Scheme 1, compound **22**), proved to be inefficient. After screening several reaction conditions, intermediate **31** was obtained in only 13% yield. However, despite this disappointingly low yield, for the purpose of this initial screening study, we continued with the Suzuki coupling reaction, followed by deprotection of the phosphonate tetraesters to obtain inhibitors **15a−c** in sufficient amounts for biological testing (Scheme 2).

3. POTENCY OF THE C6-PYRAP-BPS AND C2-PUR-BPS IN INHIBITING THE HUMAN GGPPS AND BLOCKING CANCER CELL PROLIFERATION

Scaffold hopping is a well-established strategy in medicinal chemistry for the discovery of multiple, structurally diverse analogs inhibiting the same biological target with equivalent or better biopharmaceutical profiles than the initial lead compound. Given the statistically very high attrition rate of exploratory compounds at the preclinical and clinical develop-

https://doi.org/10.1021/acs.jmedchem.3c01271
J. Med. Chem. 2023, 66, 15776−15800

Scheme 2. Synthesis of Purine-Based Inhibitors 15a−c[a]

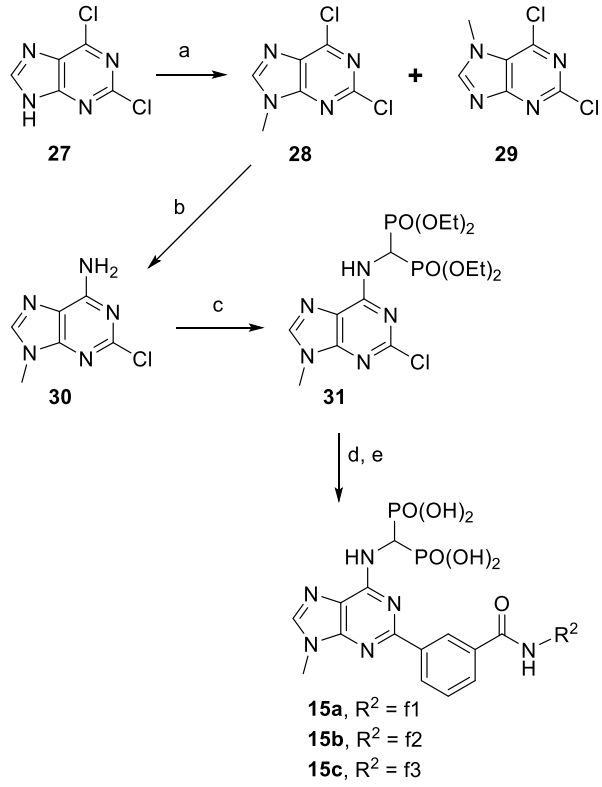

[a]Conditions: (a) K_2CO_3, MeI, DMF, rt, 60% yield of **28** and 29% of **29**; (b) 28% aqueous NH_4OH, dioxane, 95 °C, 90%; (c) $HPO(OEt)_2$, $HC(OEt)_3$, 130 °C, 13%; (d) (i) **26**, $Pd(PPh_3)_4$, 2 M K_2CO_3, dioxane, 80 °C, 38−77%; (e) (i) TMSI, DCM, 0 °C, (ii) MeOH, 51−80%.

ment stages,[36] it is highly desirable to advance several compounds in parallel in a drug discovery project. Herein, we designed a small library of representative compounds aiming to explore replacements of the thienopyrimidine scaffold of hGGPPS inhibitors (i.e., analogs **11** and **12**) with nitrogen-containing heterocycles, such as analogs **13** and **15** (Figure 2). These analogs were evaluated in our hGGPPS inhibition assay, as previously described,[9a] and their IC_{50} values are given in Table 1. The IC_{50} values reported herein represent an average of at least two independent determinations, each tested in triplicate with a standard deviation of less than 10%. In the absence of a clinically validated hGGPPS inhibitor, the best inhibitor we reported in our previous studies, CML-07-119 (Figure 1; **12c**),[9] was used as the reference control.

We previously observed very similar IC_{50} values between analogs having an amide linker (Figure 2; **11**, **X** = −NHCO−) and those having the reversed amide linker (**12**, **X** = −CONH−) connecting the C-2 phenyl thienopyrimidine core to the R^2 side chain. However, analogs **12** were consistently three- to fourfold more potent in cell-based antiproliferation assays using MM cell lines, such as RPMI-8226 (e.g., Table 1; analogs **11a−c** vs analogs **12a−c**). Based on this observation, we designed our new compounds **13−15** to have the reversed amide linker (**X** = −CONH−), with some of our previously identified best side chains as the R^2 substituent, such as fragments f1, f2, and f3 (Table 1). Dose-dependent inhibition of cell viability (EC_{50} values) was determined using standard MTS assays, and EC_{50} values reported in Table 1 represent an average of at least two independent determinations, each run in sextuplicate. It should be noted that cell viability and proliferation were typically evaluated at inhibitor concentrations ranging from 0.1 nM to 10 μM, unless otherwise indicated.

Previously, analogs containing the *m*-fluoro-*p*-methoxy side chain (i.e., R^2 = f3) were the most potent in blocking the proliferation of MM cells (RPMI-8226), and analog CML-07-119 (**12c**) was previously identified as one of our best compounds (Table 1).[9b] Interestingly, when the pyrazolopyrimidine-based inhibitor **13f** was tested in parallel with the corresponding thienopyrimidine-based analog **12c**, it was found to exhibit a slightly lower intrinsic potency (IC_{50}) and antimyeloma activity (EC_{50}) but higher selectivity in inhibiting hGGPPS vs hFPPS (Table 1). Consistent with the IC_{50} values of previous inhibitors (**11**, **12**), those containing the *p*-trifluoromethylphenyl substituent (f2) at the R^2 moiety of the side chain were often the most potent in inhibiting hGGPPS in vitro (IC_{50}). However, in contrast to previous observations,[9b] the N1-methyl analog **13e** was also the most effective compound in blocking the proliferation of RPMI-8226 cells (e.g., Table 1). Furthermore, inhibitor **13e** did not inhibit hFPPS at the highest concentration tested of 1 μM. Although the free NH analogs **13a−c** exhibited equivalent intrinsic potency (IC_{50}) to their corresponding N1 methyl derivatives (i.e., **13d−f**), these inhibitors were substantially less potent in blocking the cell proliferation of RPMI-8226 cells. This observation is not unexpected, since reduced cell membrane permeability is common for analogs with a higher number of hydrogen bond donors. Finally, we probed the effects of larger alkyl substituents at N1, and although the IC_{50} values of the ethyl (**13g−i**) and isopropyl (**13j−l**) analogs were comparable to those of most other analogs in this series, these compounds were essentially inactive in the cell-based antiproliferation assays using RPMI-8226 cells. Compounds with alkylation at N2 (e.g., **14a** and **14b**) were not intentionally synthesized (expected to be less stable); nonetheless, they were tested in our biological assays in order to probe the available space within the binding pocket and found to provide no advantages. Finally, the replacement of the core scaffold with a purine (analogs **15a−c**) also did not provide any significant advantages in intrinsic or cell-based potency. It is always possible that in a very large permutation library, where both the core scaffold and the side chains are varied simultaneously, an unexpectedly potent compound could potentially be identified. However, within the limits of the current study, the pyrazolopyrimidine-based analogs **13** appear to be the most promising new class of hGGPPS inhibitors that are worthy of further investigation. For example, analog RB-07-16 (**13e**) exhibits equivalent or slightly better potency in blocking the proliferation of several MM cell lines (e.g., JJN3, KMS12PE, KMS28PE, and RPMI-8226 cells; Figure 8) as compared to the thienopyrimidine analog CML-07-119 (**12c**), with higher selectivity in inhibiting hGGPPS vs hFPPS; whether this selectivity is an overall beneficial property remains to be determined.

We also investigated the ability of our pyrazolopyrimidine-based inhibitors (**13**) to block cell proliferation in both PDAC (MIA PaCa-2; Figure 3b) and CRC (HCT 116; Figure 3c) cells and compared to select inhibitors from series **12** and **15** (Figure 3a). Several analogs were initially prescreened at a single concentration of 1 μM using gemcitabine as a reference control. Gemcitabine, used here as a comparator control, is a key drug in the treatment of pancreatic cancer and has also been under

https://doi.org/10.1021/acs.jmedchem.3c01271
J. Med. Chem. 2023, 66, 15776−15800

Table 1. Enzyme Inhibition (IC_{50}) of the Human FPPS and GGPPS and Antiproliferation (EC_{50}) Data in MM (RPMI-8226) Cells of Analogs 11−15

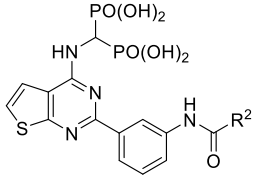

11a, R^2 = f1
11b, R^2 = f2
11c, R^2 = f3

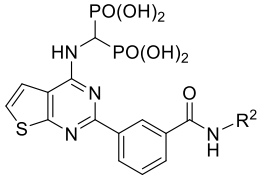

12a, R^2 = f1
12b, R^2 = f2
12c, R^2 = f3

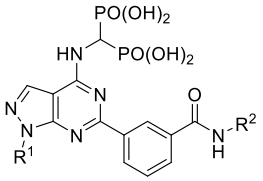

13a, R^1 = H, R^2 = f1
13b, R^1 = H, R^2 = f2
13c, R^1 = H, R^2 = f3
13d, R^1 = Me, R^2 = f1
13e, R^1 = Me, R^2 = f2
13f, R^1 = Me, R^2 = f3
13g, R^1 = Et, R^2 = f1
13h, R^1 = Et, R^2 = f2
13i, R^1 = Et, R^2 = f3
13j, R^1 = iPr, R^2 = f1
13k, R^1 = iPr, R^2 = f2
13l, R^1 = iPr, R^2 = f3

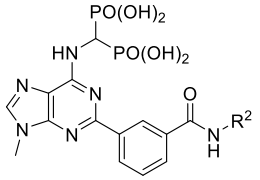

15a, R^2 = f1
15b, R^2 = f2
15c, R^2 = f3

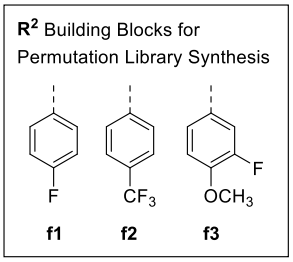

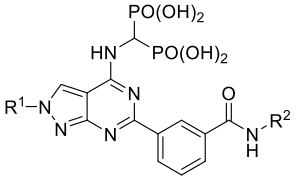

14a, R^1 = Me, R^2 = f3
14b, R^1 = Et, R^2 = f3

compound (R^2)	FPPS[a] IC_{50} (μM)	GGPPS-M4[b] IC_{50} (nM)	RPMI-8226[c] EC_{50} (nM)
11a (f1)		25	700
11b (f2)		18	710
11c (f3)		29	460
12a (f1)		18	120
12b (f2)		12	160
12c (**f3**)	**1.4**	**27**	**90**
13a (f1)		39	>1000
13b (f2)		8	>1000
13c (f3)	(10%)	25	640
13d (f1)		31	440
13e (**f2**)	(**<10%**)[d]	**12**	**70**
13f (f3)	(<10%)	48	150
13g (f1)		29	>1000
13h (f2)		30	>1000
13i (f3)	(<10%)	40	>1000
13j (f1)		30	>1000
13k (f2)		20	>1000
13l (f3)	(<10%)	41	>1000
14a (f3)	(15%)	56	520
14b (f3)		67	552
15a (f1)		41	670
15b (f2)		13	510
15c (f3)	(<10%)	58	170

[a]Some key compounds were screened at a single concentration of 1 μM ($n \geq 3$), and the % inhibition observed at 1 μM is indicated in brackets. Only CML-07-119 was tested in a full dose−response assay to determine its IC_{50} value indicated (an average of two independent assays with n = 3 determinations in each assay and a standard deviation of ±5 to 10%). All assays were run with 10 min preincubation of the enzyme with the inhibitor using zoledronic acid as the positive control (with IC_{50} of 3−5 nM). [b]The values shown are the average of ≥2 independent assays, each one run in triplicate with a standard deviation of ±5 to 10%, using CML-07-119 as the positive control. [c]EC_{50} values were determined using an MTS assay, after 72 h of incubation of the cells with or without an inhibitor; the values shown are average of $n \geq 2$ determinations, each assay run in n = 6 replicates, with a standard deviation of ≤10%, using doxorubicin as the reference control. [d]Even when this compound was tested at 10 μM, the inhibition observed was <10%.

investigation as an alternative agent in the treatment of oxaliplatin-resistant CRC.[37]

When inhibitor **12c** was compared to analogs **13c**, **13f**, **13i**, **13l**, and **15c** [all of these analogs having the same *m*-fluoro-*p*-methoxyphenyl fragment (f3) at the R^2 side chain], there was no advantage observed with any of these new compounds in their ability to block the proliferation of either the MIA PaCa-2 or the HCT 116 cells (Figure 3b,c, respectively). It should be noted that analogs **13i** and **13l** were tested to confirm that any cell-based potency observed was not simply lipophilicity-driven. As observed with the MM cell lines, inhibitor **13e** (RB-07-16) exhibited only slightly better potency than **12c** (CML-07-119) in decreasing the viability of MIA PaCa-2 cells (EC_{50} values of 790 and 1300 nM, respectively; Figure 3d). The EC_{50} values of these inhibitors (**12c** and **13e**) were identical in HCT 116 cells (EC_{50} = 580 nM; Figure 3e). Doxorubicin (Dox) and gemcitabine (Gem) were tested in parallel as reference controls and were found to exhibit EC_{50} values of 130 and 2.1 nM, respectively (Figure 3d) in MIA PaCa-2 cells, whereas the EC_{50} values in HCT 116 cells were 40 and 4.1 nM, respectively (Figure 3e). However, both of these drugs are known to exhibit significant nonselective toxicity. As an example, the toxicity of inhibitors CML-07-119 (**12c**) and RB-07-16 (**13e**) to healthy cells was evaluated in a parallel assay with doxorubicin. Dose-dependent determination of cell viability using NHBE cells revealed significant toxicity induced by doxorubicin (EC_{50} = 450 nM), whereas inhibitors CML-07-119 and RB-07-16 induced ∼30 and 0% inhibition, respectively, at the highest concentration tested of 10 μM (Figure 4a). In normal human fibroblast (IMR-90) cells, doxorubicin exhibited an EC_{50} of 360 nM, whereas GGPPS inhibitor RB-07-16 exhibited 0% inhibition at the same concentration and only ∼20% inhibition at the highest concentration tested of 10 μM (Figure 4b).

To further compare the ability of inhibitors CML-07-119 (**12c**) and RB-07-16 (**13e**) to block the proliferation of pancreatic cancer, the response of murine normal ductal

https://doi.org/10.1021/acs.jmedchem.3c01271
J. Med. Chem. 2023, 66, 15776−15800

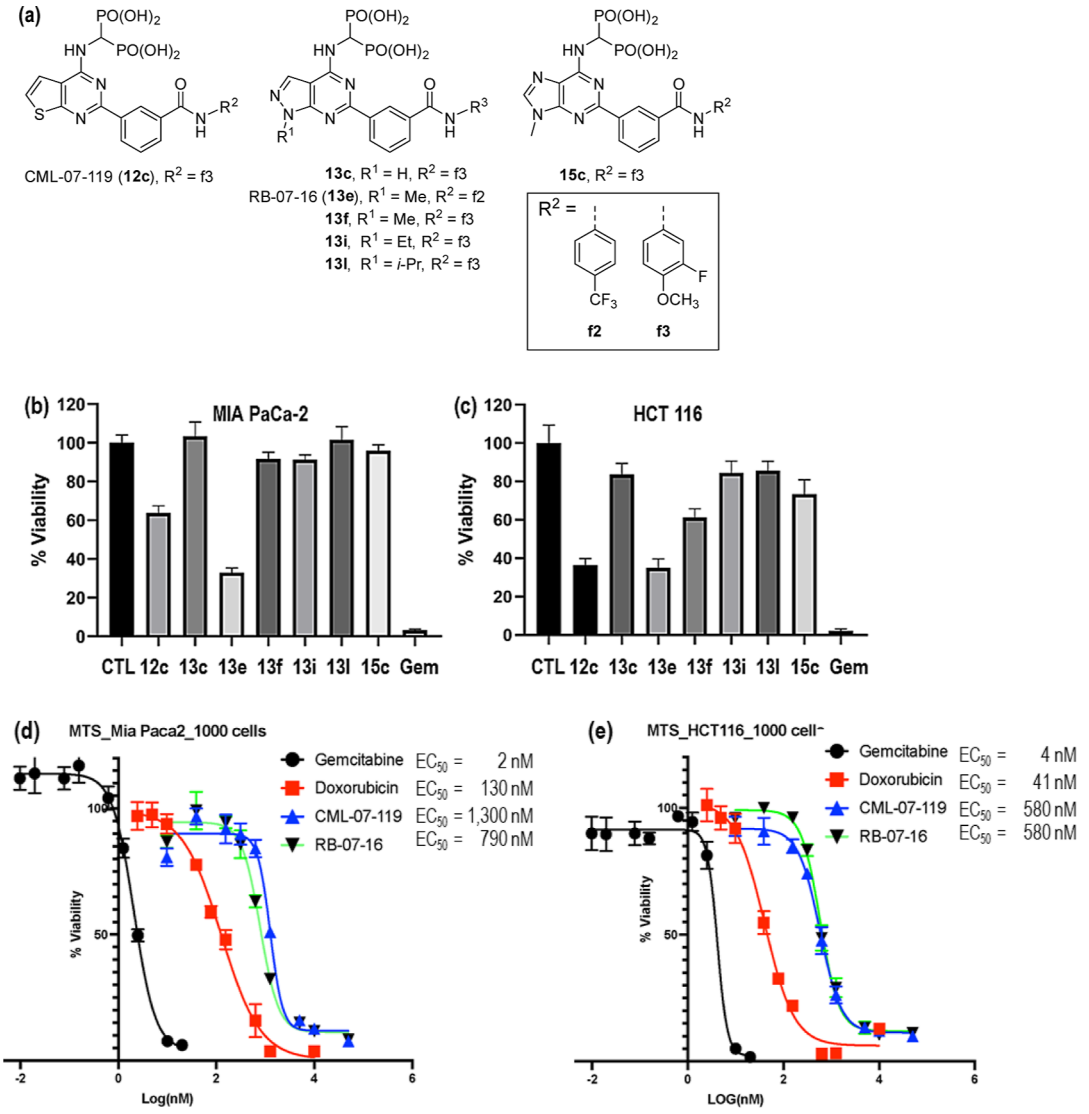

Figure 3. Preliminary evaluation of core scaffold impact in blocking the proliferation of PDAC (MIA PaCa-2) and CRC (HCT 116) cells. (a) Chemical structures of the select inhibitors tested. (b) Decrease in the viability (%) of MIA PaCa-2 cells treated at 1 μM concentration of select inhibitors. (c) Decrease in the viability (%) of HCT 116 cells treated at 1 μM concentration of select inhibitors. Dose−response inhibition curves of inhibitors CML-07-119 (**12c**), RB-07-16 (**13e**), doxorubicin, and gemcitabine for the determination of EC_{50} values in MIA PaCa-2 cells (d) and HCT 116 cells (e); data plotted in EC_{50} curves (d−e) are from quadruplicate determinations and run in parallel.

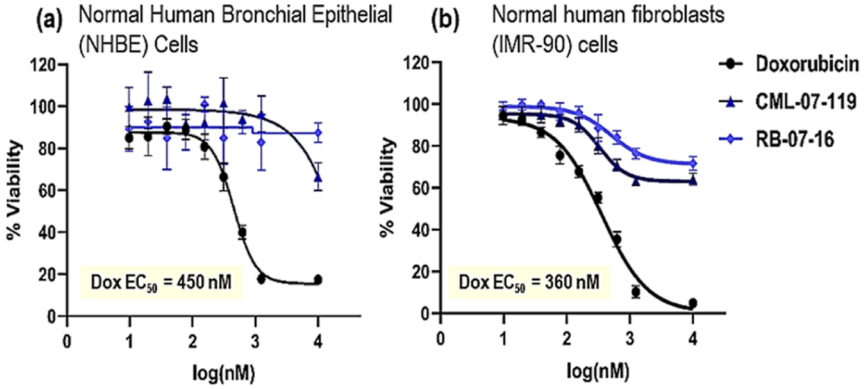

Figure 4. Evaluation of the toxicity of GGPPS inhibitors vs doxorubicin in healthy cells: (a) normal human bronchial epithelial (NHBE) cells and (b) normal human fibroblast (IMR-90) cells.

organoids [N(10128)] from wild-type mice and pancreatic tumor organoids (ccmT4) from KPC mice (KrasG12D; p53R172H; PdxCre) to these compounds was also examined.[38] Organoids are engineered to recapitulate many aspects of the

https://doi.org/10.1021/acs.jmedchem.3c01271
J. Med. Chem. 2023, 66, 15776−15800

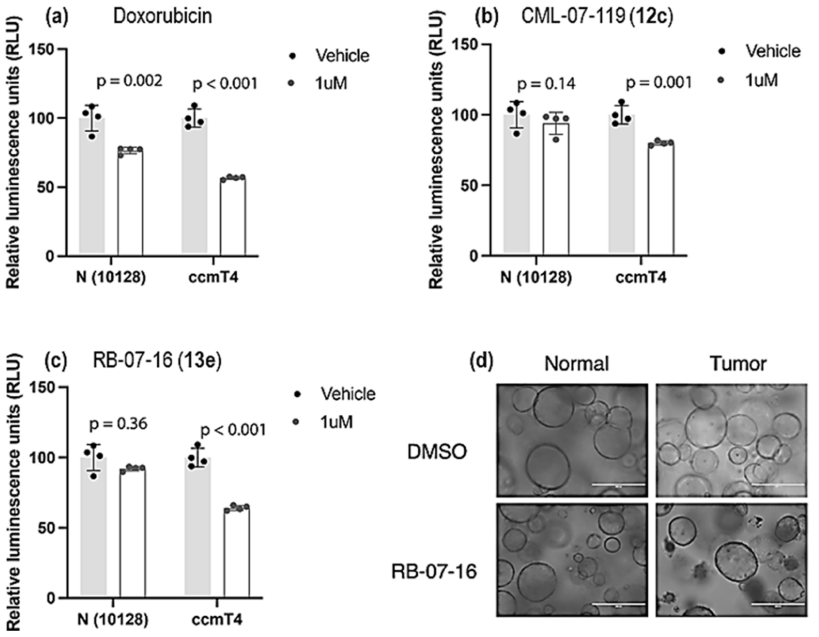

Figure 5. Inhibition of murine normal [N(10128)] and PDAC tumor (ccmT4) organoids treated with doxorubicin (a) or the GGPPS inhibitor CML-07-119 (b) or RB-07-16 (c) and images of control normal and tumor organoids treated with only media and DMSO (1:1000 dilution) or RB-07-16 dissolved in the same media mixture (d).

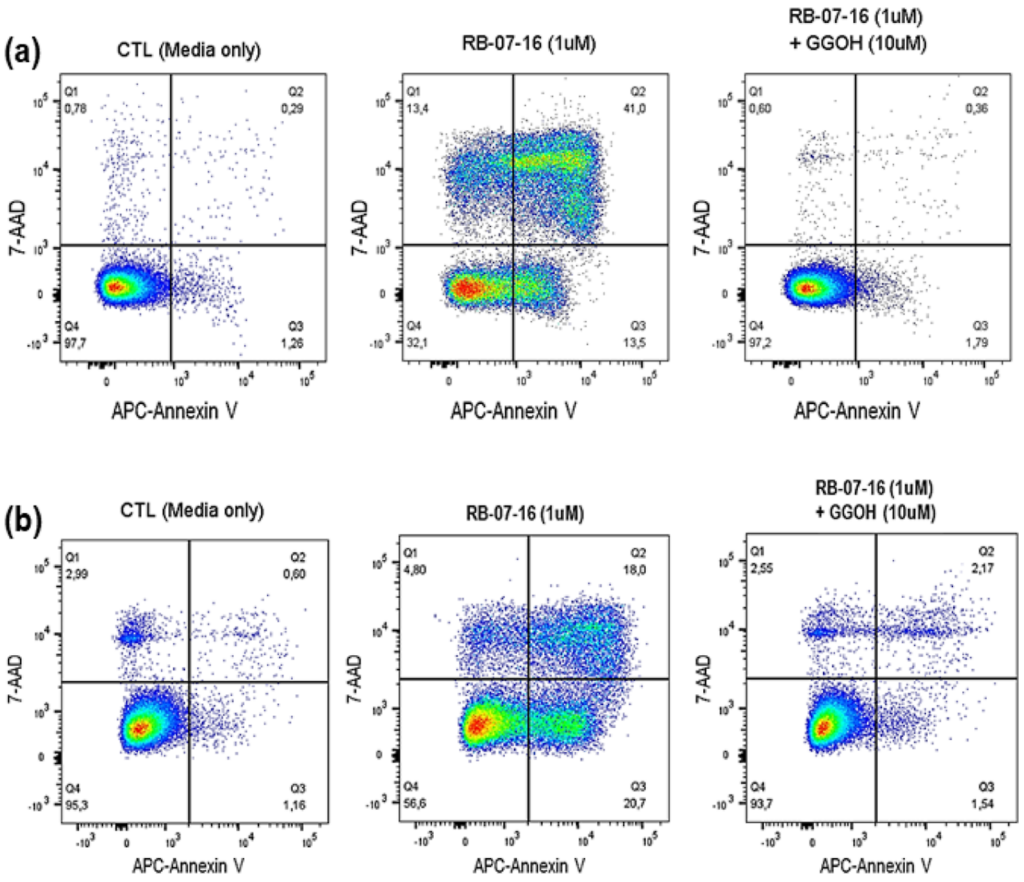

Figure 6. Confirmation of apoptosis and selective intracellular target engagement in (a) MIA PaCa-2 and (b) HCT 116 cells treated with RB-07-16 (**13e**) by flow cytometry.

complex tissue structure and function of the pancreatic tumors derived from in vivo tissues.[39] After a 72 h incubation period of the organoids with the hGGPPS inhibitors or doxorubicin, the cell viability was measured using a luminescence ATP-based assay (CellTiter-Glo, Promega) using a plate reader, and the statistical significance was calculated using Student's *t*-test (Figure 5). We also performed a sequence alignment of the murine (UniProt ID: Q9WTN0) vs the human (UniProt ID:

https://doi.org/10.1021/acs.jmedchem.3c01271
J. Med. Chem. 2023, 66, 15776−15800

O95749) GGPPS orthologue (using the cluster alignment tool[40]) and found that they share almost 94% amino acid sequence identity. This high degree of conservation suggests that inhibition of GGPPS activity in murine organoids should provide a reliable estimate of the expected effects in human PDAC organoids. Our initial data suggest that primary tumor organoids (ccmT4) are sensitive to inhibitors RB-07-16 (**13e**) and CML-07-119 (**12c**), and both compounds are relatively nontoxic to normal organoids [N(10128)] at a 1 μM concentration (Figure 5b,c). These results are consistent with the relative potency observed in the viability assay of MIA PaCa-2 cells (albeit with relatively modest activity) when treated with these inhibitors (Figure 3b,d) and suggest selective toxicity to pancreatic cancer. In contrast, doxorubicin exhibits toxicity to both normal and tumor organoids (Figure 5a); gemcitabine could not be used as a reference due to its high toxicity to normal organoids, even at low nM concentrations.

Further evaluation of inhibitor RB-07-16 (**13e**) by flow cytometry confirmed that it induces apoptosis to approximately 50% of the treated cells in both MIA PaCa-2 and HCT 116 cells at 1 μM concentration (i.e., at a concentration close to its EC_{50} values in both cell lines; Figure 6a,b, respectively). Consistent with our previous observation in MM cells treated with CML-07-119 (**12c**),[9a] complete rescue from apoptosis was observed when the MIA PaCa-2 and HCT 116 cells were simultaneously cotreated with inhibitor RB-07-16 and a nontoxic dose of GGOH(Figure 6a,b, respectively). These results strongly support a selective intracellular target engagement of GGPPS by inhibitor RB-07-16 and confirm the expected mechanism-based toxicity in both PDAC (MIA PaCa-2) and CRC (HCT 116) cells. It is noteworthy that since bisphosphonates act as bioisosteres of isoprenoid metabolites, it is conceivable that in addition to inhibiting hGGPPS, our compounds could also be inhibiting a prenyl transferase enzyme (e.g., GGTase I, II, or III), an effect that may be possible to overcome by high concentrations of GGOH. More in-depth studies are required to completely rule out any additional off-target effects.

The ability of several of our hGGPPS inhibitors, including RB-07-16 (**13e**), to disrupt the intracellular geranylgeranylation of the relevant GTPases was confirmed in both PDAC and CRC cells. For example, incubation of MIA PaCa-2 and HCT 116 cells with inhibitors CML-07-119 (**12c**) and RB-07-16 (**13e**) followed by analysis of their cell lysates by western blotting, using a Rap-1A antibody, which specifically binds to the unprenylated form of this protein, revealed a dose-dependent inhibition of Rap-1A prenylation at concentrations as low as 100 nM (Figure 7).

We also began to investigate the relationship between the downregulation of intracellular levels of GGPP and oncogenesis in cancers with different genetic drivers, particularly those that are K-RAS-dependent.[41] K-RAS mutations are dominant in approximately 85% of RAS-driven cancers and modulate tumor survival and proliferation in PDAC, CRC, and NSCLC. PDAC and CRC in particular are characterized by high mortality rates and exhibit a high rate of proliferation and metastasis. Common mutations in codons 12, 13, and 61 of K-RAS disrupt the ability of K-RAS to mediate GTP hydrolysis, locking the mutants in the signaling-activated GTP-bound state and leading to the activation of downstream pathways (primarily MAPK and PI3K) that promote cell proliferation.[42] Over the last 30 years, significant progress has been made in directly targeting K-RAS,[43] leading to the recent landmark FDA approval of sotorasib for the treatment of adults with advanced NSCLC

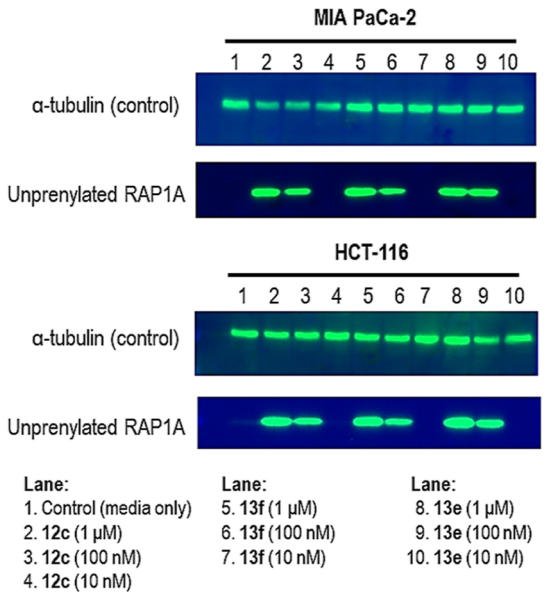

Figure 7. Western blot analyses of representative PDAC and CRC cell lines (MIA PaCa-2 and HCT 116, respectively) exposed to varying concentrations of GGPPS inhibitors.

having *K-RAS*^{G12C} mutations, who have received at least one prior systemic therapy.[44]

In search of specific biomarkers that could suggest an effective treatment for MM, PDAC, and CRC through the inhibition of hGGPPS, we investigated the potency of representative inhibitors from our structurally diverse library of compounds,[22] including CML-07-119 (**12c**) and RB-07-16 (**13e**), in a small panel of cell lines expressing wild-type or various K-RAS mutations (Figure 8). This preliminary assessment suggested that MM cell lines may be more vulnerable to hGGPPS inhibition than PDAC and CRC cells (Figure 8). There are numerous variables that can contribute to these observations, including differences in cell membrane permeability, expression of efflux pumps, and rates of metabolic breakdown of the compounds in different cell lines. Beyond activating K-RAS mutations, another key vulnerability in MM cells that may be significantly modifying their sensitivity to hGGPPS inhibitors is the added influence of constitutive ER stress that MM cells experience due to the secretory burden of immunoglobulin (M-protein) production.[45] As we have shown, analogs CML-07-119[9a] and RB-07-16 also upregulate ER stress in MM RPMI-8226 cells (Figure 9). Interestingly, a recent study reported that adenomatous polyposis coli (APC) and K-RAS double mutant CRC lead to increased biosynthesis of the GGPP metabolite, which in this context was essential for K-RAS/MEK/ERK activation,[18] suggesting that hGGPPS inhibitors could also provide clinical benefit in the context of APC/K-RAS mutant CRC tumors.[18] The preliminary results shown in Figure 8 will be followed up with investigations in a much larger panel of cell lines carrying various RAS mutations in order to more thoroughly understand the impact of hGGPPS inhibition as a potential therapeutic mechanism for cancers with different genetic drivers.

4. METABOLIC STABILITY OF RB-07-16 AND ABILITY TO INHIBIT CYP 450 ENZYMES

The metabolic stability of inhibitor RB-07-16 (**13e**) in male CD-1 mouse (MLM), Sprague−Dawley rat (RLM), beagle dog

https://doi.org/10.1021/acs.jmedchem.3c01271
J. Med. Chem. 2023, 66, 15776−15800

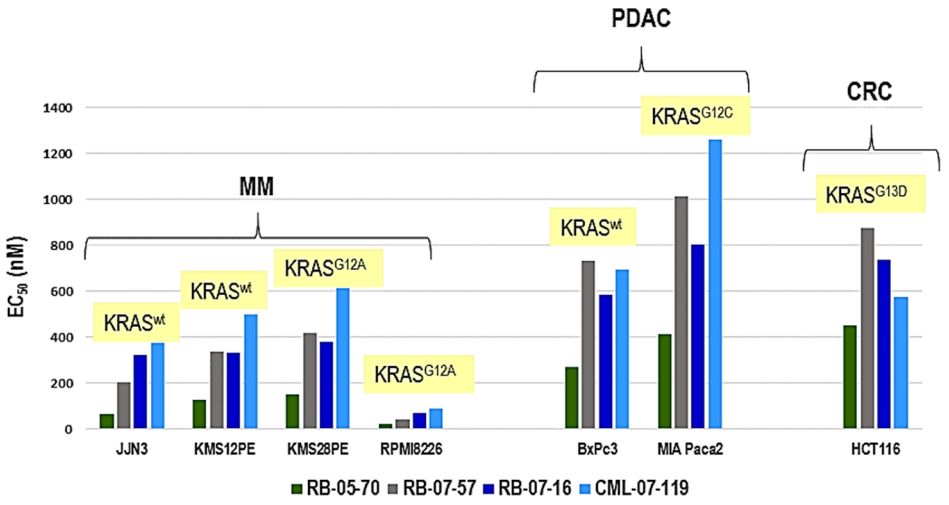

Figure 8. Examples of hGGPPS inhibitors blocking the proliferation of cancer cells from different tissue origins and bearing various K-RAS mutations.

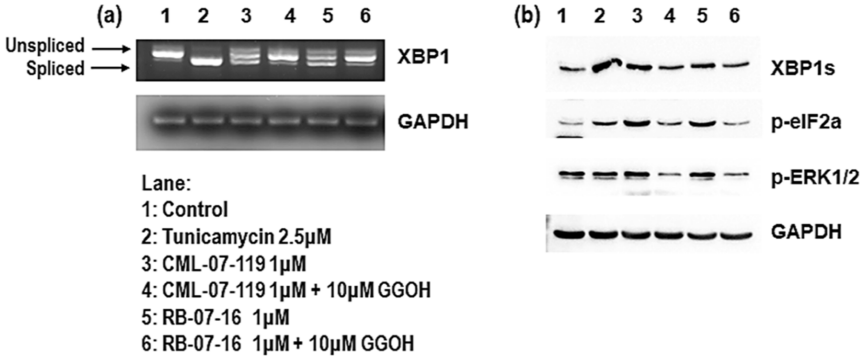

Figure 9. Induction of ER stress and modulation of ERK and AKT signaling by hGGPPS inhibitor treatment. (a) RT-PCR demonstrating specific (GGOH rescuable) induction of XBP1 mRNA splicing by inhibitors CML-07-119 (**12c**) and RB-07-16 (**13e**). (b) Western blotting results of RPMI-8226 lysates after 48 h of treatment with the indicated concentration of hGGPPS inhibitors in the presence and absence of GGOH rescue for specificity assessment.

(DLM), and human (HLM) liver microsomes was evaluated in the presence of NADPH (i.e., for primarily CYP 450-dependent metabolism) and the absence of NADPH (for non-CYP 450-dependent metabolism) using verapamil as the positive control. After a typical 45 min incubation, there was negligible metabolic degradation of this compound across all species (Table 2). Additionally, RB-07-16 did not inhibit the three most relevant isoforms of CYP 450 enzymes, 3A4, 2C9, and 2D6, which are known to be responsible for the biotransformation of most xenobiotics, including 70−80% of all clinically approved human therapeutics. Concentration-dependent inhibition assays were run in parallel with a relevant positive control for each enzyme to allow the determination of IC_{50} values shown in Table 3. The IC_{50} of GGPPS inhibitor RB-07-16 (**13e**) was determined to be greater than 40 μM for all three enzymes.

Table 2. Metabolic Stability of Inhibitor RB-07-16 (13e) in Liver Microsomes

	average % remaining with NADPH (STDEV)	average % remaining without NADPH (STDEV)
	MLM	
RB-07-16	103 (8.70)	121 (22.3)
verapamil	3.27 (0.22)	92.4 (10.9)
	RLM	
RB-07-16	89.7 (7.68)	99.3 (1.74)
verapamil	30.3 (3.03)	75.1 (8.30)
	DLM	
RB-07-16	87.7 (11.4)	81.7 (8.31)
verapamil	13.7 (0.33)	97.1 (7.48)
	HLM	
RB-07-16	107 (24.3)	100 (3.29)
verapamil	34.7 (0.61)	67.8 (5.92)

Table 3. IC_{50} Values of RB-07-16 (13e) and Relevant Controls for CYP 450 Enzymes[a]

	IC_{50} (nM) RB-07-16	IC_{50} (nM) positive control
CYP 3A4	>40,000	41.5[b]
CYP 2C9	>40,000	258[c]
CYP 2D6	>40,000	107[d]

[a]In parallel assays, the following compounds were used as the positive controls. [b]Ketoconazole. [c]Sulfaphenazole. [d]Quinidine.

5. PHARMACOKINETIC PARAMETERS OF RB-07-16 IN RAT

Pharmacokinetic (PK) parameters obtained from Sprague−Dawley (SD) rat PK (I.V. dosing at 3 mg/kg) of inhibitor RB-07-16 revealed relatively low plasma clearance, an average mean residence time (MRT) of approximately 4.7 h, and a half-life ($T_{1/2}$) of 3.8 h (Figure 10). This favorable PK profile is in sharp

https://doi.org/10.1021/acs.jmedchem.3c01271
J. Med. Chem. 2023, 66, 15776−15800

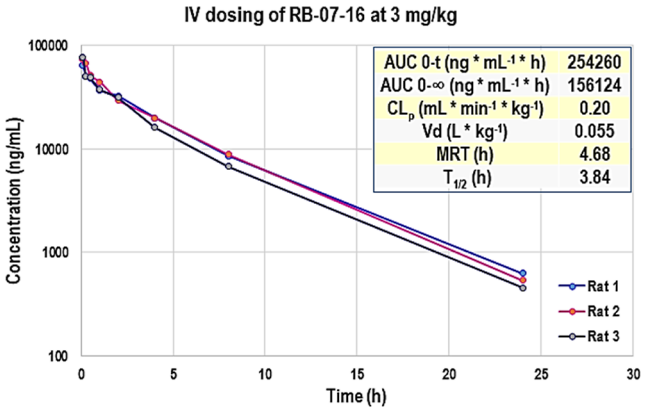

Figure 10. Pharmacokinetic measurements of RB-07-16 in rat plasma after IV injection of 3 mg/kg, as determined by LC−MS/MS at a limit of quantitation (LOQ) of 29 ng/mL; the average values (n = 3) of key pharmacokinetic parameters are indicated.

contrast to that for clinically approved bisphosphonates, such as the FPPS inhibitor zoledronic acid (**1**), which exhibits negligible systemic circulation in rats and dogs[46] as well as in humans.[47]

6. ASSESSMENT OF IN VIVO ANTITUMOR EFFICACY OF RB-07-16 IN XENOGRAFT MM AND PDAC MOUSE MODELS

The in vivo antimyeloma efficacy of inhibitor RB-07-16 (**13e**) was subsequently investigated in xenograft MM and PDAC mouse models. In the MM model, the tumor size (Figure 11)

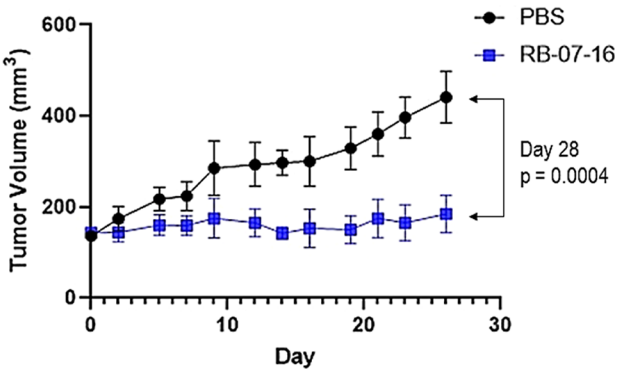

Figure 11. In vivo antimyeloma efficacy of GGPPS inhibitor RB-07-16 (**13e**) vs PBS (vehicle control) in a xenograft MM mouse model using NSG mice injected with RPMI-8226 cells. The p-value was determined with Welch's t-test correction 48 h after the last dose.

and the weight of all animals (Figure S2) were recorded before each dosing and at the end of the study. The increase in tumor volume was almost negligible in all animals (n = 9, 3 male and 6 female) treated with inhibitor RB-07-16 (**13e**), whereas in the animals given PBS vehicle control (n = 8, 2 male and 6 female), the tumor size increased significantly over the 26 day treatment period (start of dosing on day 0; Figure 11). Neither group of animals (control and compound treated) lost any weight (Figure S2). All mice from this study were euthanized 48 h after receiving the last dose, and their blood and livers were collected for further evaluation of any possible compound-induced hepatotoxicity (refer to Section 7 below).

In view of the relatively modest potency of inhibitor RB-07-16 (**13e**) in MIA PaCa-2 cells (EC_{50} = 790 nM), to evaluate the dynamic range of antitumor efficacy induced by this inhibitor, we also administered analog RB-07-16 to a xenograft PDAC mouse model. All animals, in both the vehicle control (n = 13, 6 male and 7 female) and the inhibitor-treated group (n = 14, 6 male and 8 female), continued to gain weight (Figure 12d,e) and did not exhibit any signs of distress or overt toxicity during the 26 day dosing period. Observation of these mice was continued during the postdosing period for up to 60 days, and the mice were euthanized only when their tumors became larger than 2000 mm^3, in accordance with our animal care ethics protocol. A statistically significant difference in tumor growth (Figure 12a,c) and survival rate (Figure 12b) was observed between the animals treated with RB-07-16 and those in the control group. For example, by day 58, all animals in the PBS control had been euthanized, whereas 6/14 animals in the RB-07-16 inhibitor-treated group were still alive with tumors smaller than 2000 mm^3. As expected, the antitumor efficacy of RB-07-16 in the xenograft PDAC (MIA PaCa-2) mouse model was much more modest than in the xenograft MM (RPMI-8226) mouse model (Figure 11), consistent with the nearly 10-fold difference in potency observed in RPMI-8226 cells vs the MIA PaCa-2 cells (EC_{50} values of 70 and 790 nM, respectively). These results are very encouraging and suggest that more potent and selective hGGPPS inhibitors may provide antitumor agents that could be clinically useful across a broad spectrum of tumor types.

7. EVALUATION OF COMPOUND-MEDIATED HEPATOTOXICITY

A major challenge in the identification of a new therapeutic agent is the ability to reliably select a candidate compound that has a low probability of inducing liver injury at the projected therapeutic doses.[48] Toxicity plays a major role in the attrition rate of potential therapeutics and accounts for approximately 40% of failures at the preclinical development stage (i.e., toxicity observed in animals) and ∼25% of failures in Phase I (i.e., clinical toxicity observed in humans).[36] However, toxicity is most often compound-specific and does not a priori represent a target-related safety concern. In fact, it is extremely difficult to prove a mechanism-based toxicity, which would require investigations with numerous equipotent but structurally significantly different compounds, which block the function of the same biological target and induce identical toxic effects. A significant increase of alanine aminotransferase (ALT) and aspartate aminotransferase (AST) levels in the blood of animals and humans treated with a therapeutic drug is broadly accepted to be a sensitive biomarker for compound-dependent hepatotoxicity.[49] However, several reports have shown that ALT and AST values can vary significantly depending on the exact animal species, sex, age, weight, stress levels (induced by manipulation of the animals, immobilization, or exposure to cold),[50] and even the collection site of the blood samples.[51] As two examples, the differences in the ALT and AST levels of healthy 8−10 week old male and female Nu/Nu and NOD SCID mice reported by Charles River Laboratories are summarized in Table S1.[52] Therefore, the normal levels of liver enzymes that are relevant are only those observed for the same animal species (with all other parameters identical), when treated with only vehicle control during the same study as the animals treated with the compound of interest (Table 4).

To evaluate any potential compound-dependent hepatotoxicity, all mice from the in vivo study using the xenograft MM (RPMI-8226) mouse model were euthanized 48 h after receiving the last dose, their blood was collected in serum

https://doi.org/10.1021/acs.jmedchem.3c01271
J. Med. Chem. 2023, 66, 15776−15800

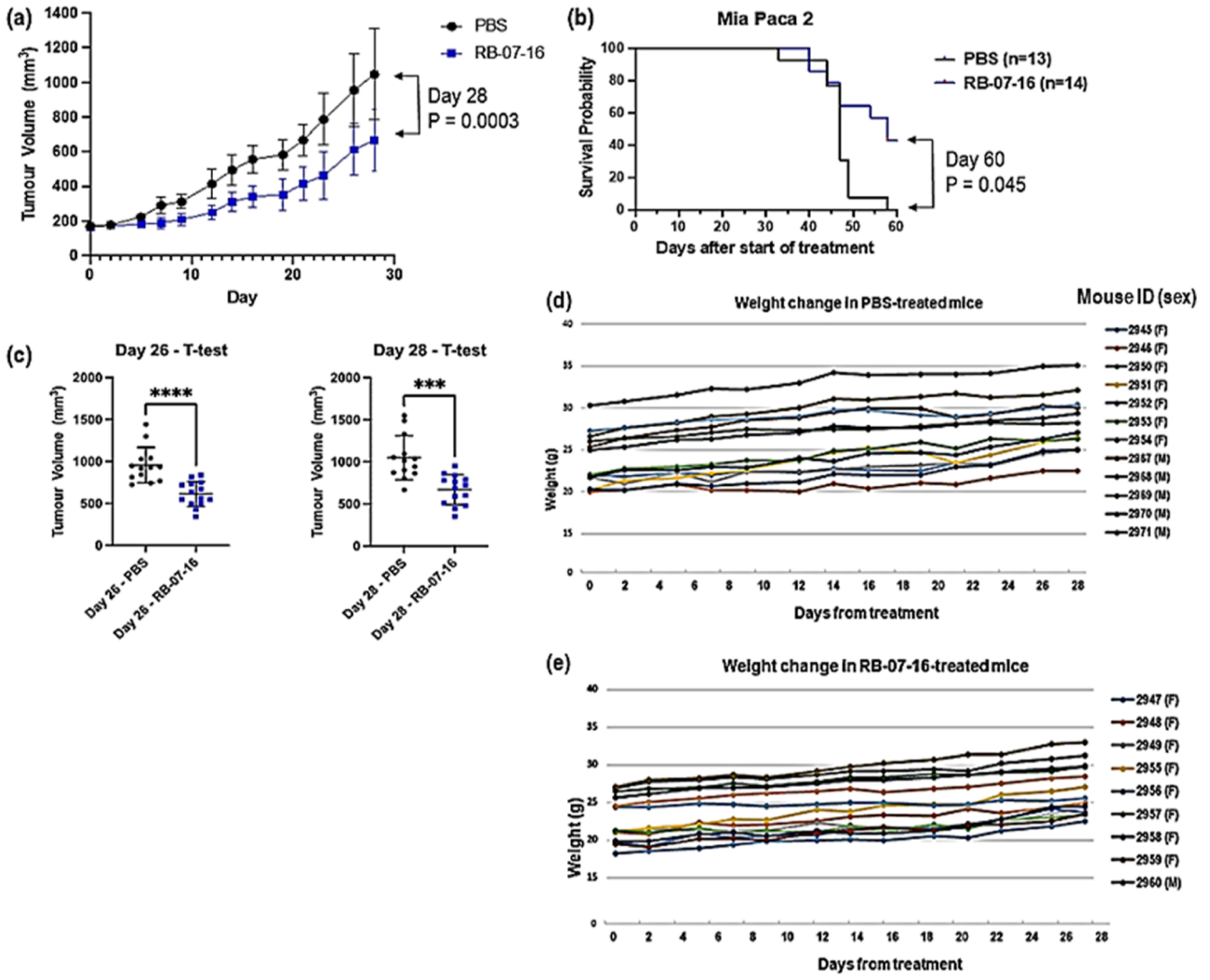

Figure 12. In vivo antitumor efficacy of hGGPPS inhibitor RB-07-16 (**13e**) vs PBS (vehicle control) in a xenograft PDAC mouse model using NSG mice injected with MIA PaCa-2 cells. (a) Tumor volume plotted using standard deviation; statistical analysis was performed using unpaired Welch's *t*-test correction. (b) Plot of survival probability. (c) *p*-Values with Welch's *t*-test correction on day 26 (when the animals received the last dose) and 48 h later (day 28). (d) Weight change of each animal treated with PBS or (e) RB-07-16 (**13e**); the ID number and sex of each animal are indicated.

separator tubes (with gel), and the serum was analyzed for any significant increase in ALT and AST; the results are shown in Table 4. Additionally, the livers (right and left lobes) of all animals were harvested immediately post-euthanasia, fixed in 10% aqueous formalin for 48 h at 4 °C, then transferred to 70% ethanol, and stored at 4 °C until embedded in paraffin, sectioned, and stained with hematoxylin and eosin (H&E) using standard methods at the RI-MUHC histology laboratory. The left and right lobes of each animal were examined without knowledge of the treatment group. The slides were graded using the scheme reported by Thoolen and co-workers[53] for the following abnormalities: eosinophilic degeneration, single-cell necrosis (apoptosis), foci of necrosis (multiple cells), inflammatory infiltrates, and bile ductular or oval cell proliferation. Vasculitis was assessed by simply counting the number of medium vessels showing subendothelial inflammatory infiltrates. Representative images of alterations from normal observed are shown in Figure 13, and detailed grading of all samples (left and right lobes) are reported in Table 5.

A well-known disadvantage to I.P. administration of drugs is the increased absorption into the liver (due to direct transport from the peritoneal cavity into the portal vein system); the latter leads to higher potential for hepatic toxicity. In spite of this effect and after multiple doses of RB-07-16 by I.P. injections over a 26 day period, our histopathology data did not reveal any serious abnormalities or significant differences between the control group of animals and those treated with this inhibitor (Table 5). Consistent with these observations, the differences in ALT and AST levels observed between the animals treated with PBS vehicle and those that received RB-07-16 (for both the male and the female animals) were less than twofold (Table 4). Such small differences in ALT and AST levels between the control group and the RB-07-16-treated group fall within the animal-to-animal variability, suggesting that there is no obvious concern with compound-induced hepatotoxicity in mice treated with an effective dose for inducing antimyeloma efficacy over a 26 day period. However, such preliminary results are no substitute for proper preclinical acute dose-ranging toxicity studies in rat and dog to more fully evaluate the safety of any potential new therapeutic agent.

8. CONCLUSIONS

We previously reported the discovery of C2-ThP-BP inhibitors of the hGGPPS,[9] which could effectively block the geranylger-

https://doi.org/10.1021/acs.jmedchem.3c01271
J. Med. Chem. 2023, 66, 15776−15800

Table 4. Levels of ALT and AST Liver Enzymes in the Serum of Xenograft MM NSG Mice Post In Vivo Antimyeloma Efficacy Study with hGGPPS Inhibitor RB-07-16 (13e); IP Dosing at 3 mg/kg for 12 Doses, 3 Times per Week, over a Period of 26 days

mouse ID	dose	ALT IU/L (sex)	AST IU/L (sex)
A808	PBS	35 (M)	76 (M)
A809	PBS	40 (M)	78 (M)
A815	PBS	**98 (F)**	**229 (F)**
A816	PBS	53 (F)	194 (F)
A817	PBS	83 (F)	194 (F)
A818	PBS	30 (F)	84 (F)
A823	PBS	33 (F)	131 (F)
A824	PBS	35 (F)	138 (F)
A810	RB-07-16	42 (M)	96 (M)
A811	RB-07-16	44 (M)	101 (M)
A812	RB-07-16	46 (M)	125 (M)
A813	RB-07-16	**148 (F)**	**280 (F)**
A814	RB-07-16	66 (F)	**250 (F)**
A819	RB-07-16	59 (F)	210 (F)
A820	RB-07-16	**152 (F)**	**316 (F)**
A821	RB-07-16	82 (F)	199 (F)
A822	RB-07-16	70 (F)	217 (F)

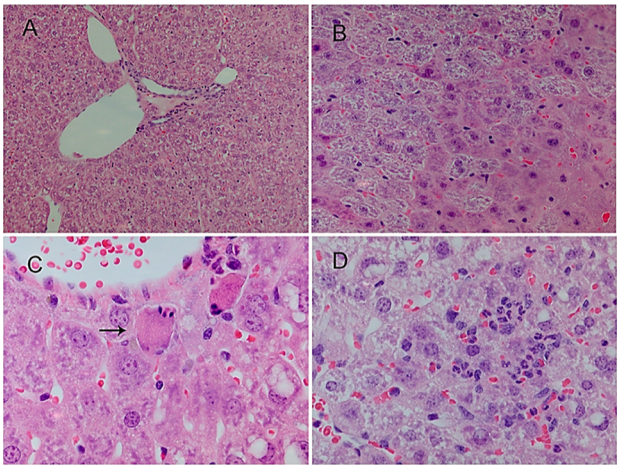

Figure 13. Light micrographs of representative lesions encountered in the mice livers (all stained with H&E). (A) Normal liver with portal tract in the center and surrounding intact hepatocytes (×100). (B) Eosinophilic degeneration in many of the hepatocytes on the right, predominantly lower right (×200). (C) Two apoptotic cells (arrow on one). Note the small pyknotic nucleus and the hypereosinophilic cytoplasm (×400). (D) Few small foci of inflammation composed predominantly of neutrophils (×400).

anylation of relevant GTPases (e.g., Rap-1A), induce the apoptosis of MM cells by selective intracellular binding to hGGPPS, exhibit a fairly long systemic circulation in rat, and block the progression of myeloma tumors in a validated animal model.[9a] In the current study, we have expanded our investigations to include novel and potent C6-PyraP-BP inhibitors of hGGPPS and have evaluated their ability to block the proliferation of MM, PDAC, and CRC cells. The current best C6-PyraP-BP inhibitor, RB-07-16 (**13e**), is slightly more potent (approximately twofold) than the previously reported best C2-ThP-BP analog, CML-07-119 (**12c**); however, it is significantly more selective in inhibiting hGGPPS vs hFPPS (Table 1). Given these advantages, RB-07-16 (**13e**) was selected for further biological profiling. RB-07-16 (**13e**) induces the desired biochemical consequences of selective intracellular target engagement, leading to apoptosis and downregulation of intracellular Rap-1A prenylation in MM, PDAC, and CRC cells. Additionally, this inhibitor was shown to have potency-dependent antitumor efficacy in xenograft mouse models of both MM and PDAC, significantly reducing tumor growth without substantially increasing liver enzymes or causing histopathologic liver alterations that are usually associated with drug-induced hepatotoxicity. Inhibitor RB-07-16 is also metabolically stable in cross-species liver microsomes, does not inhibit key CYP 450 enzymes, and exhibits good systemic circulation in rat. Collectively, our studies provide encouraging support for further optimization of the pyrazolo[3,4-*d*]pyrimidine-based hGGPPS inhibitors as potential human therapeutic agents for various cancers.

Although currently numerous small molecules and biologics are under investigation (at both the preclinical and clinical stages) for hematological cancers and solid tumors, eventual resistance to any chemotherapy is unavoidable and a major problem facing all cancer treatments.[54] Drug resistance is mainly due to tumor-induced tissue reprogramming, a mechanism largely attributable to intrinsic cellular genomic alterations induced by a given treatment,[55] underscoring the vital necessity for the discovery of novel antitumor agents, with new biochemical mechanisms of action. The recent enthusiasm for highly efficient biologic drugs (e.g., monoclonal antibodies, recombinant protein-based therapeutics, and gene and cellular therapies) does overshadow the value of small-molecule drugs, which are typically easier to manufacture, simpler to characterize (for quality control), and far less costly to prepare than complex biologics. Furthermore, the high cost of biologics has a huge impact on patients' ability to access and pay for these drugs or obtain support for these treatments from government-subsidized health-care providers;[56] according to a 2020 report by Forbes, biologic medicines are the biggest driver of rising drug prices.[57] Small molecules can also be combined with biologics for synergistic or mechanistic reasons leading to higher clinical efficacy in the treatment of cancer. For example, anti-CD38 monoclonal antibodies are often combined with small-molecule inhibitors in regimens that have proven to be very potent and durable in the treatment of myeloma.[58] A small-molecule inhibitor of the human GGPPS has the potential to provide a *first-in-class* valuable therapeutic for cancer chemotherapy.

9. EXPERIMENTAL SECTION

9.1. General Chemistry. Chemicals and solvents were purchased from commercial suppliers and used without further purification. Normal phase column chromatography on silica gel was performed using a CombiFlash instrument and the solvent gradients indicated. The homogeneity of the final inhibitors was confirmed to be ≥95% by ^{1}H and ^{31}P NMR and analytical C18 reversed-phase HPLC chromatography. Depending on the compound, two different systems were used, as indicated in the HPLC chromatogram of each compound (Supporting Information). System 1: A Waters Alliance instrument was used (e2695 with 2489 UV detector, 3100 mass spectrometer, C18 5 μm column); solvent A: H_2O, 0.1% formic acid; solvent B: CH_3CN, 0.1% formic acid; mobile phase: linear gradient from 95% A and 5% B to 0% A and 100% B in 13 min. System 2: A Waters Alliance instrument (2690 with a 996 PDA detector, Kromasil Eternity C18 5 μm HPLC Column); solvent A: H_2O, 0.2% NH_4OAc; solvent B: CH_3CN; mobile phase: linear gradient from 80% A and 20% B to 0% A and 100% B in 10 min.

https://doi.org/10.1021/acs.jmedchem.3c01271
J. Med. Chem. 2023, 66, 15776−15800

Table 5. Liver Histopathology from Mice Treated with RB-07-16 vs PBS Vehicle[a]

mouse ID	sex	dose	ED[b]	Apo[c]	FN[c]	IIn[c]	BDPr[c]	V[c]	N[d]
A808	M	PBS	0/0	0/0	0/0	0/0	0/0	0/0	0/0
A809	M	PBS	0/0	0/0	0/0	**2/2**	0/0	0/0	0/0
A815	F	PBS	1/1	0/0	0/0	0/0	0/0	0/0	0/0
A816	F	PBS	0/0	0/0	0/0	0/0	0/0	0/0	0/0
A817	F	PBS	1/0	0/0	0/0	0/0	0/0	0/0	0/0
A818	F	PBS	1/0	0/0	0/0	0/0	0/0	0/0	0/0
A823	F	PBS	0/1	0/0	0/0	0/0	0/0	0/0	0/0
A824	F	PBS	0/1	0/0	0/0	0/0	0/0	0/0	0/0
A810	M	RB-07-16	1/1	0/0	0/0	0/0	0/0	0/0	0/0
A811	M	RB-07-16	0/0	0/0	0/0	0/0	0/0	0/0	0/0
A812	M	RB-07-16	0/0	1/0	0/0	0/0	0/0	0/0	0/0
A813	F	RB-07-16	1/1	0/0	0/0	0/0	0/0	0/0	0/0
A814	F	RB-07-16	0/1	0/0	0/0	0/0	0/0	0/0	0/0
A819	F	RB-07-16	1/1	0/0	0/0	0/0	0/0	0/0	0/0
A820	F	RB-07-16	1/1	0/0	0/0	0/1	0/0	0/0	0/0
A821	F	RB-07-16	1/1	0/0	0/0	0/0	0/0	0/0	0/0
A822	F	RB-07-16	0/0	0/0	1/0	0/0	0/0	0/1	0/0

[a]The two numbers for each entry in the table indicate the score for the right (R) and left (L) lobe of each animal (R/L). [b]The following grading scheme was used for eosinophilic degeneration (ED)/change: true apoptosis (Apo) or single cell necrosis; foci of necrosis (FN); inflammatory infiltrates (IIn); and foci of bile ductular/oval cell proliferation (BDPr) based on observed abnormalities: grade 0 (none); grade 1: minimal (1−2 foci); grade 2: mild (3−6 foci); grade 3: moderate (7−12 foci); grade 4: severe (>12 foci); grade 5: very severe (diffuse).[53] [c]The grading for vessels with a vasculitis or perivasculitis (V) represents a simple count of the vessels. [d]Grading of prominent nucleoli (N): grade 1 (1−10%), grade 2 (10−25%), grade 3 (>25−50%), and grade 4 (>50%).

All final compounds were fully characterized by ^{1}H, ^{13}C, ^{31}P NMR, and HRMS analyses. Chemical shifts (δ) are reported in ppm relative to the internal deuterated solvent. The NMR spectra of all final bisphosphonate inhibitors were acquired in DMSO-d_6 or D_2O; in the latter case, they were first converted to their corresponding trisodium salt with the addition of 3 equiv of NaOD in D_2O or 0.5% NH_4OH to the D_2O solvent. The high-resolution MS spectra of final products were recorded using electrospray ionization ($ESI^{\pm}$) and Fourier transform ion cyclotron resonance mass spectrometry (FTMS).

We recently reported the synthesis and full characterization of compounds **11a**,[9a] **11b**,[9b] **11c**,[9b] and **12c**;[9a] these compounds are included in the current study for the purpose of comparison with the new structural class of hGGPPS inhibitors.

9.2. General Procedure for Bisphosphonate Deprotection. *9.2.1. Step 1.* Into an oven-dried microwave vial equipped with a stir bar, anhydrous DCM (5 mL) was added under argon, followed by hexamethyldisilane (727 mg, 1.01 mL, 2 equiv, 4.96 mmol), which had been previously dried over 4 Å molecular sieves. The septum was briefly removed to add iodine (630 mg, 1 equiv, 2.48 mmol), and then the vial was sealed quickly with a Teflon crimp cap under argon. The flask was wrapped well in aluminum foil, and the mixture was stirred at RT. Initially, the reaction mixture was a dark purple color, which slowly dissipated. After 3−4 h, the solution turned a pale pink color and was left to stir for a total of 16 h at RT to ensure complete reaction, after which time the solution became colorless. This solution was presumed to be 0.81 M TMSI in DCM and used directly in the next step.

9.2.2. Step 2. In a dry flask equipped with a stir bar, the tetraethyl ester compound (1 equiv) was dissolved in anhydrous DCM (30 mL per 1 mmol of tetraethyl ester) under argon and cooled to 0 °C in an ice bath. TMSI (25 equiv, 0.81 M solution in DCM) was added dropwise. The solution was stirred at 0 °C, and the progress of the reaction was tracked by ^{1}H NMR (DMSO-d_6), after quenching an aliquot (~0.1 mL) with MeOH. Complete conversion was typically observed in 2−4 h, at which point MeOH (30 mL/mmol) and H_2O (3 mL/mmol) were added. The mixture was stirred for 1 h at RT and then cooled at 4 °C for 1 h in order to precipitate the desired bisphosphonic acid product. The precipitated product was collected by vacuum filtration and washed with HPLC-grade MeOH. If further purification was required, the solid material was sonicated in MeOH, collected by vacuum filtration, and washed again with HPLC-grade MeOH.

*9.2.2.1. (((2-(3-((4-Fluorophenyl)carbamoyl)phenyl)thieno[2,3-d]pyrimidin-4-yl)amino)methylene)bis(phosphonic Acid) (**12a**).* Inhibitor **12a** was prepared as previously reported for this class of compounds.[9b]

The tetraester (64 mg) was deprotected using TMSI, followed by MeOH, to give inhibitor **12a** as a white solid (51 mg, quant. yield).

^{1}H NMR (500 MHz, 0.5% NH_4OH in D_2O): δ 8.79 (t, J = 1.8 Hz, 1H), 8.56 (dt, J = 7.9, 1.4 Hz, 1H), 8.04 (dt, J = 8.0, 1.5 Hz, 1H), 7.74 (t, J = 7.8 Hz, 1H), 7.66−7.55 (m, 3H), 7.51 (d, J = 6.0 Hz, 1H), 7.24 (t, J = 9.0 Hz, 2H), 5.20 (t, J = 19.0 Hz, 1H).

^{31}P NMR (203 MHz, 0.5% NH_4OH in D_2O): δ 13.88.

^{13}C NMR (201 MHz, 0.5% NH_4OH in D_2O): δ 169.6, 165.8, 160.4 (d, J = 242.8 Hz), 159.9, 157.3, 138.4, 134.3, 133.0 (d, J = 2.9 Hz), 132.2, 129.6, 129.5, 127.1, 125.3, 123.5, 119.1, 116.1, 115.9 (d, J = 22.9 Hz), 49.2 (t, J = 121.4 Hz).

HRMS [ESI^-] calcd for $C_{20}H_{16}FN_4O_7P_2S$ m/z: 537.0204; found, 537.0196 $[M-H]^-$.

*9.2.2.2. (((2-(3-((4-(Trifluoromethyl)phenyl)carbamoyl)phenyl)-thieno[2,3-d]pyrimidin-4-yl)amino)methylene)bis(phosphonic Acid) (**12b**).* Inhibitor **12b** was prepared as previously reported for this subclass of compounds.[9b]

The tetraester (52 mg) was deprotected using TMSI, followed by MeOH, to give inhibitor **12b** as a beige solid (40 mg, quant. yield).

^{1}H NMR (800 MHz, 0.5% NH_4OH in D_2O): δ 8.77 (s, 1H), 8.53 (d, J = 7.7 Hz, 1H), 8.02 (d, J = 7.6 Hz, 1H), 7.80 (d, J = 8.4 Hz, 2H), 7.77 (d, J = 8.2 Hz, 2H), 7.72 (t, J = 7.7 Hz, 1H), 7.60 (d, J = 5.8 Hz, 1H), 7.48 (d, J = 5.8 Hz, 1H), 5.15 (t, J = 18.9 Hz, 1H).

^{31}P NMR (203 MHz, 0.5% NH_4OH in D_2O): δ 13.87.

^{13}C NMR (201 MHz, 0.5% NH_4OH in D_2O): δ 169.3, 165.5, 159.7, 157.0, 140.6, 138.3, 134.2, 132.2, 129.5, 129.3, 127.0, 126.3 (q, J = 31.5 Hz), 126.2 (q, J = 4.0 Hz), 124.2 (q, J = 270.8 Hz), 123.2, 122.0, 118.9, 115.9, 49.5 (t, J = 122.5 Hz). HRMS [ESI^-] calcd for $C_{21}H_{16}F_3N_4O_7P_2S$ m/z: 587.0173; found, 587.0170 $[M-H]^-$.

*9.2.2.3. 5-Amino-1H-pyrazole-4-carboxamide (**17**).* Step 1: (ethoxymethylene)malononitrile (1.50 g, 12.3 mmol, 1.0 equiv) was added to a microwave vial and cooled in an ice bath. Hydrazine (2.0 mL, 64% in H_2O, 41.2 mmol, 3.4 equiv) was added to the vial dropwise with stirring. The reaction mixture was heated at 100 °C for 1 h, followed by TLC (100% EtOAc, R_f = 0.43). Upon complete conversion, the reaction mixture was cooled to RT, quenched with water (15 mL), and extracted with EtOAc (3× 15 mL). The combined organic extracts were

https://doi.org/10.1021/acs.jmedchem.3c01271
J. Med. Chem. 2023, 66, 15776−15800

dried over anhydrous Na_2SO_4, filtered, and concentrated under reduced pressure. The crude residue was purified on silica gel by flash chromatography, using a solvent gradient from 1 to 100% EtOAc in hexanes, to afford the 5-amino-1*H*-pyrazole-4-carbonitrile as a white solid (820 mg, 62%).

Step 2: the pyrazole (562 mg, 5.20 mmol, 1.0 equiv) was slowly added to concentrated sulfuric acid (2.0 mL) that was cooled in an ice bath and stirred over a period of 20 min at 0 °C before it was allowed to warm up to RT and stirred for 4 h. A small amount of ice was added to the reaction mixture, and it was stored in the refrigerator overnight to allow precipitation of the product. The precipitate was filtered and washed with water to afford **17** as an orange solid (569 mg, 87%).

^{1}H NMR (500 MHz, DMSO-d_6): δ 8.04 (s, 1H), 7.46 (s, 1H), 6.99 (s, 1H), 5.97 (s, 2H).

^{13}C NMR (126 MHz, DMSO-d_6): δ 165.7, 150.6, 134.3, 100.5.

MS [ESI$^+$] m/z: 127.11 [M + H$^+$]$^+$.

*9.2.3. 1,7-Dihydro-4H-pyrazolo[3,4-d]pyrimidine-4,6(5H)-dione (**18**).* Intermediate **17** (822 mg, 6.52 mmol, 1.0 equiv) and urea (1.7 g, 28 mmol, 4.3 equiv) were added to a pressure vessel and heated at 190 °C for 40 min. The precipitated solid was dissolved in boiling 1 M NaOH (12 mL) and then acidified with 1 M HCl (15 mL). The solution was cooled and then filtered, washing with excess water to obtain **18** as a yellow solid (447 mg, 45%). ^{1}H NMR (500 MHz, DMSO-d_6): δ 13.28 (s, 1H), 11.32 (s, 1H), 10.65 (s, 1H), 8.34 (s, 1H). ^{13}C NMR (126 MHz, DMSO-d_6): δ 160.2, 152.2, 151.4, 129.5, 100.8.

MS [ESI$^-$] m/z: 150.95 [M − H$^+$]$^-$.

*9.2.4. 2,4,6-Trichloropyrimidine-5-carbaldehyde (**20**).* The starting material, pyrimidine-2,4,6(1*H*,3*H*,5*H*)-trione (**19**), was prepared as previously reported.[25] A pressure vessel was purged with argon and cooled in an ice bath before $POCl_3$ (192 mL, 2.06 mol, 7.1 equiv) was added to the vessel followed by the dropwise addition of DMF (27 mL, 350 mmol, 1.2 equiv), leading to the formation of a white solid. The septum was briefly removed under argon to add intermediate **19** (37.1 g, 289 mmol, 1.0 equiv), and the reaction was heated at 120 °C for 16 h. The reaction mixture was cooled to RT and very slowly added to water (1 L), taking care that the temperature of the water did not increase substantially. The precipitated product was collected by vacuum filtration and washed with water to obtain **20** as a pale yellow solid (46.4 g, 76%). All NMR data were consistent with the literature.[60]

^{1}H NMR (500 MHz, $CDCl_3$): δ 10.44 (s, 1H).

^{13}C NMR (126 MHz, $CDCl_3$): δ 184.6, 164.1, 161.6, 123.0.

MS [APCI] m/z: 210.92 [M + H$^+$]$^+$.

*9.2.5. 4,6-Dichloro-1H-pyrazolo[3,4-d]pyrimidine (**21**).* Intermediate **20** (44.8 g, 213 mmol, 1.0 equiv) was added to a flask, which was purged with argon and cooled to 0 °C, before MeOH (600 mL) was added, followed by the dropwise addition of hydrazine (64% in H_2O, 11.3 mL, 230 mmol, 1.1 equiv) and the dropwise addition of triethylamine (30.8 mL, 221 mmol, 1.0 equiv). The reaction mixture was stirred at 0 °C and followed by TLC (25% EtOAc in hexanes, R_f = 0.36). After 1 h, the reaction mixture was dried under vacuum and purified on silica gel by flash column chromatography, using a solvent gradient from 2 to 75% EtOAc in hexanes, to obtain **21** as a white solid (21.8 g, 54%).

^{1}H NMR (500 MHz, $CDCl_3$): δ 12.28 (s, 1H), 8.31 (s, 1H).

^{13}C NMR (126 MHz, $CDCl_3$): δ 157.2, 156.2, 155.7, 134.2, 112.6.

MS [ESI$^-$] m/z: 186.93 [M − H$^+$]$^-$.

9.3. General Procedure for Bisphosphonate Synthesis. The intermediates **21** (after THP-protection of the free amine and amination) and **30** were converted to their corresponding bisphosphonates **22** and **31**, respectively, following the previously reported procedure.[9a]

*9.3.1. Tetraethyl (((6-Chloro-1-(tetrahydro-2H-pyran-2-yl)-1H-pyrazolo[3,4-d]pyrimidin-4-yl)amino)methylene)bis(phosphonate) (**22**). 9.3.1.1. Step 1.* In a round-bottom flask, intermediate **21** (17.3 g, 91.6 mmol, 1.0 equiv) and *p*TsOH monohydrate (1.86 g, 9.77 mmol, 0.11 equiv) were dissolved in a mixture of DCM (260 mL) and THF (260 mL), DHP (12.6 mL, 138 mmol, 1.5 equiv) was added, and the reaction mixture was stirred at RT. Progress of the reaction was followed by TLC (25% EtOAc in hexanes, R_f = 0.53), and after 6 h, the reaction mixture was concentrated to dryness, diluted with DCM, and washed with saturated aqueous Na_2CO_3, water, and brine, and the organic layer was dried with anhydrous $MgSO_4$. The crude product residue was purified on silica gel by flash column chromatography, using a solvent gradient from 2 to 50% EtOAc in hexanes, to obtain the THP-protected pyrazolopyrimidine as a white solid (23.3 g, 93%).

^{1}H NMR (500 MHz, $CDCl_3$): δ 8.22 (d, J = 0.6 Hz, 1H), 6.02 (dd, J = 10.5, 2.6 Hz, 1H), 4.14 (ddd, J = 11.8, 4.2, 2.1 Hz, 1H), 3.83 (td, J = 11.5, 2.6 Hz, 1H), 2.62−2.53 (m, 1H), 2.20−2.14 (m, 1H), 1.97 (ddt, J = 12.4, 3.9, 2.6 Hz, 1H), 1.85−1.76 (m, 2H), 1.70−1.65 (m, 1H). ^{13}C NMR (126 MHz, $CDCl_3$): δ 156.9, 155.5, 154.5, 133.3, 113.2, 83.0, 68.5, 29.4, 24.8, 22.7.

MS [ESI$^+$] m/z: 273.07 [M + H$^+$]$^+$.

9.3.1.2. Step 2. The THP-protected pyrazolopyrimidine intermediate (21.7 g, 79.7 mmol, 1.0 equiv) was dissolved in THF (215 mL), aqueous NH_4OH (28%, 225 mL, 1624 mmol, 20 equiv) was added, and the reaction mixture was stirred vigorously at RT. Progress of the reaction was followed by TLC (50% EtOAc in hexanes, R_f = 0.38), and after 7 h, the reaction mixture was concentrated under vacuum leading to the precipitation of the product, which was collected by vacuum filtration, washed with water and DCM to obtain the 6-chloro-1-(tetrahydro-2*H*-pyran-2-yl)-1*H*-pyrazolo[3,4-*d*]pyrimidin-4-amine product as a white solid (18.3 g, 91%).

^{1}H NMR (500 MHz, DMSO-d_6): δ 8.38−8.15 (m, 2H), 8.14 (s, 1H), 5.72 (dd, J = 10.3, 2.5 Hz, 1H), 3.93 (ddd, J = 11.6, 4.7, 2.6 Hz, 1H), 3.73−3.61 (m, 1H), 2.36 (tdd, J = 12.8, 10.3, 4.1 Hz, 1H), 2.03−1.94 (m, 1H), 1.83 (dq, J = 12.9, 3.4 Hz, 1H), 1.73 (ddtd, J = 16.8, 10.9, 7.5, 6.9, 3.5 Hz, 1H), 1.55 (hept, J = 3.9 Hz, 2H).

^{13}C NMR (126 MHz, DMSO-d_6): δ 159.1, 158.1, 154.9, 133.6, 99.7, 82.2, 67.5, 29.2, 25.1, 22.7. MS [ESI$^+$]

m/z: 254.17 [M + H$^+$]$^+$.

9.3.1.3. Step 3. Following the general procedure for bisphosphonate synthesis previously reported,[9a] the bisphosphonate tetraethyl ester intermediate **22** was obtained as a white solid (17.1 g, 50%).

^{1}H NMR (500 MHz, $CDCl_3$): δ 8.14 (s, 1H), 6.59 (s, 1H), 5.95 (dd, J = 10.6, 2.5 Hz, 1H), 5.67 (td, J = 21.9, 9.8 Hz, 1H), 4.38−4.09 (m, 8H), 3.82 (td, J = 11.6, 2.5 Hz, 1H), 2.55 (tdd, J = 12.4, 10.4, 4.2 Hz, 1H), 2.14 (dd, J = 10.2, 4.4 Hz, 1H), 1.97−1.89 (m, 1H), 1.86−1.73 (m, 3H), 1.67−1.61 (m, 1H), 1.36−1.27 (m, 12H).

^{31}P NMR (203 MHz, $CDCl_3$): δ 15.98−15.40 (m).

^{13}C NMR (126 MHz, $CDCl_3$): δ 158.0, 155.9, 154.8, 132.7, 100.3, 82.2, 68.5, 63.9 (dt, J = 28.5, 5.1 Hz), 44.8 (t, J = 147.0 Hz), 29.6, 25.0, 22.9, 16.9−15.8 (m).

MS [ESI$^-$] m/z: 538.18 [M − H$^+$]$^-$.

*9.3.2. Tetraethyl (((6-Chloro-1H-pyrazolo[3,4-d]pyrimidin-4-yl)-amino)methylene)bis(phosphonate) (**23**).* Intermediate **22** (1.80 g, 3.33 mmol, 1.0 equiv) was dissolved in MeOH (16 mL), HCl (4 M in dioxane, 40 mL, 160 mmol, 48 equiv) was added, and the reaction mixture was stirred at 40 °C followed by TLC (10% MeOH in EtOAc, R_f = 0.47). Complete conversion was observed after 1.5 h, at which point the reaction mixture was concentrated under vacuum, the crude residue was diluted with saturated aqueous $NaHCO_3$ (50 mL), extracted with EtOAc (3× 30 mL), and dried over anhydrous Mg_2SO_4. The crude residue was purified on silica gel by flash chromatography using a gradient from 0 to 20% MeOH in EtOAc to obtain **23** as a white solid (1.25 g, 82%).

^{1}H NMR (500 MHz, $CDCl_3$): δ 13.75 (s, 1H), 8.85 (d, J = 10.1 Hz, 1H), 8.64 (s, 1H), 5.82 (td, J = 22.4, 10.0 Hz, 1H), 4.39−3.97 (m, 8H), 1.33 (t, J = 7.1 Hz, 6H), 1.11 (t, J = 7.1 Hz, 6H).

^{31}P NMR (203 MHz, $CDCl_3$): δ 16.19.

^{13}C NMR (126 MHz, $CDCl_3$): δ 158.6, 156.5, 155.7, 132.2, 99.9, 64.0 (dt, J = 91.6, 3.2 Hz), 44.8 (t, J = 147.4 Hz), 16.2 (dt, J = 27.7, 3.0 Hz).

MS [ESI$^-$] m/z: 454.16 [M − H$^+$]$^-$.

9.4. General Procedure for Alkylation of Pyrazole 23. Intermediate **23** (1.0 equiv) was dissolved in anhydrous DMF (0.1 M) and cooled to 0 °C, before K_2CO_3 (5.0 equiv) was added, followed by the addition of an alkyl iodide (1.1 equiv). The reaction mixture was stirred at RT followed by LCMS. Upon complete conversion of the starting material, the reaction mixture was concentrated, diluted with brine, and extracted with EtOAc (3×). The product crude residue was

https://doi.org/10.1021/acs.jmedchem.3c01271
J. Med. Chem. 2023, 66, 15776−15800

purified on silica gel by flash column chromatography, using a solvent gradient from 0 to 20% MeOH in EtOAc.

*9.4.1. Tetraethyl (((6-Chloro-1-methyl-1H-pyrazolo[3,4-d]-pyrimidin-4-yl)amino)methylene)bis(phosphonate) (**24a**).* Intermediate **23** (249 mg) was alkylated to give intermediate **24a** as a white solid (174 mg, 68%).

^{1}H NMR (500 MHz, $CDCl_3$): δ 8.09 (s, 1H), 6.77 (s, 1H), 5.70 (td, J = 22.0, 9.9 Hz, 1H), 4.34−4.14 (m, 8H), 4.02 (s, 3H), 1.34 (t, J = 7.0 Hz, 6H), 1.28 (t, J = 7.1 Hz, 6H).

^{31}P NMR (203 MHz, $CDCl_3$): δ 15.82.

^{13}C NMR (126 MHz, $CDCl_3$): δ 157.6, 155.9, 154.5, 131.3, 100.0, 63.9 (d, J = 29.9 Hz), 44.8 (t, J = 146.8 Hz), 34.2, 16.5−16.2 (m).

MS [ESI$^-$] m/z: 468.23 [M − H$^+$]$^-$.

*9.4.2. Tetraethyl (((6-Chloro-2-methyl-2H-pyrazolo[3,4-d]-pyrimidin-4-yl)amino)methylene)bis(phosphonate) (**25a**).* Intermediate **23** (249 mg) was alkylated to give intermediate **25a** as a white solid (40 mg, 16%).

^{1}H NMR (500 MHz, $CDCl_3$): δ 8.30 (s, 1H), 7.45 (d, J = 9.7 Hz, 1H), 5.76 (td, J = 22.0, 9.7 Hz, 1H), 4.37−4.08 (m, 11H), 1.36 (t, J = 7.1 Hz, 6H), 1.23 (t, J = 7.1 Hz, 6H).

^{31}P NMR (203 MHz, $CDCl_3$): δ 15.86.

^{13}C NMR (126 MHz, $CDCl_3$): δ 161.3, 157.9, 157.2, 125.2, 101.00, 64.0 (d, J = 24.9 Hz), 44.4 (t, J = 146.0 Hz), 40.9, 16.3.

MS [ESI$^-$] m/z: 468.22 [M − H$^+$]$^-$.

*9.4.3. Tetraethyl (((6-Chloro-1-ethyl-1H-pyrazolo[3,4-d]-pyrimidin-4-yl)amino)methylene)bis(phosphonate) (**24b**).* Intermediate **23** (204 mg) was alkylated to give intermediate **24b** as a white solid (137 mg, 63%).

^{1}H NMR (500 MHz, $CDCl_3$): δ 8.04 (s, 1H), 6.36 (d, J = 9.9 Hz, 1H), 5.67 (td, J = 21.8, 9.8 Hz, 1H), 4.43 (q, J = 7.3 Hz, 2H), 4.36−4.16 (m, 8H), 1.52 (t, J = 7.2 Hz, 3H), 1.34 (t, J = 7.0 Hz, 6H), 1.30 (t, J = 7.1 Hz, 6H).

^{31}P NMR (203 MHz, $CDCl_3$): δ 15.86.

^{13}C NMR (201 MHz, $CDCl_3$): δ 157.5, 155.7, 153.9, 130.7, 99.9, 63.9 (d, J = 70.1 Hz), 44.8 (t, J = 147.3 Hz), 42.4, 16.4 (d, J = 12.3 Hz), 14.8.

MS [ESI$^-$] m/z: 482.13 [M − H$^+$]$^-$.

*9.4.4. Tetraethyl (((6-Chloro-2-ethyl-2H-pyrazolo[3,4-d]-pyrimidin-4-yl)amino)methylene)bis(phosphonate) (**25b**).* Intermediate **23** (204 mg) was alkylated to give intermediate **25b** as a white solid (47 mg, 22%).

^{1}H NMR (500 MHz, $CDCl_3$): δ 8.38 (s, 1H), 7.74 (d, J = 9.8 Hz, 1H), 5.77 (td, J = 22.0, 9.8 Hz, 1H), 4.39 (q, J = 7.3 Hz, 2H), 4.35−4.05 (m, 8H), 1.62 (t, J = 7.3 Hz, 3H), 1.35 (t, J = 7.1 Hz, 6H), 1.21 (t, J = 7.1 Hz, 6H).

^{31}P NMR (203 MHz, $CDCl_3$): δ 15.89.

^{13}C NMR (126 MHz, $CDCl_3$): δ 161.1, 157.8, 157.3, 123.9, 100.6, 64.0 (d, J = 20.5 Hz), 49.1, 44.3 (t, J = 146.9 Hz), 16.3 (d, J = 3.3 Hz), 15.3.

MS [ESI$^-$] m/z: 482.14 [M − H$^+$]$^-$.

*9.4.5. Tetraethyl (((6-Chloro-1-isopropyl-1H-pyrazolo[3,4-d]-pyrimidin-4-yl)amino)methylene)bis(phosphonate) (**24c**).* Intermediate **23** (252 mg) was alkylated to give intermediate **24c** as a white solid (171 mg, 62%).

^{1}H NMR (500 MHz, $CDCl_3$): δ 8.07 (s, 1H), 6.61 (d, J = 9.8 Hz, 1H), 5.68 (td, J = 21.9, 9.9 Hz, 1H), 5.10 (hept, J = 6.7 Hz, 1H), 4.36−4.12 (m, 8H), 1.55 (d, J = 6.7 Hz, 6H), 1.34 (t, J = 7.1 Hz, 6H), 1.29 (t, J = 7.1 Hz, 6H).

^{31}P NMR (203 MHz, $CDCl_3$): δ 15.92.

^{13}C NMR (126 MHz, $CDCl_3$): δ 157.3, 155.9, 153.5, 131.1, 100.1, 64.0 (dt, J = 37.2, 3.2 Hz), 49.1, 44.9 (t, J = 146.9 Hz), 22.1, 16.46 (dt, J = 6.3, 3.0 Hz).

MS [ESI$^-$] m/z: 496.23 [M − H$^+$]$^-$.

9.5. General Procedure for the Suzuki Coupling Reaction. Intermediates **22**, **24**, **25**, and **31** were coupled to side chains **26** using the protocol we previously reported,[59] with very minor variations for individual compounds in temperature (80−90 °C) and in the base used (KF or aqueous K_2CO_3).

9.6. General Procedure for the Synthesis of Bisphosphonic Acid Inhibitors 13a−l, 14a,b, and 15a−c. *9.6.1. Step 1.* Pd-catalyzed Suzuki coupling reaction of intermediates **22**, **24**, **25**, and **31** with the boronic acids **26** was carried out as previously reported[59] to give the tetraester precursors of the final inhibitors **13a−l**, **14a,b**, and **15a−c**.

9.6.2. Step 2. In the case of intermediate **22**, the THP group was removed under standard acidic conditions before proceeding to the final bisphosphonate tetraester deprotection in step 3.

Note: The crude products from steps 1 and 2 were doubly purified, first on silica gel by flash column chromatography (using a solvent gradient from 0 to 20% MeOH in EtOAc), followed by purification on C18 silica gel by reverse phase column chromatography (using a solvent gradient from 10 to 100% MeCN in H_2O) in order to ensure that the bisphosphonate tetraester precursors of all final compounds were isolated in very high purity.

9.6.3. Step 3. Deprotection of the bisphosphonate tetraesters with TMSI followed by MeOH was achieved using the general protocol described above.

*9.6.4. (((6-(3-((4-Fluorophenyl)carbamoyl)phenyl)-1H-pyrazolo-[3,4-d]pyrimidin-4-yl)amino)methylene)bis(phosphonic Acid) (**13a**). 9.6.4.1. Step 1.* Coupling of intermediate **22** (201 mg) with boronic acid **26** (R^2 = f1) gave the product as a white solid (131 mg, 49%).

^{1}H NMR (500 MHz, $CDCl_3$): δ 9.34 (s, 1H), 9.00 (s, 1H), 8.71 (dt, J = 7.8, 1.4 Hz, 1H), 8.26 (s, 1H), 8.17 (d, J = 7.7 Hz, 1H), 7.86 (dd, J = 8.9, 4.8 Hz, 2H), 7.64 (t, J = 7.8 Hz, 1H), 7.21 (s, 1H), 7.13−7.04 (m, 2H), 6.14 (dd, J = 10.5, 2.5 Hz, 1H), 5.76 (td, J = 22.9, 8.8 Hz, 1H), 4.30−4.07 (m, 8H), 3.88 (td, J = 11.5, 2.5 Hz, 1H), 2.64 (tdd, J = 12.7, 10.5, 4.3 Hz, 1H), 2.22−2.15 (m, 1H), 2.03−1.95 (m, 1H), 1.90−1.77 (m, 3H), 1.71−1.65 (m, 1H), 1.29−1.21 (m, 12H).

^{31}P NMR (203 MHz, $CDCl_3$): δ 16.87 (d, J = 4.4 Hz).

MS [ESI$^-$] m/z: 717.46 [M − H$^+$]$^-$.

9.6.4.2. Step 2. Removal of the THP group of the above intermediate (117 mg) gave the tetraester precursor of **13a** as a white solid (70 mg, 68%).

^{1}H NMR (500 MHz, DMSO-d_6): δ 13.65 (s, 1H), 10.52 (s, 1H), 9.10 (d, J = 9.4 Hz, 1H), 8.94 (s, 1H), 8.57 (dt, J = 7.8, 1.5 Hz, 1H), 8.51 (s, 1H), 8.06 (dt, J = 7.7, 1.5 Hz, 1H), 7.87−7.80 (m, 2H), 7.70 (t, J = 7.7 Hz, 1H), 7.26−7.18 (m, 2H), 6.01 (t, J = 22.8 Hz, 1H), 4.20−4.03 (m, 8H), 1.17 (t, J = 7.1 Hz, 6H), 1.11 (t, J = 7.0 Hz, 6H).

^{31}P NMR (203 MHz, DMSO): δ 16.98.

MS [ESI$^-$] m/z: 633.36 [M − H$^+$]$^-$.

9.6.4.3. Step 3. The tetraester precursor (47 mg) was deprotected with TMSI, followed by MeOH, to give the inhibitor **13a** as a white solid (28 mg, 69%).

^{1}H NMR (400 MHz, DMSO-d_6): δ 10.49 (s, 1H), 8.94 (d, J = 1.9 Hz, 1H), 8.63 (d, J = 7.8 Hz, 1H), 8.49 (s, 2H), 8.05 (d, J = 7.7 Hz, 1H), 7.90−7.80 (m, 2H), 7.68 (t, J = 7.8 Hz, 1H), 7.27−7.16 (m, 2H), 5.60 (td, J = 21.8, 9.0 Hz, 1H).

^{31}P NMR (162 MHz, DMSO-d_6): δ 14.04.

^{13}C NMR (201 MHz, DMSO-d_6): δ 166.1, 159.9, 158.8 (d, J = 240.6 Hz), 156.4, 156.0, 139.0, 136.1, 135.6, 133.8, 131.8, 129.6, 128.9, 127.9, 122.7 (d, J = 7.9 Hz), 115.7 (d, J = 22.3 Hz), 100.0, 47.7 (t, J = 139.6 Hz).

HRMS [ESI$^-$] calcd for $C_{19}H_{17}FN_6O_7P_2$ m/z: 521.0545; found, 521.0527 [M − H]$^-$.

*9.6.5. (((6-(3-((4-(Trifluoromethyl)phenyl)carbamoyl)phenyl)-1H-pyrazolo[3,4-d]pyrimidin-4-yl)amino)methylene)bis(phosphonic Acid) (**13b**). 9.6.5.1. Step 1.* Coupling of intermediate **22** (501 mg) with boronic acid **26** (R^2 = f2) gave the product as a white solid (402 mg, 56%).

^{1}H NMR (500 MHz, $CDCl_3$): δ 9.41 (d, J = 25.6 Hz, 2H), 8.74 (dt, J = 7.8, 1.4 Hz, 1H), 8.28 (s, 1H), 8.22 (dt, J = 7.7, 1.5 Hz, 1H), 8.09 (d, J = 8.4 Hz, 2H), 7.71−7.61 (m, 3H), 7.35 (s, 1H), 6.14 (dd, J = 10.5, 2.5 Hz, 1H), 5.70 (td, J = 23.1, 8.6 Hz, 1H), 4.29−4.05 (m, 8H), 3.88 (td, J = 11.4, 2.4 Hz, 1H), 2.71−2.59 (m, 1H), 2.23−2.15 (m, 1H), 2.04−1.96 (m, 1H), 1.90−1.78 (m, 3H), 1.72−1.66 (m, 1H), 1.30−1.21 (m, 12H).

^{31}P NMR (203 MHz, $CDCl_3$): δ 16.95.

MS [ESI$^-$] m/z: 767.37 [M − H$^+$]$^-$.

https://doi.org/10.1021/acs.jmedchem.3c01271
J. Med. Chem. 2023, 66, 15776−15800

9.6.5.2. Step 2. Removal of the THP group of the above product (141 mg) gave the tetraester precursor of **13b** as a white solid (55 mg, 44%).

^{1}H NMR (500 MHz, DMSO): δ 13.65 (s, 1H), 10.81 (s, 1H), 9.11 (d, J = 9.7 Hz, 1H), 8.95 (s, 1H), 8.59 (dt, J = 7.9, 1.4 Hz, 1H), 8.51 (s, 1H), 8.12−8.03 (m, 3H), 7.78−7.69 (m, 3H), 6.01 (s, 1H), 4.19−4.03 (m, 8H), 1.17 (t, J = 7.0 Hz, 6H), 1.11 (t, J = 7.0 Hz, 6H).

^{31}P NMR (203 MHz, DMSO): δ 16.97.

MS [ESI$^-$] m/z: 683.35 [M − H$^+$]$^-$.

9.6.5.3. Step 3. The tetraester precursor (38 mg) was deprotected using TMSI followed by MeOH to give inhibitor **13b** as a white solid (23 mg, 71%).

^{1}H NMR (400 MHz, DMSO-d_6): δ 10.79 (s, 1H), 8.96 (s, 1H), 8.65 (d, J = 7.8 Hz, 1H), 8.50 (s, 2H), 8.08 (dd, J = 8.8, 2.8 Hz, 3H), 7.78−7.66 (m, 3H), 5.61 (td, J = 21.9, 9.1 Hz, 1H).

^{31}P NMR (162 MHz, DMSO-d_6): δ 14.05.

^{13}C NMR (201 MHz, DMSO-d_6): δ 166.7, 159.8, 156.4, 156.1, 143.4, 139.1, 135.3, 133.8, 132.1, 129.8, 128.9, 128.0, 126.4 (d, J = 4.4 Hz), 125.1 (q, J = 270.0 Hz), 124.1 (q, J = 31.5 Hz), 120.6, 100.0, 47.7 (t, J = 139.3 Hz).

HRMS [ESI$^-$] calcd for $C_{20}H_{17}F_3N_6O_7P_2$ m/z: 571.0513; found, 571.0494 [M − H]$^-$.

*9.6.6. (((6-(3-((3-Fluoro-4-methoxyphenyl)carbamoyl)phenyl)-1H-pyrazolo[3,4-d]pyrimidin-4-yl)amino)methylene)bis-(phosphonic Acid) (**13c**). 9.6.6.1. Step 1.* Coupling of intermediate **22** (507 mg) with boronic acid **26** (R^2 = f3) gave the product as a white solid (392 mg, 56%).

^{1}H NMR (500 MHz, $CDCl_3$): δ 9.37 (s, 1H), 9.06 (s, 1H), 8.74−8.64 (m, 1H), 8.22 (s, 1H), 8.17 (d, J = 7.9 Hz, 1H), 7.81−7.67 (m, 2H), 7.62 (t, J = 7.7 Hz, 1H), 7.09−6.99 (m, 1H), 6.96 (t, J = 9.0 Hz, 1H), 6.13 (dd, J = 10.5, 2.5 Hz, 1H), 5.77−5.55 (m, 1H), 4.32−4.01 (m, 8H), 3.91 (s, 3H), 3.86 (td, J = 11.1, 2.3 Hz, 1H), 2.63 (q, J = 10.3, 9.0 Hz, 1H), 2.17 (s, 1H), 1.98 (d, J = 13.1 Hz, 1H), 1.83 (t, J = 10.2 Hz, 2H), 1.75−1.61 (m, 2H), 1.31−1.13 (m, 12H).

^{31}P NMR (203 MHz, $CDCl_3$): δ 16.97.

MS [ESI$^-$] m/z: 747.43 [M − H$^+$]$^-$.

9.6.6.2. Step 2. Removal of the THP group of the above product (233 mg) gave the tetraester precursor of **13c** as a white solid (142 mg, 69%).

^{1}H NMR (500 MHz, DMSO-d_6): δ 13.65 (s, 1H), 10.48 (s, 1H), 9.10 (d, J = 9.5 Hz, 1H), 8.94 (s, 1H), 8.57 (dt, J = 7.9, 1.4 Hz, 1H), 8.51 (s, 1H), 8.05 (dt, J = 8.0, 1.3 Hz, 1H), 7.78 (dd, J = 13.7, 2.5 Hz, 1H), 7.69 (t, J = 7.8 Hz, 1H), 7.56 (dt, J = 8.8, 1.9 Hz, 1H), 7.19 (t, J = 9.4 Hz, 1H), 6.02 (t, J = 22.9 Hz, 1H), 4.23−3.98 (m, 8H), 3.84 (s, 3H), 1.17 (d, J = 7.0 Hz, 6H), 1.11 (t, J = 7.1 Hz, 6H).

^{31}P NMR (203 MHz, DMSO): δ 16.98.

MS [ESI$^-$] m/z: 663.40 [M − H$^+$]$^-$.

9.6.6.3. Step 3. The tetraester precursor (61 mg) was deprotected using TMSI followed by MeOH to give inhibitor **13c** as a white solid (15 mg, 29%).

^{1}H NMR (400 MHz, DMSO-d_6): δ 10.53 (s, 1H), 9.00 (d, J = 1.8 Hz, 1H), 8.70 (dt, J = 7.7, 1.4 Hz, 1H), 8.58 (s, 2H), 8.11 (dt, J = 7.7, 1.5 Hz, 1H), 7.87 (dd, J = 13.8, 2.5 Hz, 1H), 7.75 (t, J = 7.8 Hz, 1H), 7.63 (dt, J = 8.8, 1.8 Hz, 1H), 7.25 (t, J = 9.4 Hz, 1H), 5.69 (td, J = 21.9, 9.3 Hz, 1H), 3.92 (s, 3H).

^{31}P NMR (162 MHz, DMSO-d_6): δ 14.09.

^{13}C NMR (201 MHz, DMSO-d_6): δ 165.9, 159.9, 156.4, 156.1, 151.3 (d, J = 241.7 Hz), 143.7 (d, J = 10.6 Hz), 139.0, 135.5, 133.8, 133.1 (d, J = 9.5 Hz), 131.8, 129.6, 128.9, 127.8, 116.8, 114.4, 109.2 (d, J = 22.5 Hz), 100.0, 56.6, 47.7 (t, J = 140.1 Hz).

HRMS [ESI$^-$] calcd for $C_{20}H_{19}FN_6O_8P_2$ m/z: 551.0651; found, 551.0652 [M − H]$^-$.

*9.6.7. (((6-(3-((4-Fluorophenyl)carbamoyl)phenyl)-1-methyl-1H-pyrazolo[3,4-d]pyrimidin-4-yl)amino)methylene)bis(phosphonic Acid) (**13d**). 9.6.7.1. Step 1.* Coupling of intermediate **24a** (250 mg) with boronic acid **26** (R^2 = f1) gave the bisphosphonate tetraester precursor of **13d** as a white solid (214 mg, 62%).

^{1}H NMR (500 MHz, $CDCl_3$): δ 9.35 (s, 1H), 9.05 (s, 1H), 8.62 (dt, J = 7.8, 1.5 Hz, 1H), 8.23 (s, 1H), 8.14 (dt, J = 7.8, 1.5 Hz, 1H), 7.89 (dd, J = 8.6, 4.8 Hz, 2H), 7.62 (t, J = 7.7 Hz, 1H), 7.50 (d, J = 10.3 Hz, 1H), 7.13−7.05 (m, 2H), 5.83 (td, J = 23.0, 9.1 Hz, 1H), 4.30−4.09 (m, 8H), 3.83 (s, 3H), 1.31−1.19 (m, 12H).

^{31}P NMR (203 MHz, $CDCl_3$): δ 17.03.

MS [ESI$^-$] m/z: 647.32 [M − H$^+$]$^-$.

9.6.7.2. Step 2. The tetraester precursor (100 mg) was deprotected using TMSI followed by MeOH to give inhibitor **13d** as a white solid (75 mg, 91%).

^{1}H NMR (400 MHz, DMSO-d_6): δ 10.49 (s, 1H), 8.96 (t, J = 1.8 Hz, 1H), 8.67 (dt, J = 7.8, 1.4 Hz, 1H), 8.58 (d, J = 9.7 Hz, 1H), 8.48 (s, 1H), 8.06 (dt, J = 7.7, 1.5 Hz, 1H), 7.89−7.81 (m, 2H), 7.69 (t, J = 7.7 Hz, 1H), 7.27−7.16 (m, 2H), 5.64 (td, J = 21.9, 9.6 Hz, 1H), 4.01 (s, 3H).

^{31}P NMR (162 MHz, DMSO-d_6): δ 14.10.

^{13}C NMR (201 MHz, DMSO-d_6): δ 166.2, 160.0, 158.8 (d, J = 240.5 Hz), 156.4, 154.4, 139.1, 136.0 (d, J = 2.5 Hz), 135.6, 133.0, 131.9, 129.6, 128.8, 127.9, 122.7 (d, J = 7.8 Hz), 115.7 (d, J = 22.0 Hz), 100.3, 47.8 (t, J = 139.6 Hz), 34.0.

HRMS [ESI$^-$] calcd for $C_{20}H_{19}FN_6O_7P_2$ m/z: 535.0702; found, 535.0694 [M − H]$^-$.

*9.6.8. (((1-Methyl-6-(3-((4-(trifluoromethyl)phenyl)carbamoyl)-phenyl)-1H-pyrazolo[3,4-d]pyrimidin-4-yl)amino)methylene)bis-(phosphonic Acid) (**13e**). 9.6.8.1. Step 1.* Coupling of intermediate **24a** (88 mg) with boronic acid **26** (R^2 = f2) gave the bisphosphonate tetraester precursor of **13e** as a white solid (70 mg, 53%).

^{1}H NMR (400 MHz, $CDCl_3$): δ 9.37 (s, 1H), 9.25 (s, 1H), 8.70 (dt, J = 7.9, 1.5 Hz, 1H), 8.19 (dd, J = 7.5, 1.8 Hz, 1H), 8.13 (s, 1H), 8.08 (d, J = 8.4 Hz, 2H), 7.71−7.62 (m, 3H), 6.70 (s, 1H), 5.72 (td, J = 22.9, 9.0 Hz, 1H), 4.30−4.10 (m, 8H), 4.00 (s, 3H), 1.32−1.19 (m, 12H).

^{31}P NMR (162 MHz, $CDCl_3$): δ 16.91.

MS [ESI$^-$] m/z: 697.27 [M − H$^+$]$^-$.

9.6.8.2. Step 2. The tetraester precursor (101 mg) was deprotected using TMSI followed by MeOH to give inhibitor **13e** as a white solid (69 mg, 81%). ^{1}H NMR (400 MHz, DMSO-d_6): δ 10.78 (s, 1H), 8.98 (d, J = 1.9 Hz, 1H), 8.69 (dt, J = 7.7, 1.4 Hz, 1H), 8.60 (d, J = 9.9 Hz, 1H), 8.48 (s, 1H), 8.11−8.06 (m, 3H), 7.73 (dd, J = 20.2, 8.2 Hz, 3H), 5.64 (td, J = 21.8, 9.6 Hz, 1H), 4.01 (s, 3H).

^{31}P NMR (162 MHz, DMSO-d_6): δ 14.11.

^{13}C NMR (201 MHz, DMSO-d_6): δ 166.7, 159.9, 156.5, 154.4, 143.3, 139.2, 135.3, 133.1, 132.1, 129.8, 128.9, 128.1, 126.4, 125.1 (q, J = 271.0 Hz), 124.1 (q, J = 31.5, 30.8 Hz), 120.7, 100.4, 47.7 (t, J = 139.8 Hz), 34.0.

HRMS [ESI$^-$] calcd for $C_{21}H_{19}F_3N_6O_7P_2$ m/z: 585.0670; found, 585.0675 [M − H]$^-$.

*9.6.9. (((6-(3-((3-Fluoro-4-methoxyphenyl)carbamoyl)phenyl)-1-methyl-1H-pyrazolo[3,4-d]pyrimidin-4-yl)amino)methylene)bis-(phosphonic Acid) (**13f**). 9.6.9.1. Step 1.* Coupling of intermediate **24a** (38 mg) with boronic acid **26** (R^2 = f3) gave the bisphosphonate tetraester precursor of inhibitor **13f** as a white solid (29 mg, 54%).

^{1}H NMR (500 MHz, $CDCl_3$): δ 9.25 (s, 1H), 9.02 (s, 1H), 8.69 (dt, J = 7.8, 1.4 Hz, 1H), 8.17 (d, J = 7.7 Hz, 1H), 8.09 (s, 1H), 7.75 (dd, J = 13.0, 2.5 Hz, 1H), 7.68 (d, J = 9.1 Hz, 1H), 7.65 (t, J = 7.7 Hz, 1H), 6.99 (t, J = 9.1 Hz, 1H), 6.52 (s, 1H), 5.73 (dt, J = 23.0, 11.5 Hz, 1H), 4.29−4.11 (m, 8H), 4.07 (s, 3H), 3.93 (s, 3H), 1.28 (t, J = 7.1 Hz, 6H), 1.24 (t, J = 7.0 Hz, 6H).

^{31}P NMR (162 MHz, $CDCl_3$): δ 16.92.

MS [ESI$^-$] m/z: 677.33 [M − H$^+$]$^-$.

9.6.9.2. Step 2. The tetraester precursor (38 mg) was deprotected using TMSI followed by MeOH to give inhibitor **13f** as a white solid (14 mg, 46%).

^{1}H NMR (400 MHz, DMSO-d_6): δ 10.50 (s, 1H), 9.01 (d, J = 1.9 Hz, 1H), 8.72 (dt, J = 7.9, 1.4 Hz, 1H), 8.63−8.58 (m, 1H), 8.54 (s, 1H), 8.10 (dt, J = 7.8, 1.5 Hz, 1H), 7.85 (dd, J = 13.7, 2.5 Hz, 1H), 7.74 (t, J = 7.7 Hz, 1H), 7.61 (dt, J = 9.0, 1.9 Hz, 1H), 7.24 (t, J = 9.4 Hz, 1H), 5.68 (td, J = 22.0, 9.6 Hz, 1H), 4.06 (s, 3H), 3.90 (s, 3H).

^{31}P NMR (162 MHz, DMSO-d_6): δ 14.08.

^{13}C NMR (201 MHz, DMSO-d_6): δ 165.6, 159.6, 156.0 (d, J = 4.4 Hz), 154.0, 150.8 (d, J = 241.7 Hz), 143.3 (d, J = 10.8 Hz), 138.7, 135.1, 132.7, 132.6, 131.4, 129.1, 128.4, 127.4, 116.4 (d, J = 3.3 Hz), 113.9 (d, J = 2.5 Hz), 108.8 (d, J = 22.6 Hz), 100.0, 56.2, 47.3 (t, J = 139.9 Hz), 33.6.

https://doi.org/10.1021/acs.jmedchem.3c01271
J. Med. Chem. 2023, 66, 15776−15800

HRMS [ESI$^-$] calcd for $C_{21}H_{21}FN_6O_8P_2$ m/z: 565.0807; found, 565.0816 [M − H]$^-$

*9.6.10. (((1-Ethyl-6-(3-((4-fluorophenyl)carbamoyl)phenyl)-1H-pyrazolo[3,4-d]pyrimidin-4-yl)amino)methylene)bis(phosphonic Acid) (**13g**). 9.6.10.1. Step 1.* Coupling of intermediate **24b** (46 mg) with boronic acid **26** (R^2 = f1) gave the bisphosphonate tetraester precursor of **13g** as a white solid (26 mg, 41%).

^{1}H NMR (500 MHz, $CDCl_3$): δ 9.16 (s, 1H), 9.06 (s, 1H), 8.64 (dt, J = 7.8, 1.4 Hz, 1H), 8.14 (s, 1H), 8.11 (dt, J = 7.8, 1.5 Hz, 1H), 7.83 (dd, J = 8.6, 4.8 Hz, 2H), 7.61 (t, J = 7.7 Hz, 1H), 7.09−7.04 (m, 2H), 7.01 (s, 1H), 5.79 (td, J = 22.8, 9.1 Hz, 1H), 4.40 (q, J = 7.2 Hz, 2H), 4.26−4.09 (m, 8H), 1.51 (t, J = 7.3 Hz, 3H), 1.25−1.19 (m, 12H).

^{31}P NMR (203 MHz, $CDCl_3$): δ 17.00.

MS [ESI$^-$] m/z: 661.39 [M − H$^+$]$^-$.

9.6.10.2. Step 2. The tetraester precursor (128 mg) was deprotected using TMSI followed by MeOH to give inhibitor **13g** as a white solid (76 mg, 72%). ^{1}H NMR (400 MHz, DMSO-d_6): δ 10.49 (s, 1H), 8.94 (t, J = 1.9 Hz, 1H), 8.66 (dt, J = 7.8, 1.4 Hz, 1H), 8.57 (d, J = 9.8 Hz, 1H), 8.50 (s, 1H), 8.05 (dt, J = 7.7, 1.5 Hz, 1H), 7.89−7.81 (m, 2H), 7.69 (t, J = 7.7 Hz, 1H), 7.27−7.17 (m, 2H), 5.63 (td, J = 22.0, 9.6 Hz, 1H), 4.44 (q, J = 7.2 Hz, 2H), 1.44 (t, J = 7.2 Hz, 3H).

^{31}P NMR (162 MHz, DMSO-d_6): δ 14.08.

^{13}C NMR (201 MHz, DMSO-d_6): δ 166.2, 159.9, 158.8 (d, J = 240.5 Hz), 156.4, 153.9, 139.2, 136.0, 135.6, 133.1, 131.9, 129.5, 128.8, 127.9, 122.71 (d, J = 7.9 Hz), 115.7 (d, J = 21.9 Hz), 100.4, 47.8 (t, J = 139.2 Hz), 41.8, 15.4.

HRMS [ESI$^-$] calcd for $C_{21}H_{21}FN_6O_7P_2$ m/z: 549.0858; found, 549.0858 [M − H]$^-$.

*9.6.11. (((1-Ethyl-6-(3-((4-(trifluoromethyl)phenyl)carbamoyl)-phenyl)-1H-pyrazolo[3,4-d]pyrimidin-4-yl)amino)methylene)bis-(phosphonic Acid) (**13h**). 9.6.11.1. Step 1.* Coupling of intermediate **24b** (95 mg) with boronic acid **26** (R^2 = f2) gave the bisphosphonate tetraester precursor of **13h** as a white solid (40 mg, 28%). ^{1}H NMR (400 MHz, $CDCl_3$): δ 9.32 (s, 1H), 9.22 (s, 1H), 8.75−8.69 (m, 1H), 8.19 (d, J = 7.7 Hz, 1H), 8.07 (d, J = 9.9 Hz, 3H), 7.71−7.62 (m, 3H), 6.34 (s, 1H), 5.69 (td, J = 22.9, 8.9 Hz, 1H), 4.52 (q, J = 7.3 Hz, 2H), 4.32−4.06 (m, 8H), 1.58 (t, J = 7.3 Hz, 3H), 1.29 (t, J = 7.1 Hz, 6H), 1.24 (t, J = 7.1 Hz, 6H).

^{31}P NMR (162 MHz, $CDCl_3$): δ 16.90.

MS [ESI$^-$] m/z: 711.43 [M − H$^+$]$^-$.

9.6.11.2. Step 2. The tetraester precursor (26 mg) was deprotected using TMSI followed by MeOH to give inhibitor **13h** as a white solid (19 mg, 86%).

^{1}H NMR (400 MHz, DMSO-d_6): δ 10.78 (s, 1H), 8.97 (d, J = 2.0 Hz, 1H), 8.71−8.65 (m, 1H), 8.51 (d, J = 12.2 Hz, 2H), 8.08 (dd, J = 8.8, 2.7 Hz, 3H), 7.78−7.66 (m, 3H), 5.61 (td, J = 21.9, 9.5 Hz, 1H), 4.44 (q, J = 7.2 Hz, 2H), 1.44 (t, J = 7.2 Hz, 3H).

^{31}P NMR (162 MHz, DMSO-d_6): δ 14.00.

^{13}C NMR (201 MHz, DMSO-d_6): δ 166.7, 159.8, 156.4, 153.9, 143.4, 139.2, 135.3, 133.2, 132.1, 129.7, 128.9, 128.1, 126.4, 125.1 (q, J = 271.9 Hz), 124.1 (q, J = 32.3, 31.0 Hz), 120.7, 100.5, 47.7 (t, J = 140.2 Hz), 41.8, 15.4.

HRMS [ESI$^-$] calcd for $C_{22}H_{21}F_3N_6O_7P_2$ m/z: 599.0826; found, 599.0810 [M − H]$^-$.

*9.6.12. (((1-Ethyl-6-(3-((3-fluoro-4-methoxyphenyl)carbamoyl)-phenyl)-1H-pyrazolo[3,4-d]pyrimidin-4-yl)amino)methylene)bis-(phosphonic Acid) (**13i**). 9.6.12.1. Step 1.* Coupling of intermediate **24b** (134 mg) with boronic acid **26** (R^2 = f3) gave the bisphosphonate tetraester precursor of **13i** as a white solid (118 mg, 62%).

^{1}H NMR (500 MHz, $CDCl_3$): δ 9.26 (s, 1H), 9.05 (s, 1H), 8.66 (dt, J = 7.8, 1.4 Hz, 1H), 8.18−8.12 (m, 1H), 8.11 (s, 1H), 7.73 (dd, J = 13.0, 2.5 Hz, 1H), 7.70−7.65 (m, 1H), 7.62 (t, J = 7.8 Hz, 1H), 6.97 (t, J = 9.1 Hz, 1H), 6.78 (s, 1H), 5.71 (td, J = 22.7, 8.6 Hz, 1H), 4.47 (q, J = 7.3 Hz, 2H), 4.27−4.07 (m, 8H), 3.91 (s, 3H), 1.54 (t, J = 7.3 Hz, 3H), 1.29−1.18 (m, 12H).

^{31}P NMR (203 MHz, $CDCl_3$): δ 17.03.

MS [ESI$^-$] m/z: 691.45 [M − H$^+$]$^-$.

9.6.12.2. Step 2. The tetraester precursor (43 mg) was deprotected using TMSI followed by MeOH to give inhibitor **13i** as a white solid (19 mg, 52%).

^{1}H NMR (400 MHz, DMSO-d_6): δ 10.45 (s, 1H), 8.94 (t, J = 1.8 Hz, 1H), 8.65 (dt, J = 7.8, 1.4 Hz, 1H), 8.55 (d, J = 9.9 Hz, 1H), 8.50 (s, 1H), 8.04 (dt, J = 7.8, 1.5 Hz, 1H), 7.80 (dd, J = 13.8, 2.5 Hz, 1H), 7.68 (t, J = 7.7 Hz, 1H), 7.56 (dt, J = 9.2, 1.9 Hz, 1H), 7.19 (t, J = 9.4 Hz, 1H), 5.62 (td, J = 21.9, 9.4 Hz, 1H), 4.44 (q, J = 7.2 Hz, 2H), 3.85 (s, 3H), 1.44 (t, J = 7.2 Hz, 3H).

^{31}P NMR (162 MHz, DMSO-d_6): δ 14.06.

^{13}C NMR (201 MHz, DMSO-d_6): δ 166.0, 159.9, 156.4, 153.9, 151.3 (d, J = 241.6 Hz), 143.7 (d, J = 10.7 Hz), 139.2, 135.6, 133.2, 133.1 (d, J = 9.5 Hz), 131.9, 129.5, 128.8, 127.9, 116.8, 114.4, 109.2 (d, J = 22.5 Hz), 100.5, 56.6, 47.7 (t, J = 140.2 Hz), 41.8, 15.4.

HRMS [ESI$^-$] calcd for $C_{22}H_{23}FN_6O_8P_2$ m/z: 579.0964; found, 579.0971 [M − H$^+$]$^-$.

*9.6.13. (((6-(3-((4-Fluorophenyl)carbamoyl)phenyl)-1-isopropyl-1H-pyrazolo[3,4-d]pyrimidin-4-yl)amino)methylene)bis-(phosphonic Acid) (**13j**). 9.6.13.1. Step 1.* Coupling of intermediate **24c** (151 mg) with boronic acid **26** (R^2 = f1) gave the bisphosphonate tetraester precursor of **13j** as a white solid (133 mg, 65%).

^{1}H NMR (500 MHz, $CDCl_3$): δ 9.23 (s, 1H), 8.68 (dt, J = 7.8, 1.4 Hz, 2H), 8.14−8.08 (m, 1H), 8.02 (s, 1H), 7.80 (dd, J = 8.9, 4.9 Hz, 2H), 7.62 (t, J = 7.8 Hz, 1H), 7.12−7.03 (m, 2H), 6.00 (d, J = 9.3 Hz, 1H), 5.73 (td, J = 22.5, 9.1 Hz, 1H), 5.30 (hept, J = 6.8 Hz, 1H), 4.28−4.09 (m, 8H), 1.61 (d, J = 6.7 Hz, 6H), 1.27 (t, J = 7.1 Hz, 6H), 1.22 (t, J = 7.1 Hz, 6H).

^{31}P NMR (203 MHz, $CDCl_3$): δ 16.85.

MS [ESI$^-$] m/z: 675.35 [M − H$^+$]$^-$.

9.6.13.2. Step 2. The tetraester precursor (92 mg) was deprotected using TMSI followed by MeOH to give inhibitor **13j** as a white solid (68 mg, 89%).

^{1}H NMR (400 MHz, DMSO-d_6): δ 10.41 (s, 1H), 8.86 (t, J = 1.8 Hz, 1H), 8.58 (dt, J = 7.8, 1.5 Hz, 1H), 8.43 (d, J = 4.0 Hz, 2H), 7.97 (dt, J = 7.7, 1.5 Hz, 1H), 7.82−7.74 (m, 2H), 7.61 (t, J = 7.8 Hz, 1H), 7.20−7.09 (m, 2H), 5.53 (td, J = 21.7, 9.3 Hz, 1H), 5.10 (p, J = 6.7 Hz, 1H), 1.43 (d, J = 6.6 Hz, 6H).

^{31}P NMR (162 MHz, DMSO-d_6): δ 14.05.

^{13}C NMR (201 MHz, DMSO-d_6): δ 166.2, 159.7, 158.8 (d, J = 240.4 Hz), 156.4, 153.5, 139.2, 136.0, 135.6, 132.9, 131.9, 129.5, 128.8, 127.9, 122.72 (d, J = 8.1 Hz), 115.7 (d, J = 22.2 Hz), 100.6, 48.4, 47.52 (t, J = 138.4 Hz), 22.5.

HRMS [ESI$^-$] calcd for $C_{22}H_{23}FN_6O_7P_2$ m/z: 563.1015; found, 563.1029 [M − H]$^-$.

*9.6.14. (((1-Isopropyl-6-(3-((4-(trifluoromethyl)phenyl)-carbamoyl)phenyl)-1H-pyrazolo[3,4-d]pyrimidin-4-yl)amino)-methylene)bis(phosphonic Acid) (**13k**). 9.6.14.1. Step 1.* Coupling of intermediate **24c** (154 mg) with boronic acid **26** (R^2 = f2) gave the bisphosphonate tetraester precursor of **13k** as a white solid (175 mg, 76%).

^{1}H NMR (500 MHz, $CDCl_3$): δ 9.35 (s, 1H), 9.12 (s, 1H), 8.73 (dt, J = 7.8, 1.4 Hz, 1H), 8.18 (d, J = 7.7 Hz, 1H), 8.08−8.03 (m, 3H), 7.70−7.63 (m, 3H), 6.16 (d, J = 9.1 Hz, 1H), 5.70 (td, J = 22.7, 8.9 Hz, 1H), 5.32 (hept, J = 6.7 Hz, 1H), 4.32−4.07 (m, 8H), 1.64 (d, J = 6.7 Hz, 6H), 1.29 (t, J = 7.1 Hz, 6H), 1.24 (t, J = 7.1 Hz, 6H).

^{31}P NMR (203 MHz, $CDCl_3$): 16.92.

MS [ESI$^-$] m/z: 725.40 [M − H$^+$]$^-$.

9.6.14.2. Step 2. The tetraester precursor (102 mg) was deprotected using TMSI followed by MeOH to give inhibitor **13k** as a white solid (80 mg, 93%).

^{1}H NMR (400 MHz, DMSO-d_6): δ 10.71 (s, 1H), 8.89 (d, J = 1.8 Hz, 1H), 8.60 (dt, J = 7.9, 1.5 Hz, 1H), 8.44 (d, J = 5.8 Hz, 2H), 8.03−7.98 (m, 3H), 7.68 (d, J = 8.6 Hz, 2H), 7.63 (t, J = 7.8 Hz, 1H), 5.53 (td, J = 21.9, 9.6 Hz, 1H), 5.10 (p, J = 6.7 Hz, 1H), 1.44 (d, J = 6.7 Hz, 6H).

^{31}P NMR (162 MHz, DMSO-d_6): δ 14.04.

^{13}C NMR (201 MHz, DMSO-d_6): δ 166.3, 159.2, 155.9, 153.0, 142.9, 138.8, 134.8, 132.4, 131.7, 129.2, 128.4, 127.6, 126.0, 124.5 (q, J = 273.4 Hz), 123.7 (q, J = 35.1 Hz), 120.2, 100.1, 47.9, 47.4 (t, J = 131.7 Hz), 22.0.

HRMS [ESI$^-$] calcd for $C_{23}H_{23}F_3N_6O_7P_2$ m/z: 613.0983; found, 613.0984 [M − H]$^-$.

9.6.15. (((6-(3-((3-Fluoro-4-methoxyphenyl)carbamoyl)phenyl)-1-isopropyl-1H-pyrazolo[3,4-d]pyrimidin-4-yl)amino)methylene)-

https://doi.org/10.1021/acs.jmedchem.3c01271
J. Med. Chem. 2023, 66, 15776−15800

*bis(phosphonic Acid) (**13l**). 9.6.15.1. Step 1.* Coupling of intermediate **24c** (153 mg) with boronic acid **26** (R^2 = f3) gave the bisphosphonate tetraester precursor of **13l** as a white solid (114 mg, 52%).

^{1}H NMR (500 MHz, $CDCl_3$): δ 9.30 (s, 1H), 8.83 (s, 1H), 8.68 (dt, J = 7.8, 1.4 Hz, 1H), 8.14 (d, J = 7.7 Hz, 1H), 8.02 (s, 1H), 7.71 (dd, J = 13.0, 2.5 Hz, 1H), 7.63 (q, J = 7.7 Hz, 2H), 6.97 (t, J = 9.1 Hz, 1H), 6.07 (s, 1H), 5.68 (dt, J = 25.3, 12.7 Hz, 1H), 5.30 (hept, J = 6.9 Hz, 1H), 4.28−4.08 (m, 8H), 3.91 (s, 3H), 1.61 (d, J = 6.7 Hz, 6H), 1.27 (t, J = 7.1 Hz, 6H), 1.22 (t, J = 7.1 Hz, 6H).

^{31}P NMR (203 MHz, $CDCl_3$): δ 16.93.

MS [ESI$^-$] m/z: 705.37 [M − H$^+$]$^-$.

9.6.15.2. Step 2. The tetraester precursor (80 mg) was deprotected using TMSI followed by MeOH to give inhibitor **13l** as a white solid (59 mg, 87%).

^{1}H NMR (400 MHz, DMSO-d_6): δ 10.37 (s, 1H), 8.86 (t, J = 1.8 Hz, 1H), 8.57 (dt, J = 7.9, 1.5 Hz, 1H), 8.43 (s, 2H), 7.97 (dt, J = 7.8, 1.5 Hz, 1H), 7.72 (dd, J = 13.7, 2.5 Hz, 1H), 7.60 (t, J = 7.8 Hz, 1H), 7.48 (dt, J = 8.9, 1.9 Hz, 1H), 7.11 (t, J = 9.4 Hz, 1H), 5.53 (td, J = 21.8, 9.4 Hz, 1H), 5.10 (p, J = 6.7 Hz, 1H), 3.77 (s, 3H), 1.44 (d, J = 6.7 Hz, 6H).

^{31}P NMR (162 MHz, DMSO-d_6): δ 14.05.

^{13}C NMR (201 MHz, DMSO-d_6): δ 166.0, 159.7, 156.4, 153.5, 151.3 (d, J = 242.0 Hz), 143.7 (d, J = 10.7 Hz), 139.2, 135.6, 133.1 (d, J = 9.4 Hz), 132.9, 131.9, 129.5, 128.8, 127.9, 116.8, 114.4, 109.2 (d, J = 22.6 Hz), 100.6, 56.6, 48.4, 47.4 (t, J = 138.9 Hz), 22.5.

HRMS [ESI$^-$] calcd for $C_{23}H_{25}FN_6O_8P_2$ m/z: 593.1120; found, 593.1120 [M − H]$^-$.

*9.6.16. (((6-(3-((3-Fluoro-4-methoxyphenyl)carbamoyl)phenyl)-2-methyl-2H-pyrazolo[3,4-d]pyrimidin-4-yl)amino)methylene)bis-(phosphonic Acid) (**14a**). 9.6.16.1. Step 1.* Coupling of intermediate **25a** (45 mg) with boronic acid **26** (R^2 = f3) gave the bisphosphonate tetraester precursor of **14a** as a white solid (49 mg, 76%).

^{1}H NMR (500 MHz, DMSO-d_6): δ 10.48 (s, 1H), 9.08 (d, J = 9.6 Hz, 1H), 8.93 (s, 1H), 8.67 (s, 1H), 8.57 (dt, J = 7.8, 1.4 Hz, 1H), 8.02 (dt, J = 7.9, 1.4 Hz, 1H), 7.77 (dd, J = 13.7, 2.5 Hz, 1H), 7.67 (t, J = 7.7 Hz, 1H), 7.59−7.53 (m, 1H), 7.18 (t, J = 9.4 Hz, 1H), 6.11−5.93 (m, 1H), 4.21−4.01 (m, 11H), 3.84 (s, 3H), 1.17 (t, J = 7.0 Hz, 6H), 1.11 (t, J = 7.0 Hz, 6H).

^{31}P NMR (203 MHz, DMSO-d_6): δ 16.89.

MS [ESI$^-$] m/z: 677.41 [M − H$^+$]$^-$.

9.6.16.2. Step 2. The tetraester precursor (30 mg) was deprotected using TMSI followed by MeOH to give inhibitor **14a** as a white solid (20 mg, 81%).

^{1}H NMR (800 MHz, DMSO-d_6, 333 K): δ 10.36 (s, 1H), 9.02 (s, 1H), 8.72 (s, 1H), 8.64 (d, J = 7.7 Hz, 1H), 8.09 (d, J = 7.6 Hz, 1H), 7.84 (dd, J = 13.7, 2.5 Hz, 1H), 7.70 (t, J = 7.7 Hz, 1H), 7.62 (dd, J = 8.8, 2.5 Hz, 1H), 7.21 (t, J = 9.3 Hz, 1H), 5.44 (t, J = 21.3 Hz, 1H), 4.13 (s, 3H), 3.90 (s, 3H).

^{31}P NMR (162 MHz, DMSO-d_6, 313 K): δ 13.58.

^{13}C NMR (201 MHz, DMSO-d_6, 333 K): δ 165.8, 158.9, 157.2, 151.5 (d, J = 242.1 Hz), 143.9 (d, J = 10.7 Hz), 138.1, 135.5, 133.2 (d, J = 9.5 Hz), 131.8, 129.9, 128.9, 128.0, 127.6, 117.0, 114.8, 109.4 (d, J = 22.7 Hz), 101.5, 56.9, 49.2 (t, J = 131.9 Hz), 40.8.

HRMS [ESI$^-$] calcd for $C_{21}H_{19}FN_6Na_2O_8P_2$ m/z: 609.0446; found, 609.0436 [M − H]$^-$.

*9.6.17. (((2-Ethyl-6-(3-((3-fluoro-4-methoxyphenyl)carbamoyl)-phenyl)-2H-pyrazolo[3,4-d]pyrimidin-4-yl)amino)methylene)bis-(phosphonic Acid) (**14b**). 9.6.17.1. Step 1.* Coupling of intermediate **25b** (106 mg) with boronic acid **26** (R^2 = f3) gave the bisphosphonate tetraester precursor of **14b** as a white solid (115 mg, 76%).

^{1}H NMR (500 MHz, DMSO-d_6): δ 10.48 (s, 1H), 9.05 (d, J = 9.7 Hz, 1H), 8.98−8.91 (m, 1H), 8.73 (s, 1H), 8.58 (dt, J = 8.0, 1.3 Hz, 1H), 8.02 (ddd, J = 7.6, 1.9, 1.2 Hz, 1H), 7.77 (dd, J = 13.7, 2.5 Hz, 1H), 7.67 (t, J = 7.8 Hz, 1H), 7.57 (dt, J = 9.1, 1.9 Hz, 1H), 7.18 (t, J = 9.3 Hz, 1H), 6.11−5.91 (m, 1H), 4.42 (q, J = 7.3 Hz, 2H), 4.19−4.03 (m, 8H), 3.84 (s, 3H), 1.53 (t, J = 7.3 Hz, 3H), 1.53 (t, J = 7.3 Hz, 3H), 1.17 (t, J = 7.1 Hz, 6H), 1.11 (t, J = 7.0 Hz, 6H).

^{31}P NMR (203 MHz, DMSO-d_6): δ 16.92.

MS [ESI$^-$] m/z: 691.45 [M − H$^+$]$^-$.

9.6.17.2. Step 2. The tetraester precursor (98 mg) was deprotected using TMSI followed by MeOH to give inhibitor **14b** as a white solid (63 mg, 77%).

^{1}H NMR (800 MHz, DMSO-d_6, 333 K): δ 10.36 (s, 1H), 9.04 (s, 1H), 8.79 (s, 1H), 8.64 (d, J = 7.7 Hz, 1H), 8.09 (d, J = 7.6 Hz, 1H), 7.84 (dd, J = 13.7, 2.5 Hz, 1H), 7.70 (t, J = 7.7 Hz, 1H), 7.63 (dd, J = 8.8, 2.4 Hz, 1H), 7.21 (t, J = 9.3 Hz, 1H), 5.43 (t, J = 21.1 Hz, 1H), 4.42 (q, J = 7.3 Hz, 2H), 3.90 (s, 3H), 1.56 (t, J = 7.3 Hz, 3H).

^{31}P NMR (162 MHz, DMSO-d_6, 313 K): δ 13.60.

^{13}C NMR (201 MHz, DMSO-d_6, 333 K): δ 165.8, 158.8, 157.3, 152.1, 150.9, 143.9 (d, J = 10.9 Hz), 137.7, 135.5, 133.2 (d, J = 9.5 Hz), 131.8, 130.1, 128.9, 128.0, 126.5, 117.0, 114.8, 109.4 (d, J = 22.7 Hz), 101.2, 56.9, 49.7 (t, J = 132.6 Hz), 48.7, 15.4.

HRMS [ESI$^-$] calcd for $C_{22}H_{23}FN_6O_8P_2$ m/z: 579.0964; found, 579.0968 [M − H]$^-$.

*9.6.18. 2,6-Dichloro-9-methyl-9H-purine (**28**).* 2,6-Dichloro-7*H*-purine (**27**, 10.0 g, 52.9 mmol, 1.0 equiv) was dissolved in anhydrous DMF (100 mL), and K_2CO_3 (36.8 g, 266 mmol, 5.0 equiv) was added followed by MeI (9.9 mL, 159 mmol, 3.0 equiv). The reaction mixture was stirred at room temperature for 1.5 h. The reaction was subsequently diluted with brine, extracted with EtOAc (3× 50 mL), dried over anhydrous $MgSO_4$, and concentrated under vacuum. The crude mixture was purified on silica gel by flash chromatography, using a solvent gradient from 0 to 20% MeOH in EtOAc. Intermediate **28** was isolated as a white solid (6.46 g, 60%).

^{1}H NMR (400 MHz, $CDCl_3$): δ 8.11 (s, 1H), 3.94 (s, 3H).

^{13}C NMR (126 MHz, $CDCl_3$): δ 153.5, 153.0, 151.7, 146.4, 130.7, 30.5.

MS [ESI$^+$] m/z: 203.06 [M + H$^+$]$^+$.

*9.6.19. 2-Chloro-9-methyl-9H-purin-6-amine (**30**).* Intermediate **28** (4.65 g, 23.0 mmol, 1.0 equiv) and dioxane (20 mL) were added to a pressure vessel followed by aqueous NH_4OH (28%, 81 mL, 583 mmol, 25 equiv), and the reaction was stirred at 95 °C for 16 h. The reaction mixture was cooled to RT and concentrated under vacuum, leading to the precipitation of the product, which was collected by vacuum filtration and washed with water to obtain **30** as a white solid (3.78 g, 90%).

^{1}H NMR (400 MHz, DMSO-d_6): δ 8.10 (s, 1H), 7.72 (s, 2H), 3.69 (s, 3H).

^{13}C NMR (126 MHz, DMSO-d_6): δ 157.2, 153.4, 151.4, 142.5, 118.1, 30.0.

MS [ESI$^+$] m/z: 184.13 [M + H$^+$]$^+$.

*9.6.20. Tetraethyl (((2-Chloro-9-methyl-9H-purin-6-yl)amino)-methylene)bis(phosphonate) (**31**).* Following the general procedure for bisphosphonate synthesis previously reported,[9a] the bisphosphonate tetraethyl ester intermediate **31** was obtained from **30** (3.78 g) as a white solid (1.30 g, 13%).

^{1}H NMR (400 MHz, $CDCl_3$): δ 7.79 (s, 1H), 6.55 (d, J = 10.1 Hz, 1H), 5.59 (td, J = 22.0, 10.1 Hz, 1H), 4.32−4.17 (m, 8H), 3.83 (s, 3H), 1.37−1.21 (m, 12H).

^{31}P NMR (162 MHz, $CDCl_3$): δ 16.01.

^{13}C NMR (126 MHz, $CDCl_3$): δ 154.0, 153.6, 151.4, 141.6, 119.0, 63.7 (d, J = 10.1 Hz), 44.7 (t, J = 146.3 Hz), 30.1, 16.33 (d, J = 8.4 Hz).

MS [ESI$^-$] m/z: 468.18 [M − H$^+$]$^-$.

*9.6.21. (((2-(3-((4-Fluorophenyl)carbamoyl)phenyl)-9-methyl-9H-purin-6-yl)amino)methylene)bis(phosphonic Acid) (**15a**). 9.6.21.1. Step 1.* Coupling of intermediate **31** (150 mg) with boronic acid **26** (R^2 = f1) gave the bisphosphonate tetraester precursor of **15a** as a white solid (159 mg, 77%).

^{1}H NMR (400 MHz, $CDCl_3$): δ 9.24 (s, 1H), 8.77 (s, 1H), 8.67 (d, J = 7.8 Hz, 1H), 8.11 (d, J = 7.7 Hz, 1H), 7.87−7.78 (m, 3H), 7.62 (t, J = 7.7 Hz, 1H), 7.09 (t, J = 8.6 Hz, 2H), 6.21 (d, J = 9.3 Hz, 1H), 5.67 (td, J = 22.6, 9.3 Hz, 1H), 4.32−4.12 (m, 8H), 3.94 (s, 3H), 1.30 (t, J = 7.1 Hz, 6H), 1.22 (t, J = 7.0 Hz, 6H).

^{31}P NMR (162 MHz, $CDCl_3$): δ 16.83.

MS [ESI$^-$] m/z: 647.32 [M − H$^+$]$^-$.

9.6.21.2. Step 2. The tetraester precursor (49 mg) was deprotected using TMSI followed by MeOH to give inhibitor **15a** as a white solid (21 mg, 51%).

https://doi.org/10.1021/acs.jmedchem.3c01271
J. Med. Chem. 2023, 66, 15776−15800

^{1}H NMR (800 MHz, D_2O, 333 K): δ 9.09 (s, 1H), 8.87 (d, J = 7.3 Hz, 1H), 8.34 (s, 1H), 8.32 (d, J = 7.8 Hz, 1H), 8.02 (t, J = 7.7 Hz, 1H), 7.90 (dd, J = 8.8, 5.0 Hz, 2H), 7.54 (t, J = 8.9 Hz, 2H), 5.40 (t, J = 18.7 Hz, 1H), 4.18 (s, 3H).

^{31}P NMR (162 MHz, D_2O, 313 K): δ 14.10.

^{13}C NMR (201 MHz, D_2O, 333 K): δ 169.8, 160.6 (d, J = 241.8 Hz), 159.8, 154.7, 150.0, 142.9, 139.3, 134.7, 133.7, 132.5, 129.6, 129.5, 127.3, 125.6 (d, J = 8.4 Hz), 118.7, 116.1 (d, J = 22.8 Hz), 51.5 (t, J = 126.2 Hz), 30.2.

HRMS [ESI$^-$] calcd for $C_{20}H_{19}FN_6O_7P_2$ m/z: 535.0702; found, 535.0702 [M − H]$^-$.

*9.6.22. (((9-Methyl-2-(3-((4-(trifluoromethyl)phenyl)carbamoyl)-phenyl)-9H-purin-6-yl)amino)methylene)bis(phosphonic Acid) (**15b**). 9.6.22.1. Step 1.* Coupling of intermediate **31** (151 mg) with boronic acid **26** (R^2 = f2) gave the bisphosphonate tetraester precursor of **15b** as a white solid (86 mg, 38%).

^{1}H NMR (400 MHz, $CDCl_3$): δ 9.27 (d, J = 13.2 Hz, 2H), 8.66−8.59 (m, 1H), 8.08 (dd, J = 18.7, 8.2 Hz, 3H), 7.83 (s, 1H), 7.65−7.53 (m, 3H), 6.22 (dd, J = 9.3, 3.2 Hz, 1H), 5.65 (td, J = 22.7, 9.1 Hz, 1H), 4.32−4.08 (m, 8H), 3.87 (s, 3H), 1.31 (t, J = 7.1 Hz, 6H), 1.22 (t, J = 7.1 Hz, 6H).

^{31}P NMR (162 MHz, $CDCl_3$): δ 16.83.

MS [ESI$^-$] m/z: 697.31 [M − H$^+$]$^-$.

9.6.22.2. Step 2. The tetraester precursor (56 mg) was deprotected using TMSI followed by MeOH to give inhibitor **15b** as a white solid (30 mg, 70%).

^{1}H NMR (800 MHz, D_2O, 333 K): δ 9.12 (s, 1H), 8.89 (d, J = 7.6 Hz, 1H), 8.34 (d, J = 6.5 Hz, 2H), 8.15−8.08 (m, 4H), 8.03 (t, J = 7.8 Hz, 1H), 5.41 (t, J = 18.8 Hz, 1H), 4.18 (s, 3H).

^{31}P NMR (162 MHz, D_2O, 313 K): δ 14.09.

^{13}C NMR (201 MHz, D_2O, 333 K): δ 169.7, 159.8, 154.7, 150.0, 142.9, 141.6, 139.3, 134.8, 132.6, 132.2, 129.6 (d, J = 8.2 Hz), 127.4, 126.7, 126.5, 124.6 (q, J = 272.9 Hz), 122.7, 118.7, 51.5 (t, J = 126.0 Hz), 30.2.

HRMS [ESI$^-$] calcd for $C_{21}H_{19}F_3N_6O_7P_2$ m/z: 585.0670; found, 585.0657 [M − H]$^-$.

*9.6.23. (((2-(3-((3-Fluoro-4-methoxyphenyl)carbamoyl)phenyl)-9-methyl-9H-purin-6-yl)amino)methylene)bis(phosphonic Acid) (**15c**). 9.6.23.1. Step 1.* Coupling of intermediate **31** (101 mg) with boronic acid **26** (R^2 = f3) gave the bisphosphonate tetraester precursor of **15c** as a white solid (81 mg, 56%).

^{1}H NMR (400 MHz, $CDCl_3$): δ 9.15 (s, 1H), 8.87 (s, 1H), 8.53 (dt, J = 7.8, 1.3 Hz, 1H), 8.01 (d, J = 7.7 Hz, 1H), 7.74 (s, 1H), 7.63 (dd, J = 13.1, 2.5 Hz, 1H), 7.51 (dt, J = 15.4, 8.4 Hz, 2H), 6.86 (t, J = 9.1 Hz, 1H), 6.15 (d, J = 9.2 Hz, 1H), 5.54 (td, J = 22.7, 9.2 Hz, 1H), 4.24−3.98 (m, 8H), 3.81 (d, J = 2.3 Hz, 6H), 1.20 (t, J = 7.1 Hz, 6H), 1.11 (t, J = 7.0 Hz, 5H).

^{31}P NMR (162 MHz, $CDCl_3$): δ 16.89.

MS [ESI$^-$] m/z: 677.24 [M − H$^+$]$^-$.

9.6.23.2. Step 2. The tetraester precursor (64 mg) was deprotected using TMSI followed by MeOH to give inhibitor **15c** as a white solid (43 mg, 80%).

^{1}H NMR (800 MHz, D_2O, 333 K): δ 9.08 (s, 1H), 8.87 (d, J = 7.8 Hz, 1H), 8.34 (s, 1H), 8.31 (d, J = 7.8 Hz, 1H), 8.02 (t, J = 7.8 Hz, 1H), 7.85−7.80 (m, 1H), 7.65 (d, J = 8.8 Hz, 1H), 7.53 (t, J = 9.1 Hz, 1H), 5.39 (t, J = 18.9 Hz, 1H), 4.25 (d, J = 0.8 Hz, 3H), 4.18 (s, 3H).

^{31}P NMR (162 MHz, D_2O, 313 K): δ 13.89.

^{13}C NMR (201 MHz, D_2O, 333 K): δ 169.6, 159.8, 154.7, 152.1 (d, J = 242.2 Hz), 150.0, 145.0 (d, J = 10.8 Hz), 142.9, 139.3, 134.7, 132.5, 131.3 (d, J = 9.5 Hz), 129.6, 129.5, 127.3, 119.7, 118.7 (d, J = 5.9 Hz), 115.1, 111.9 (d, J = 21.5 Hz), 57.2, 51.5 (t, J = 126.1 Hz), 30.2 (d, J = 4.1 Hz).

HRMS [ESI$^-$] calcd for $C_{21}H_{21}FN_6O_8P_2$ m/z: 565.0807; found, 565.0826 [M − H]$^-$.

9.7. Protocols for the In Vivo Efficacy Studies. Immunodeficient laboratory mice (NSG) were bred at the Research Institute of the McGill University Health Center (RI-MUHC), maintained in a pathogen-free standard animal facility with a light/dark cycle of 12 h, and provided with food and water ad libitum. Aged mice (n = 17, 5 male and 12 female; average 8 weeks old) were injected subcutaneously with 50 μL of pathogen-free MM cells (8×10^6 RPMI-8226 cells) premixed with 50 μL of Matrigel matrix and allowed to grow for another 8−10 days for their tumor size to reach approximately 120−150 mm^3 (measured using a calliper), before initiation of dosing with inhibitor RB-07-16 or vehicle control. At that point, the mice were randomly divided into two groups and dosed by intraperitoneal injection (I.P.) three times per week for a total of 12 doses with either vehicle control (PBS, n = 8, 2 male and 6 female) or 3 mg/kg of inhibitor RB-07-16 dissolved in PBS (n = 9, 3 male and 6 female) as the trisodium salt. The animals were observed daily for any signs of overt toxicity, such as significant weight loss, decreased mobility, skin lesions, inflammation at the site of injection, or morbidity, according to the Facility Animal Care Committees protocol number MUHC-7242 from the RI-MUHC (Glen site) and in accordance with the Policies and Guidelines of the Canadian Council on Animal Care (CCAC). We acknowledge that in this study, the number of male and female animals was not equal due to the limited number of male animals available at the time of this study in our own facility.

Using a similar protocol to the above, pathogen-free MIA PaCa-2 cells (4×10^6), suspended in a solution of Matrigel matrix and PBS (1:1), were injected subcutaneously into the right flanks of 6 week-old NSG mice (n = 27). The mice were maintained in a pathogen-free standard animal facility with a light/dark cycle of 12 h and provided with food and water ad libitum. Dosing was initiated 6 days later, when the tumors had reached approximately 150 mm^3 size. The animals were randomly divided into two groups of approximately the same number of male/female animals and dosed I.P. with either PBS vehicle (n = 13, 6M/7F) or 3 mg/kg of RB-07-16 dissolved in PBS as the trisodium salt (n = 14, 6M/8F), three times per week for a total of 12 doses. The animals were observed daily for any signs of overt toxicity, such as weight loss, decreased mobility, skin lesions, and inflammation at the site of injection, or morbidity, according to the Facility Animal Care Committees protocol number MUHC-10021.

■ ASSOCIATED CONTENT

Supporting Information

The Supporting Information is available free of charge at https://pubs.acs.org/doi/10.1021/acs.jmedchem.3c01271.

Methods for biological assays; and ^{1}H, ^{13}C, ^{31}P NMR spectra and HPLC chromatograms for final inhibitors (PDF)

Molecular formula strings and biological data (CSV)

■ AUTHOR INFORMATION

Corresponding Author

Youla S. Tsantrizos − *Department of Chemistry, McGill University, Montreal, Québec H3A 0B8, Canada; Department of Biochemistry, McGill University, Montreal, Québec H3G 1Y6, Canada;* orcid.org/0000-0002-6231-7498; Email: youla.tsantrizos@mcgill.ca

Authors

Rebecca Boutin − *Department of Chemistry, McGill University, Montreal, Québec H3A 0B8, Canada*

Hiu-Fung Lee − *Department of Chemistry, McGill University, Montreal, Québec H3A 0B8, Canada*

Tian Lai Guan − *Department of Chemistry, McGill University, Montreal, Québec H3A 0B8, Canada; Department of Biochemistry, McGill University, Montreal, Québec H3G 1Y6, Canada*

Tan Trieu Nguyen − *Department of Medicine, McGill University, Montreal, Québec H3A 1A1, Canada*

Xian Fang Huang − *Department of Medicine, McGill University, Montreal, Québec H3A 1A1, Canada*

Daniel D. Waller − *Terry Fox Laboratory, BC Cancer Research Institute, Vancouver, British Columbia V5Z 1L3, Canada*

Jordan Lu − *Institute for Cancer Genetics, Department of Genetics and Development, Columbia University Irving Medical Center, New York, New York 10032, United States*
Iok In Christine Chio − *Institute for Cancer Genetics, Department of Genetics and Development and Herbert Irving Comprehensive Cancer Center, Columbia University Irving Medical Center, New York, New York 10032, United States*
René P. Michel − *Department of Pathology, McGill University, Montréal, Québec H3A 1A1, Canada*
Michael Sebag − *Department of Medicine, McGill University, Montreal, Québec H3A 1A1, Canada; Division of Hematology, McGill University Health Center, Montreal, Québec H4A 3J1, Canada*

Complete contact information is available at:
https://pubs.acs.org/10.1021/acs.jmedchem.3c01271

Author Contributions

Y.S.T. conceptualized and coordinated this project and wrote the manuscript; R.B., H.-F.L., M.S., D.D.W, I.I.C., R.P.M. participated in the editing of the final manuscript; M.S. coordinated the hematology, cellular, and in vivo studies. R.B. and H.-F.L synthesized the inhibitors; T.L.G. performed the in vitro inhibition assays; D.D.W. guided the cell-based assays and the CRISPR spCas9-mediated knockout studies for *GGPS1* and *FDPS* and evaluated the SD of the results observed in the in vivo study in the xenograft PDAC (MIA PaCa-2) model; T.T.N. and T.L.G. performed the cell-based assays; D.D.W. and X.F.H. performed and analyzed the in vivo efficacy studies; I.I.C and J.L. performed and wrote the section on the PDAC organoids; and R.P.M. coordinated the processing of the livers for histopathology, performed the grading of the putative histopathologic findings, and wrote the related sections of the manuscript.

Notes

The authors declare no competing financial interest.

■ ACKNOWLEDGMENTS

We are grateful for ADME and PK studies conducted by Kathryn Skorey, Linh Nguyen, Harun Rashid, Julien Breault-Turcot, and Annie Run Qi Shao at NuChem Sciences Inc. We also wish to thank Mònica Gómez Palou for initiating the CRISPER knockout studies for *GGPS1* and *FDPS*. Financial support for this work was provided by the Canadian Institute of Health Research (CIHR) grants to M.S. and Y.S.T.

■ ABBREVIATIONS

C2-Pur-BP, C2-substituted purine-based bisphosphonate; C6-PyraP-BP, C6-substituted pyrazolopyrimidine-based bisphosphonate; C2-ThP-BP, C2-substituted thienopyrimidine-based bisphosphonate; CRC, colorectal cancer; DLM, dog liver microsomes; FTase, farnesyl transferase; GGTase I, II, and III, geranylgeranyl transferase I, II, and III; GTPases, small GTP-binding proteins; hFPPS, human farnesyl pyrophosphate synthase; hGGPPS, human geranylgeranyl pyrophosphate synthase; HLM, human liver microsomes; IP, intraperitoneal injection; IV, intravenous injection; MLM, mouse liver microsomes; MM, multiple myeloma; PBS, phosphate buffered saline; PDAC, pancreatic ductal adenocarcinoma; RLM, rat liver microsomes

■ REFERENCES

(1) Reviews: (a) Hessler, G.; Baringhaus, K.-H. The scaffold hopping potential of pharmacophores. *Drug Discovery Today: Technol.* **2010**, *7*, e263−e269. (b) Hu, Y.; Stumpfe, D.; Bajorath, J. Recent advances in scaffold hopping. *J. Med. Chem.* **2017**, *60*, 1238−1246. (c) Recent examples: Tanaka, Y.; Seto, M.; Kakegawa, K.; Takami, K.; Kikuchi, F.; Yamamoto, T.; Nakamura, M.; Daini, M.; Murakami, M.; Ohashi, T.; Kasahara, T.; Wang, J.; Ikeda, Z.; Wada, Y.; Puenner, F.; Fujii, T.; Inazuka, M.; Sato, S.; Suzaki, T.; Oak, J.-H.; Takai, Y.; Kohara, H.; Kimoto, K.; Oki, H.; Mikami, S.; Sasaki, M.; Tanaka, Y. Discovery of Brain-Penetrant Glucosylceramide Synthase Inhibitors with a Novel Pharmacophore. *J. Med. Chem.* **2022**, *65*, 4270−4290. (d) Szabó, G.; Éliás, O.; Erdélyi, P.; Potor, A.; Túrós, G. I.; Károlyi, B. I.; Varró, G.; Vaskó, Á. G.; Bata, I.; Kapus, G. L.; Dohányos, Z.; Bobok, A. Á.; Fodor, L.; Thán, M.; Vastag, M.; Komlódi, Z.; Soukupné Kedves, R. É.; Makó, É.; Süveges, B.; Greiner, I. Multiparameter optimization of naphthyridine derivatives as selective α5-GABA$_A$ receptor negative allosteric modulators. *J. Med. Chem.* **2022**, *65*, 7876−7895. (e) Zhang, J.; Jiang, H.; Lin, S.; Wu, D.; Tian, H.; Jiang, L.; Cui, Y.; Jin, J.; Chen, X.; Xu, H. Design and optimization of thienopyrimidine derivatives as potent and selective PI3Kδ inhibitors for the treatment of B-cell malignancies. *J. Med. Chem.* **2022**, *65*, 8011−8028. (f) Wang, W.; He, J.; Yang, J.; Zhang, C.; Cheng, Z.; Zhang, Y.; Zhang, Q.; Wang, P.; Tang, S.; Wang, X.; Liu, M.; Lu, W.; Zhang, H.-K. Scaffold hopping strategy to identify prostanoid EP4 receptor antagonists for cancer immunotherapy. *J. Med. Chem.* **2022**, *65*, 7896−7917. (h) Ladduwahetty, T.; Lee, M. R.; Maillard, M. C.; Cachope, R.; Todd, D.; Barnes, M.; Beaumont, V.; Chauhan, A.; Gallati, C.; Haughan, A. F.; Kempf, G.; Luckhurst, C. A.; Matthews, K.; McAllister, G.; Mitchell, P.; Patel, H.; Rose, M.; Saville-Stones, E.; Steinbacher, S.; Stott, A. J.; Thatcher, E.; Tierney, J.; Urbonas, L.; Munoz-Sanjuan, I.; Dominguez, C. Identification of a potent, selective, and brain-penetrant Rho kinase inhibitor and its activity in a mouse model of Huntington's disease. *J. Med. Chem.* **2022**, *65*, 9819−9845.

(2) (a) Fader, L. D.; Carson, R.; Morin, S.; Bilodeau, F.; Chabot, C.; Halmos, T.; Bailey, M. D.; Kawai, S. H.; Coulombe, R.; Laplante, S.; Mekhssian, K.; Jakalian, A.; Garneau, M.; Duan, J.; Mason, S. W.; Simoneau, B.; Fenwick, C.; Tsantrizos, Y.; Yoakim, C. Minimizing the Contribution of Enterohepatic Recirculation to Clearance in Rat for the NCINI Class of Inhibitors of HIV. *ACS Med. Chem. Lett.* **2014**, *5*, 711−716. (b) Fader, L. D.; Bailey, M.; Beaulieu, E.; Bilodeau, F.; Bonneau, P.; Bousquet, Y.; Carson, R. J.; Chabot, C.; Coulombe, R.; Duan, J.; Fenwick, C.; Garneau, M.; Halmos, T.; Jakalian, A.; James, C.; Kawai, S. H.; Landry, S.; LaPlante, S. R.; Mason, S. W.; Morin, S.; Rioux, N.; Simoneau, B.; Surprenant, S.; Thavonekham, B.; Thibeault, C.; Trinh, T.; Tsantrizos, Y. S.; Tsoung, J.; Yoakim, C.; Wernic, D. Aligning potency and pharmacokinetic properties for pyridine-based NCINIs. *ACS Med. Chem. Lett.* **2016**, *7*, 797−801.

(3) Owen, D. R.; Allerton, C. M. N.; Anderson, A. S.; Aschenbrenner, L.; Avery, M.; Berritt, S.; Boras, B.; Cardin, R. D.; Carlo, A.; Coffman, K. J.; Dantonio, A.; Di, L.; Eng, H.; Ferre, R. A.; Gajiwala, K. S.; Gibson, S. A.; Greasley, S. E.; Hurst, B. L.; Kadar, E. P.; Kalgutkar, A. S.; Lee, J. C.; Lee, J.; Liu, W.; Mason, S. W.; Noell, S.; Novak, J. J.; Obach, R. S.; Ogilvie, K.; Patel, N. C.; Pettersson, M.; Rai, D. K.; Reese, M. R.; Sammons, M. F.; Sathish, J. G.; Singh, R. S. P.; Steppan, C. M.; Stewart, A. E.; Tuttle, J. B.; Updyke, L.; Verhoest, P. R.; Wei, L.; Yang, Q.; Zhu, Y. An oral SARS-CoV-2 M^{pro} inhibitor clinical candidate for the treatment of COVID-19. *Science* **2021**, *374*, 1586−1593.

(4) (a) Lin, Y.-S.; Park, J.; De Schutter, J. W.; Huang, X. F.; Berghuis, A. M.; Sebag, M.; Tsantrizos, Y. S. Design and synthesis of active site inhibitors of the human farnesyl pyrophosphate synthase: Apoptosis and inhibition of ERK phosphorylation in multiple myeloma cells. *J. Med. Chem.* **2012**, *55*, 3201−3215. (b) Leung, C. Y.; Park, J.; De Schutter, J. W.; Sebag, M.; Berghuis, A. M.; Tsantrizos, Y. S. Thienopyrimidine bisphosphonate (ThPBP) inhibitors of the human farnesyl pyrophosphate synthase: Optimization and characterization of the mode of inhibition. *J. Med. Chem.* **2013**, *56*, 7939−7950. (c) Park, J.; Leung, C. Y.; Matralis, A. N.; Lacbay, C. M.; Tsakos, M.; Fernandez De Troconiz, G.; Berghuis, A. M.; Tsantrizos, Y. S. Pharmacophore mapping of thienopyrimidine-based monophosphonate (ThP-MP) inhibitors of the human farnesyl pyrophosphate synthase. *J. Med. Chem.* **2017**, *60*, 2119−2134.

(5) (a) De Schutter, J. W.; Park, J.; Leung, C. Y.; Gormley, P.; Lin, Y.-S.; Hu, Z.; Berghuis, A. M.; Poirier, J.; Tsantrizos, Y. S. Multistage Screening Reveals Chameleon Ligands of the Human Farnesyl Pyrophosphate Synthase: Implications to Drug Discovery for Neurodegenerative Diseases. *J. Med. Chem.* **2014**, *57*, 5764−5776. (b) Pelleieux, S.; Picard, C.; Lamarre-Théroux, L.; Dea, D.; Leduc, V.; Tsantrizos, Y. S.; Poirier, J. Isoprenoids and tau pathology in sporadic Alzheimer's disease. *Neurobiol. Aging* **2018**, *65*, 132−139.

(6) (a) Reviews: Karnoub, A. E.; Weinberg, R. A. Ras oncogenes: split personalities. *Nat. Rev. Mol. Cell Biol.* **2008**, *9*, 517−531. (b) Simanshu, D. K.; Nissley, D. V.; McCormick, F. RAS proteins and their regulators in human disease. *Cell* **2017**, *170*, 17−33.

(7) For a review see: Lawson, C. D.; Ridley, A. J. Rho GTPase signaling complexes in cell migration and invasion. *J. Cell Biol.* **2018**, *217*, 447−457.

(8) Some representative examples: (a) Shull, L. W.; Wiemer, A. J.; Hohl, R. J.; Wiemer, D. F. Synthesis and biological activity of isoprenoid bisphosphonates. *Bioorg. Med. Chem.* **2006**, *14*, 4130−4136. (b) Zhang, Y.; Cao, R.; Yin, F.; Hudock, M. P.; Guo, R.-T.; Krysiak, K.; Mukherjee, S.; Gao, Y.-G.; Robinson, H.; Song, Y.; No, J. H.; Bergan, K.; Leon, A.; Cass, L.; Goddard, A.; Chang, T.-K.; Lin, F.-Y.; Beek, E. V.; Papapoulos, S.; Wang, A. H.-J.; Kubo, T.; Ochi, M.; Mukkamala, D.; Oldfield, E. Lipophilic Bisphosphonates as Dual Farnesyl/Geranylgeranyl Diphosphate Synthase Inhibitors: An X-ray and NMR Investigation. *J. Am. Chem. Soc.* **2009**, *131*, 5153−5162. (c) Zhang, Y.; Cao, R.; Yin, F.; Lin, F.-Y.; Wang, H.; Krysiak, K.; No, J.-H.; Mukkamala, D.; Houlihan, K.; Li, J.; Morita, C. T.; Oldfield, E. Lipophilic pyridinium bisphosphonates: Potent $\gamma\delta$ T cell stimulators. *Angew. Chem., Int. Ed.* **2010**, *49*, 1136−1138. (d) Wills, V. S.; Allen, C.; Holstein, S. A.; Wiemer, D. F. Potent triazole bisphosphonate inhibitor of geranylgeranyl diphosphate synthase. *ACS Med. Chem. Lett.* **2015**, *6*, 1195−1198. (e) Haney, S. L.; Chhonker, Y. S.; Varney, M. L.; Talmon, G.; Smith, L. M.; Murry, D. J.; Holstein, S. A. In vivo evaluation of isoprenoid triazole bisphosphonate inhibitors of geranylgeranyl diphosphate synthase: Impact of olefin stereochemistry on toxicity and biodistribution. *J. Pharmacol. Exp. Therapeut.* **2019**, *371*, 327−338.

(9) (a) Lacbay, C. M.; Waller, D. D.; Park, J.; Gómez Palou, M.; Vincent, F.; Huang, X. F.; Ta, V.; Berghuis, A. M.; Sebag, M.; Tsantrizos, Y. S. Unraveling the prenylation-cancer paradox in multiple myeloma with novel geranylgeranyl pyrophosphate synthase (GGPPS) inhibitors. *J. Med. Chem.* **2018**, *61*, 6904−6917. (b) Lee, H.-F.; Lacbay, C. M.; Boutin, R.; Matralis, A. N.; Park, J.; Waller, D. D.; Guan, T. L.; Sebag, M.; Tsantrizos, Y. S. Synthesis and evaluation of structurally diverse C-2 substituted thienopyrimidine-based inhibitors of the human geranylgeranyl pyrophosphate synthase. *J. Med. Chem.* **2022**, *65*, 2471−2496.

(10) (a) Mullen, P. J.; Yu, R.; Longo, J.; Archer, M. C.; Penn, L. Z. The interplay between cell signalling and the mevalonate pathway in cancer. *Nat. Rev. Cancer* **2016**, *16*, 718−731. (b) Clendening, J. W.; Pandyra, A.; Boutros, P. C.; Ghamrasni, S. E.; Khosravi, F.; Trentin, G. A.; Martirosyan, A.; Hakem, A.; Hakem, R.; Jurisica, I.; Penn, L. Z. Dysregulation of the mevalonate pathway promotes transformation. *Proc. Natl. Acad. Sci. U.S.A.* **2010**, *107*, 15051−15056. (c) Sorrentino, G.; Ruggeri, N.; Specchia, V.; Cordenonsi, M.; Mano, M.; Dupont, S.; Manfrin, A.; Ingallina, E.; Sommaggio, R.; Piazza, S.; Rosato, A.; Piccolo, S.; Del Sal, G. Metabolic control of YAP and TAZ by the mevalonate pathway. *Nat. Cell Biol.* **2014**, *16*, 357−366. (d) Laggner, U.; Lopez, J. S.; Perera, G.; Warbey, V. S.; Sita-Lumsden, A.; O'Doherty, M. J.; Hayday, A.; Harries, M.; Nestle, F. O. Regression of melanoma metastases following treatment with the n-bisphosphonate zoledronate and localised radiotherapy. *Clin. Immunol.* **2009**, *131*, 367−373.

(11) Kazi, A.; Xiang, S.; Yang, H.; Chen, L.; Kennedy, P.; Ayaz, M.; Fletcher, S.; Cummings, C.; Lawrence, H. R.; Beato, F.; Kang, Y.; Kim, M. P.; Delitto, A.; Underwood, P. W.; Fleming, J. B.; Trevino, J. G.; Hamilton, A. D.; Sebti, S. M. Dual farnesyl and geranylgeranyl transferase inhibitor thwarts mutant KRAS-driven patient derived pancreatic tumors. *Clin. Cancer Res.* **2019**, *25*, 5984−5996.

(12) (a) Holstein, S. A.; Hohl, R. J. Isoprenoid biosynthetic pathway inhibition disrupts monoclonal protein secretion and induces the unfolded protein response pathway in multiple myeloma cells. *Leuk. Res.* **2011**, *35*, 551−559. (b) Haney, S. L.; Varney, M. L.; Chhonker, Y. S.; Shin, S.; Mehla, K.; Crawford, A. J.; Smith, H. J.; Smith, L. M.; Murry, D. J.; Hollingsworth, M. A.; Holstein, S. A. Inhibition of geranylgeranyl diphosphate synthase is a novel therapeutic strategy for pancreatic ductal adenocarcinoma. *Oncogene* **2019**, *38*, 5308−5320.

(13) Martin, N. E.; Brunner, T. B.; Kiel, K. D.; DeLaney, T. F.; Regine, W. F.; Mohiuddin, M.; Rosato, E. F.; Haller, D. G.; Stevenson, J. P.; Smith, D.; Pramanik, B.; Tepper, J.; Tanaka, W. K.; Morrison, B.; Deutsch, P.; Gupta, A. K.; Muschel, R. J.; McKenna, W. G.; Bernhard, E. J.; Hahn, S. M. A phase I trial of the dual farnesyltransferase and geranylgeranyltransferase inhibitor L-778,123 and radiotherapy for locally advanced pancreatic cancer. *Clin. Cancer Res.* **2004**, *10*, 5447−5454.

(14) Takai, Y.; Sasaki, T.; Matozaki, T. Small GTP-binding proteins. *Physiol. Rev.* **2001**, *81*, 153−208.

(15) Nguyen, U. T. T.; Guo, Z.; Delon, C.; Wu, Y.; Deraeve, C.; Fränzel, B.; Bon, R. S.; Blankenfeldt, W.; Goody, R. S.; Waldmann, H.; Wolters, D.; Alexandrov, K. Analysis of the eukaryotic prenylome by isoprenoid affinity tagging. *Nat. Chem. Biol.* **2009**, *5*, 227−235.

(16) (a) Yokoyama, K.; Zimmerman, K.; Scholten, J.; Gelb, M. H. Differential prenyl pyrophosphate binding to mammalian protein geranylgeranyl transferase-I and protein farnesyltransferase and its consequence on the specificity of protein prenylation. *J. Biol. Chem.* **1997**, *272*, 3944−3952. (b) Rowinsky, E. K. Lately, it occurs to me what a long, strange trip it's been for the farnesyltransferase inhibitors. *J. Clin. Oncol.* **2006**, *24*, 2981−2984.

(17) Pandyra, A. A.; Mullen, P. J.; Goard, C. A.; Ericson, E.; Sharma, P.; Kalkat, M.; Yu, R.; Pong, J. T.; Brown, K. R.; Hart, T.; Gebbia, M.; Lang, K. S.; Giaever, G.; Nislow, C.; Moffat, J.; Penn, L. Z. Genome-wide RNAi analysis reveals that simultaneous inhibition of specific mevalonate pathway genes potentiates tumor cell death. *Oncotarget* **2015**, *6*, 26909−26921.

(18) Wong, C. C.; Wu, J.-L.; Ji, F.; Kang, W.; Bian, X.; Chen, H.; Chan, L.-S.; Luk, S. T. Y.; Tong, S.; Xu, J.; Zhou, Q.; Liu, D.; Su, H.; Gou, H.; Cheung, A. H.-K.; To, K. F.; Cai, Z.; Shay, J. W.; Yu, J. The cholesterol uptake regulator PCSK9 promotes and is a therapeutic target in APC/KRAS-mutant colorectal cancer. *Nat. Commun.* **2022**, *13*, 3971.

(19) Review: Deer, E. L.; González-Hernández, J.; Coursen, J. D.; Shea, J. E.; Ngatia, J.; Scaife, C. L.; Firpo, M. A.; Mulvihill, S. J. Phenotype and genotype of pancreatic cancer cell lines. *Pancreas* **2010**, *39*, 425−435.

(20) Sakamoto, K.; Qi, Y.; Miyako, E. Nanoformulation of the K-Ras(G12D)-inhibitory peptide KS-58 suppresses colorectal and pancreatic cancer-derived tumors. *Sci. Rep.* **2023**, *13*, 518.

(21) (a) Jahnke, W.; Rondeau, J.-M.; Cotesta, S.; Marzinzik, A.; Pellé, X.; Geiser, M.; Strauss, A.; Götte, M.; Bitsch, F.; Hemmig, R.; Henry, C.; Lehmann, S.; Glickman, J. F.; Roddy, T. P.; Stout, S. J.; Green, J. R. Allosteric non-bisphosphonate FPPS inhibitors identified by fragment-based discovery. *Nat. Chem. Biol.* **2010**, *6*, 660−666. (b) Marzinzik, A. L.; Amstutz, R.; Bold, G.; Bourgier, E.; Cotesta, S.; Glickman, J. F.; Götte, M.; Henry, C.; Lehmann, S.; Hartwieg, J. C. D.; Ofner, S.; Pellé, X.; Roddy, T. P.; Rondeau, J.-M.; Stauffer, F.; Stout, S. J.; Widmer, A.; Zimmermann, J.; Zoller, T.; Jahnke, W. Discovery of Novel Allosteric Non-Bisphosphonate Inhibitors of Farnesyl Pyrophosphate Synthase by Integrated Lead Finding. *ChemMedChem* **2015**, *10*, 1884−1891.

(22) Tsantrizos, Y. S.; Sebag, M. Substituted bicyclic pyrimidine-based compounds and composition and uses thereof. WO 2018137036 A1, 2018.

(23) Singla, P.; Luxami, V.; Singh, R.; Tandon, V.; Paul, K. Novel pyrazolo[3,4-d]pyrimidine with 4-(1*H*-benzimidazol-2-yl)-phenylamine as broad spectrum anticancer agents: Synthesis, cell based assay, topoisomerase inhibition, DNA intercalation and bovine serum albumin studies. *Eur. J. Med. Chem.* **2017**, *126*, 24−35.

(24) (a) Chuaqui, C. E.; Huang, S.; Ioannidis, S.; Shi, J.; Su, M.; Su, Q. Heterocyclic JAK kinase inhibitors. WO 2010038060 A1, 2010. (b) Gray, N. S.; Zhou, W. Compounds that modulate EGFR activity and methods for treating or preventing conditions therewith. WO 2011079231 A1, 2011. (c) Zeng, Q.; Huang, B.; Danielsen, K.; Shukla,

https://doi.org/10.1021/acs.jmedchem.3c01271
J. Med. Chem. 2023, 66, 15776−15800

R.; Nagy, T. Facile and practical synthesis of 2,6-dichloropurine. *Org. Process Res. Dev.* **2004**, *8*, 962−963.
(25) Mailyan, A. K.; Chen, J. L.; Li, W.; Keller, A. A.; Sternisha, S. M.; Miller, B. G.; Zakarian, A. Short Total Synthesis of [$^{15}N_5$]-Cylindrospermopsins from $^{15}NH_4Cl$ Enables Precise Quantification of Freshwater Cyanobacterial Contamination[$^{15}N_5$]-cylindrospermopsins from $^{15}NH_4Cl$ enables precise quantification of freshwater cyanobacterial contamination. *J. Am. Chem. Soc.* **2018**, *140*, 6027−6032.
(26) Liang, C.; Li, Z. PI3K/MTOR Kinase inhibitors. WO 2010056320 A2, 2010.
(27) Su, Q.; Ioannidis, S.; Chuaqui, C.; Almeida, L.; Alimzhanov, M.; Bebernitz, G.; Bell, K.; Block, M.; Howard, T.; Huang, S.; Huszar, D.; Read, J. A.; Rivard Costa, C.; Shi, J.; Su, M.; Ye, M.; Zinda, M. Discovery of 1-methyl-1*H*-imidazole derivatives as potent Jak2 inhibitors. *J. Med. Chem.* **2014**, *57*, 144−158.
(28) Hao, E. J.; Li, G. X.; Liang, Y. R.; Xie, M. S.; Wang, D. C.; Jiang, X. H.; Cheng, J. Y.; Shi, Z. X.; Wang, Y.; Guo, H. M. Design, synthesis, and activity evaluation of novel acyclic nucleosides as potential anticancer agents in vitro and in vivo. *J. Med. Chem.* **2021**, *64*, 2077−2109.
(29) Hopkins, B. T.; Ma, B.; Chan, T. R.; Kumaravel, G.; Miao, H.; Bertolotti-Ciarlet, A.; Otipoby, K. Biaryl compounds useful for the treatment of human diseases in oncology, neurology and immunology. WO 2015089327 A1, 2015.
(30) Boyle, R. G.; Walker, D. W. Substituted quinoxalines and benzotriazine P70S6 kinase inhibitors. WO 2016170163 A1, 2016.
(31) Bookser, B. C.; Weinhouse, M. I.; Burns, A. C.; Valiere, A. N.; Valdez, L. J.; Stanczak, P.; Na, J.; Rheingold, A. L.; Moore, C. E.; Dyck, B. Solvent-controlled, site-selective N-alkylation reactions of azolo-fused ring heterocycles at N1-N2-and N3-positions, including pyrazolo[3,4-*d*]pyrimidines, purines, [1,2,3]triazolo[4,5]pyridines, and related deaza-compounds. *J. Org. Chem.* **2018**, *83*, 6334−6353.
(32) (a) Kim, D. C.; Lee, Y. R.; Yang, B.-S.; Shin, K. J.; Kim, D. J.; Chung, B. Y.; Yoo, K. H. Synthesis and biological evaluations of pyrazolo[3,4-d]pyrimidines as cyclin-dependent kinase 2 inhibitors. *Eur. J. Med. Chem.* **2003**, *38*, 525−532. (b) Yin, Y.; Chen, C. J.; Yu, R. N.; Shu, L.; Zhang, T. T.; Zhang, D. Y. Discovery of novel selective Janus kinase 2 (JAK2) inhibitors bearing a 1*H*-pyrazolo[3,4-*d*]-pyrimidin-4-amino scaffold. *Bioorg. Med. Chem.* **2019**, *27*, 1562−1576.
(33) van de Bittner, G.; Hooker, J. M. Imaging agents for neural flux. WO 2016011394 A1, 2016.
(34) (a) McKenna, C. E.; Higa, M. T.; Cheung, N. H.; McKenna, M.-C. The facile dealkylation of phosphonic acid dialkyl esters by bromotrimethylsilane. *Tetrahedron Lett.* **1977**, *18*, 155−158. (b) Błażewska, K. M. McKenna reaction-which oxygen attacks bromotrimethylsilane? *J. Org. Chem.* **2014**, *79*, 408−412.
(35) Olah, G. A.; Narang, S. C.; Gupta, B. G. B.; Malhotra, R. Hexamethyldisilane/iodine: Convenient in situ generation of iodotrimethylsilane. *Angew. Chem., Int. Ed.* **1979**, *18*, 612−614.
(36) Waring, M. J.; Arrowsmith, J.; Leach, A. R.; Leeson, P. D.; Mandrell, S.; Owen, R. M.; Pairaudeau, G.; Pennie, W. D.; Pickett, S. D.; Wang, J.; Wallace, O.; Weir, A. An analysis of the attrition of drug candidates from four major pharmaceutical companies. *Nat. Rev. Drug Discovery* **2015**, *14*, 475−486.
(37) Chocry, M.; Leloup, L.; Parat, F.; Messé, M.; Pagano, A.; Kovacic, H. Gemcitabine: An alternative treatment for oxaliplatin-resistant colorectal cancer. *Cancers* **2022**, *14*, 5894.
(38) He, D.; Feng, H.; Sundberg, B.; Yang, J.; Powers, J.; Christian, A. H.; Wilkinson, J. E.; Monnin, C.; Avizonis, D.; Thomas, C. J.; Friedman, R. A.; Kluger, M. D.; Hollingsworth, M. A.; Grandgenett, P. M.; Klute, K. A.; Toste, F. D.; Chang, C. J.; Chio, I. I. C. Methionine oxidation activates pyruvate kinase M2 to promote pancreatic cancer metastasis. *Mol. Cell* **2022**, *82*, 3045−3060.e11.
(39) Recent Review: (a) Boj, S. F.; Hwang, C.-I.; Baker, L. A.; Chio, I. I. C.; Engle, D. D.; Corbo, V.; Jager, M.; Ponz-Sarvise, M.; Tiriac, H.; Spector, M. S.; Gracanin, A.; Oni, T.; Yu, K. H.; van Boxtel, R.; Huch, M.; Rivera, K. G.; Wilson, J. P.; Feigin, M. E.; Öhlund, D.; Handly-Santana, A.; Ardito-Abraham, C. M.; Ludwig, M.; Elyada, E.; Alagesan, B.; Biffi, G.; Yordanov, G. N.; Delcuze, B.; Creighton, B.; Wright, K.; Park, Y.; Morsink, F. H. M.; Molenaar, I. Q.; Borel Rinkes, I.; Cuppen, E.; Hao, Y.; Jin, Y.; Nijman, I. J.; Iacobuzio-Donahue, C.; Leach, S. D.; Pappin, D. J.; Hammell, M.; Klimstra, D. S.; Basturk, O.; Hruban, R. H.; Offerhaus, G. J.; Vries, R. G. J.; Clevers, H.; Tuveson, D. A. Organoid models of human and mouse ductal pancreatic cancer. *Cell* **2015**, *160*, 324−338. (b) Chio, I. I. C.; Jafarnejad, S. M.; Ponz-Sarvise, M.; Park, Y.; Rivera, K.; Palm, W.; Wilson, J.; Sangar, V.; Hao, Y.; Öhlund, D.; Wright, K.; Filippini, D.; Lee, E. J.; Da Silva, B.; Schoepfer, C.; Wilkinson, J. E.; Buscaglia, J. M.; DeNicola, G. M.; Tiriac, H.; Hammell, M.; Crawford, H. C.; Schmidt, E. E.; Thompson, C. B.; Pappin, D. J.; Sonenberg, N.; Tuveson, D. A. NRF2 Promotes tumor maintenance by modulating mRNA translation in pancreatic cancer. *Cell* **2016**, *166*, 963−976.
(40) Madeira, F.; Pearce, M.; Tivey, A. R. N.; Basutkar, P.; Lee, J.; Edbali, O.; Madhusoodanan, N.; Kolesnikov, A.; Lopez, R. Search and sequence analysis tools services from EMBL-EBI in 2022. *Nucleic Acids Res.* **2022**, *50*, W276−W279.
(41) Hobbs, G. A.; Der, C. J.; Rossman, K. L. RAS isoforms and mutations in cancer at a glance. *J. Cell Sci.* **2016**, *129*, 1287−1292.
(42) Review: Moore, A. R.; Rosenberg, S. C.; McCormick, F.; Malek, S. RAS-targeted therapies: is the undruggable drugged? *Nat. Rev. Drug Discovery* **2020**, *19*, 533−552.
(43) (a) Lanman, B. A.; Allen, J. R.; Allen, J. G.; Amegadzie, A. K.; Ashton, K. S.; Booker, S. K.; Chen, J. J.; Chen, N.; Frohn, M. J.; Goodman, G.; Kopecky, D. J.; Liu, L.; Lopez, P.; Low, J. D.; Ma, V.; Minatti, A. E.; Nguyen, T. T.; Nishimura, N.; Pickrell, A. J.; Reed, A. B.; Shin, Y.; Siegmund, A. C.; Tamayo, N. A.; Tegley, C. M.; Walton, M. C.; Wang, H.-L.; Wurz, R. P.; Xue, M.; Yang, K. C.; Achanta, P.; Bartberger, M. D.; Canon, J.; Hollis, L. S.; McCarter, J. D.; Mohr, C.; Rex, K.; Saiki, A. Y.; San Miguel, T.; Volak, L. P.; Wang, K. H.; Whittington, D. A.; Zech, S. G.; Lipford, J. R.; Cee, V. J. Discovery of a covalent inhibitor of $KRAS^{G12C}$ (AMG 510) for the treatment of solid tumors. *J. Med. Chem.* **2020**, *63*, 52−65. (b) Lim, S.; Boyer, N.; Boo, N.; Huang, C.; Venkatachalam, G.; Angela Juang, Y. C.; Garrigou, M.; Kaan, H. Y. K.; Duggal, R.; Peh, K. M.; Sadruddin, A.; Gopal, P.; Yuen, T. Y.; Ng, S.; Kannan, S.; Brown, C. J.; Verma, C. S.; Orth, P.; Peier, A.; Ge, L.; Yu, X.; Bhatt, B.; Chen, F.; Wang, E.; Li, N. J.; Gonzales, R. J.; Stoeck, A.; Henry, B.; Sawyer, T. K.; Lane, D. P.; Johannes, C. W.; Biswas, K.; Partridge, A. W. Discovery of cell active macrocyclic peptides with on-target inhibition of KRAS signaling. *Chem. Sci.* **2021**, *12*, 15975−15987.
(44) Nakajima, E. C.; Drezner, N.; Li, X.; Mishra-Kalyani, P. S.; Liu, Y.; Zhao, H.; Bi, Y.; Liu, J.; Rahman, A.; Wearne, E.; Ojofeitimi, I.; Hotaki, L. T.; Spillman, D.; Pazdur, R.; Beaver, J. A.; Singh, H. FDA approval summary: Sotorasib for $KRAS^{G12C}$-mutated metastatic NSCLC. *Clin. Cancer Res.* **2022**, *28*, 1482−1486.
(45) Maura, F.; Bolli, N.; Angelopoulos, N.; Dawson, K. J.; Leongamornlert, D.; Martincorena, I.; Mitchell, T. J.; Fullam, A.; Gonzalez, S.; Szalat, R.; Abascal, F.; Rodriguez-Martin, B.; Samur, M. K.; Glodzik, D.; Roncador, M.; Fulciniti, M.; Tai, Y. T.; Minvielle, S.; Magrangeas, F.; Moreau, P.; Corradini, P.; Anderson, K. C.; Tubio, J. M. C.; Wedge, D. C.; Gerstung, M.; Avet-Loiseau, H.; Munshi, N.; Campbell, P. J. Genomic landscape and chronological reconstruction of driver events in multiple myeloma. *Nat. Commun.* **2019**, *10*, 3835.
(46) Weiss, H. M.; Pfaar, U.; Schweitzer, A.; Wiegand, H.; Skerjanec, A.; Schran, H. Biodistribution and plasma protein binding of zoledronic acid. *Drug Metab. Dispos.* **2008**, *36*, 2043−2049.
(47) Skerjanec, A.; Berenson, J.; Hsu, C.; Major, P.; Miller, W. H.; Ravera, C.; Schran, H.; Seaman, J.; Waldmeier, F. The pharmacokinetics and pharmacodynamics of zoledronic acid in cancer patients with varying degrees of renal function. *J. Clin. Pharmacol.* **2003**, *43*, 154−162.
(48) Review: (a) Onakpoya, I. J.; Heneghan, C. J.; Aronson, J. K. Worldwide withdrawal of medicinal products because of adverse drug reactions: a systematic review and analysis. *Crit. Rev. Toxicol.* **2016**, *46*, 477−489. (b) Monroe, J. J.; Tanis, K. Q.; Podtelezhnikov, A. A.; Nguyen, T.; Machotka, S. V.; Lynch, D.; Evers, R.; Palamanda, J.; Miller, R. R.; Pippert, T.; Cabalu, T. D.; Johnson, T. E.; Aslamkhan, A. G.; Kang, W.; Tamburino, A. M.; Mitra, K.; Agrawal, N. G. B.; Sistare, F. D. Application of a Rat Liver Drug Bioactivation Transcriptional

https://doi.org/10.1021/acs.jmedchem.3c01271
J. Med. Chem. 2023, 66, 15776−15800

Response Assay Early in Drug Development That Informs Chemically Reactive Metabolite Formation and Potential for Drug-induced Liver Injury. *Toxicol. Sci.* **2020**, *177*, 281−299.
(49) Robles-Diaz, M.; Lucena, M. I.; Kaplowitz, N.; Stephens, C.; Medina−Cáliz, I.; González−Jimenez, A.; Ulzurrun, E.; Gonzalez, A. F.; Fernandez, M. C.; Romero−Gómez, M.; Jimenez-Perez, M.; Bruguera, M.; Prieto, M.; Bessone, F.; Hernandez, N.; Arrese, M.; Andrade, R. J. Use of Hy's Law and a new composite algorithm to predict acute liver failure in patients with drug-induced liver injury. *Gastroenterology* **2014**, *147*, 109−118.e5.
(50) Sánchez, O.; Arnau, A.; Pareja, M.; Poch, E.; Ramírez, I.; Soley, M. Acute stress-induced tissue injury in mice: differences between emotional and social stress. *Cell Stress Chaperones* **2002**, *7*, 36−46.
(51) Fernández, I.; Peña, A.; Del Teso, N.; Pérez, V.; Rodríguez-Cuesta, J. Clinical biochemistry parameters in C57BL/6J mice after blood collection from the submandibular vein and retroorbital plexus. *J. Am. Assoc. Lab. Anim. Sci.* **2010**, *49*, 202−206.
(52) Data for NOD SCID and Nu/Nu Mouse Biochemistry found on the Charles River Laboratory Wed site for Clinical Pathology Data. https://www.criver.com/sites/default/files/resources/doc_a/NODSCIDMouseClinicalPathologyData.pdf, https://www.criver.com/sites/default/files/resources/doc_a/NUNUMouseClinicalPathologyData.pdf.
(53) Thoolen, B.; Maronpot, R. R.; Harada, T.; Nyska, A.; Rousseaux, C.; Nolte, T.; Malarkey, D. E.; Kaufmann, W.; Küttler, K.; Deschl, U.; Nakae, D.; Gregson, R.; Vinlove, M. P.; Brix, A. E.; Singh, B.; Belpoggi, F.; Ward, J. M. Proliferative and nonproliferative lesions of the rat and mouse hepatobiliary system. *Toxicol. Pathol.* **2010**, *38*, 5S−81S.
(54) Awad, M. M.; Liu, S.; Rybkin, I. I.; Arbour, K. C.; Dilly, J.; Zhu, V. W.; Johnson, M. L.; Heist, R. S.; Patil, T.; Riely, G. J.; Jacobson, J. O.; Yang, X.; Persky, N. S.; Root, D. E.; Lowder, K. E.; Feng, H.; Zhang, S. S.; Haigis, K. M.; Hung, Y. P.; Sholl, L. M.; Wolpin, B. M.; Wiese, J.; Christiansen, J.; Lee, J.; Schrock, A. B.; Lim, L. P.; Garg, K.; Li, M.; Engstrom, L. D.; Waters, L.; Lawson, J. D.; Olson, P.; Lito, P.; Ou, S.-H. I.; Christensen, J. G.; Jänne, P. A.; Aguirre, A. J. Acquired resistance to $KRAS^{G12C}$ inhibition in cancer. *N. Engl. J. Med.* **2021**, *384*, 2382−2393.
(55) Lindner, A. U.; Salvucci, M.; McDonough, E.; Cho, S.; Stachtea, X.; O'Connell, E. P.; Corwin, A. D.; Santamaria-Pang, A.; Carberry, S.; Fichtner, M.; Van Schaeybroeck, S.; Laurent-Puig, P.; Burke, J. P.; McNamara, D. A.; Lawler, M.; Sood, A.; Graf, J. F.; Rehm, M.; Dunne, P. D.; Longley, D. B.; Ginty, F.; Prehn, J. H. M. An atlas of inter- and intra-tumor heterogeneity of apoptosis competency in colorectal cancer tissue at single-cell resolution. *Cell Death Differ.* **2022**, *29*, 806−817.
(56) Review: Makurvet, F. D. Biologics vs. small molecules: Drug costs and patient access. *Med. Drug Discov.* **2021**, *9*, 100075.
(57) Forbes. Biologic medicines: the biggest driver of rising drug prices, 2019. https://www.forbes.com/sites/theapothecary/2019/03/08/biologic-medicines-the-biggest-driver-of-rising-drug-prices/?sh=731a940218b0 (accessed 13 April, 2020).
(58) Facon, T.; Kumar, S.; Plesner, T.; Orlowski, R. Z.; Moreau, P.; Bahlis, N.; Basu, S.; Nahi, H.; Hulin, C.; Quach, H.; Goldschmidt, H.; O'Dwyer, M.; Perrot, A.; Venner, C. P.; Weisel, K.; Mace, J. R.; Raje, N.; Attal, M.; Tiab, M.; Macro, M.; Frenzel, L.; Leleu, X.; Ahmadi, T.; Chiu, C.; Wang, J.; Van Rampelbergh, R.; Uhlar, C. M.; Kobos, R.; Qi, M.; Usmani, S. Z. Daratumumab plus lenalidomide and dexamethasone for untreated myeloma. *N. Engl. J. Med.* **2019**, *380*, 2104−2115.
(59) Leung, C.-Y.; Langille, A. M.; Mancuso, J.; Tsantrizos, Y. S. Discovery of thienopyrimidine-based inhibitors of the human farnesyl pyrophosphate synthase - Parallel synthesis of analogs via a trimethylsilyl ylidene intermediate. *Bioorg. Med. Chem.* **2013**, *21*, 2229−2240.
(60) Nowak, P.; Cole, D. C.; Brooijmans, N.; Bursavich, M. G.; Curran, K. J.; Ellingboe, J. W.; Gibbons, J. J.; Hollander, I.; Hu, Y.; Kaplan, J.; Malwitz, D. J.; Toral-Barza, L.; Verheijen, J. C.; Zask, A.; Zhang, W.-G.; Yu, K. Discovery of Potent and Selective Inhibitors of the Mammalian Target of Rapamycin (mTOR) Kinase. *J. Med. Chem.* **2009**, *52*, 7081−7089.

https://doi.org/10.1021/acs.jmedchem.3c01271
J. Med. Chem. 2023, 66, 15776−15800